การศึกษาเปรียบเทียบผลของขนาดผลึกและอุณหภูมิการเผาต่อความเสถียรทางความร้อน

ของโลหะออกไซด์แบบสไปเนล

นาย ปริญญา สมร่าง

วิทยานิพนธ์นี้เป็นส่วนหนึ่งของการศึกษาตามหลักสูตรปริญญาวิศวกรรมศาสตรมหาบัณฑิต
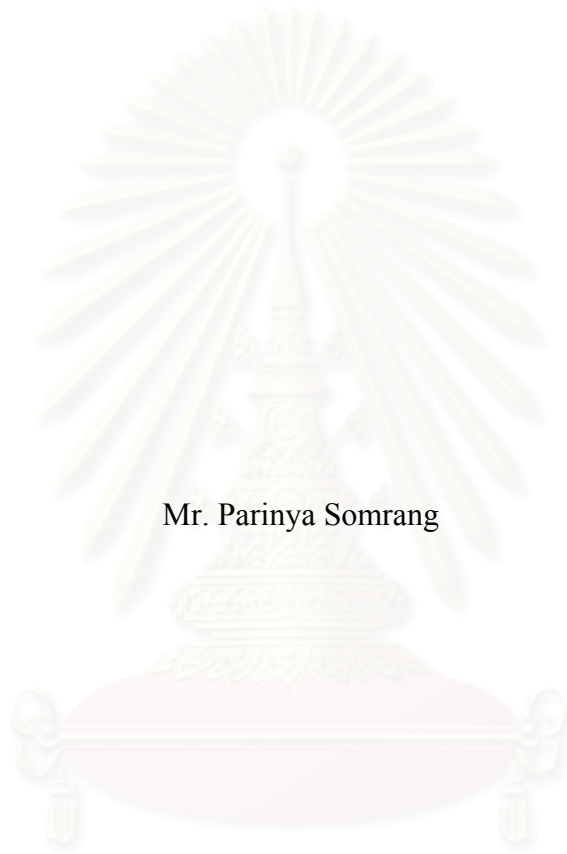
สาขาวิชาวิศวกรรมเคมี ภาควิชาวิศวกรรมเคมี

คณะวิศวกรรมศาสตร์ จุฬาลงกรณ์มหาวิทยาลัย

ปีการศึกษา 2544

COMPARATIVE EFFECT OF CRYSTALLITE SIZE AND CALCINATION
TEMPERATURE ON THE THERMAL STABILITY OF
SPINEL TYPE METAL OXIDE

Mr. Parinya Somrang

Thesis Title	Comparative effect of crystallite size and calcination temperature on the thermal stability of spinel type metal oxide
By	Mr. Parinya Somrang
Field of Study	Chemical Engineering
Thesis Advisor	Mr. Suphot Phatanasri, D.Eng.
Thesis Co-advisor	Miss Waraporn Tanakulrungsank, D.Eng.

Accepted by the Faculty of Engineering, Chulalongkorn University in Partial Fulfillment of the Requirements for the Master's Degree

.... Dean of Faculty of Engineering

(Professor Somsak Panyakeow, D.Eng.)

Thesis Committee

.... Chairman

(Associate Professor Ura Pancharoen, D.Eng.Sc.)

.... Thesis Advisor

(Suphot Phatanasri, D.Eng.)

.... Thesis Co-advisor

(Waraporn Tanakulrungsank, D.Eng.)

.... Member

(Professor Piyasan Praserthdam, Dr.Ing.)

.... Member

(Assistant Professor Supakanok Thongyai, Ph.D.)

นายปริญญา สมร่าง: การศึกษาเปรียบเทียบผลของขนาดผลึกและอุณหภูมิการเผาต่อความเสถียรทาง
ความร้อนของโลหะออกไซด์แบบสไปเนล (COMPARATIVE EFFECT OF CRYSTALLITE SIZE
AND CALCINATION TEMPERATURE ON THE THERMAL STABILITY OF SPINEL TYPE
METAL OXIDE) อ.ที่ปรึกษา: อ.ดร.สุพจน์ พัฒนะศรี, อ.ที่ปรึกษาร่วม: อ.ดร.วราภรณ์ ธนกุลรังสรรค์
99 หน้า. ISBN 974-03-1325-6

โครงสร้างผลึกระดับนาโนเมตร ของซิงค์โครไมท์ ซิงค์แมงกาไนท์ ซิงค์เฟอไรท์ และ ซิงค์โคบอลไทท์
ถูกเตรียมขึ้นด้วยปฏิกิริยาทางความร้อนของซิงค์อะซิเตตและโลหะอะเซทติลอะซิโตเนต   ในอัตราส่วนโดย
อะตอมของสังกะสีต่อโลหะเท่ากับ 0.5 ในตัวทำละลายอินทรีย์ 1,4-บิวเทนไดออล ที่อุณหภูมิการทำปฏิกิริยา
300℃ เป็นเวลา 2 ชั่วโมง ภายใต้สภาวะการเพิ่มขึ้นของความดันตามอุณหภูมิ และอัตราการเพิ่มอุณหภูมิที่แตก
ต่างกันคือ 2.5 และ 1.0℃ ต่อนาที ซิงค์โครไมท์และซิงค์เฟอไรท์เกิดขึ้นโดยตรงจากปฏิกิริยาทางความร้อนด้วย
ไกลคอล ในขณะที่ซิงค์แมงกาไนท์และซิงค์โคบอลไทท์ เกิดผ่านตัวกลางที่ต้องผ่านการเผาก่อนเพื่อให้เกิดเป็น
โครงสร้างสไปเนล จากการศึกษาได้พบว่าอัตราการเพิ่มอุณหภูมิมีผลกระทบต่อขนาดผลึกที่สังเคราะห์ได้ ขนาด
ผลึกที่วัดด้วยวิธีการกล้องจุลทรรศน์อิเล็กตรอนแบบส่องผ่าน   จะมีขนาดใกล้เคียงกับที่วัดด้วยวิธีการกระเจิงรังสี
เอ็กซ์ ซึ่งแสดงให้เห็นว่าผลึกที่ได้เป็นผลึกเดี่ยว เมื่อนำโลหะออกไซด์แบบสไปเนลที่เตรียมได้ เผาที่อุณหภูมิ
ระหว่าง 600 ถึง 1000℃ พบว่าความเสถียรทางความร้อนของโลหะออกไซด์แบบสไปเนลนั้นอยู่มีความสัมพันธ์
ดังนี้

$$ZnCr_2O_4 > ZnMn_2O_4 > ZnFe_2O_4 \approx ZnCo_2O_4$$
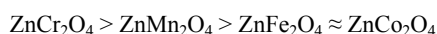
โดยความเสถียรทางความร้อนของผลิตภัณฑ์   จะกำหนดจากอัตราส่วนระหว่างขนาดผลึกหลังจากการ
เผาต่อขนาดผลึกก่อนการเผา สมบัติทางโครงสร้างสไปเนลที่เตรียมได้ทั้งก่อนและหลังจากการเผาจะคล้ายกัน ถึง
แม้ว่าจะผ่านการเผาที่อุณหภูมิสูง

ภาควิชา...วิศวกรรมเคมี... ลายมือชื่อนิสิต..

สาขาวิชา...วิศวกรรมเคมี... ลายมือชื่ออาจารย์ที่ปรึกษา..

ปีการศึกษา...2544... ลายมือชื่ออาจารย์ที่ปรึกษาร่วม...................................

PARINYA SOMRANG: COMPARATIVE EFFECT OF CRYSTALLITE SIZE AND CALCINATION TEMPERATURE ON THE THERMAL STABILITY OF SPINEL TYPE METAL OXIDE. THESIS ADVISOR: SUPHOT PHATANASRI, D.Eng. THESIS CO-ADVISOR: WARAPORN TANAKULRUNGSANK, D.Eng. 99 pp. ISBN 974-03-1325-6

The nanostructured material zinc chromite, zinc manganite, zinc ferrite and zinc cobaltite were synthesized via the thermal reaction of zinc acetate and metal acetylacetonate, stoichiometric ratios of Zn/Metal equal to 0.5, in 1,4-butanediol at 300°C for 2 hours under autogenous pressure with different reaction heating rate of 2.5 and 1.0°C/min. Zinc chromite and zinc ferrite were directly formed after glycothermal reaction, while zinc manganite and zinc cobaltite which were formed via an undetermined intermediate phase had to be calcined at a desired temperature before forming spinel phase. It was found that the reaction heating rate affected significantly on the crystallite size of the as-synthesized products. The crystallite size of the as-synthesized products observed by TEM was close to that examined by XRD. This suggested that each particle was a single crystal. After calcination at various temperatures, the results indicated that the thermal stability of the spinel type metal oxides lied in the correlation of,

$$ZnCr_2O_4 > ZnMn_2O_4 > ZnFe_2O_4 \approx ZnCo_2O_4$$
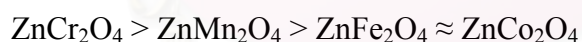
The thermal stability of the product was designed from the ratio of the crystallite size of the product after calcined (d) to the crystallite size of the as-synthesized sample (d_0). The spinel structure, before and after calcination, revealed the same performance even after calcined at high temperature.

Department...Chemical Engineering......   Student's signature...............................

Field of study...Chemical Engineering....   Advisor's signature..............................

Academic year...2001..............................   Co-advisor's signature..........................

ACKNOWLEDGEMENT

CONTENTS

CONTENTS (CONT.)

LIST OF TABLES

LIST OF FIGURES

LIST OF FIGURES (CONT.)

LIST OF FIGURES (CONT.)

LIST OF FIGURES (CONT.)

LIST OF FIGURES (CONT.)

CHAPTER I

INTRODUCTION

Of particular interest to the material scientists is the fact that nanostructure materials have assumed high importance due to unique features associated with their size. They are materials of great interest because of their large number of technological applications. They are produced as thin films, powders, colloids, and encapsulated materials. Due to their extremely small dimensions, nanostructure materials can exhibit novel electronic, optical, magnetic, and chemical properties.

Nanostructure have higher surface areas than do conventional materials. Activity due to their small particle size and enormous surface area has been the focus of the intense study in physics, chemistry and materials science. The impact of nanostructure on the properties of high surface area materials is an area of increasing importance to understanding, creating, and improving materials for diverse applications. High surface areas can be attained either fabricating small particles or clusters where the surface-to-volume ratio of each particle is high, or by creating materials where the void surface area (pores) is high compared to the amount of bulk support material. Materials such as highly dispersed supported metal catalyst and gas phase clusters fall into the former category, and microporous (nanometer-pored) materials such as zeolites, high surface area inorganic oxides, porous carbons, and amorphous silicas fall into the latter category.

There are many areas of current academic and industrial activity where the use of the nanostructure approach to high surface area materials may have significant impact. In catalysis, majority of the product volume from chemical process industries directly originates from catalytic technology. In recent years, catalytic technology was improved to find the most suitable catalyst for each works. The key goal is to promote reactions that have high selectivity with high yield. It is anticipated that this goal will be more closely approached through a catalyst particle via nanoparticle synthesis and assembly so that it performs only specific chemical conversions, performs these at high yield, and does so with greater energy efficiency. Manufacture of materials with

greatly improved properties in one or more areas such as strength, toughness, or ductility may become commonplace. In addition, many laboratories around the world are actively pursuing the potential to create novel thermal barrier materials whose bonding and strength depend upon the surface area and morphology of the nanoscale constituents.

In the search for improved properties of catalytic materials, great interest has focused on spinel-type structured. The name is derived from the mineral spinel, $MgAl_2O_4$. This structure can be described on the basis of the cubic close packing of the anions. A spinel structure presents two types of interstitial sites: tetrahedral and octahedral; these sites are surrounded by four and six oxygen atom, respectively. The formula of the spinel is AB_2O_4 where A^{2+} and B^{3+} are the cations occupying the tetrahedral and the octahedral sites, respectively. A^{2+} cations can be Mg, Ca or any divalent cations of the first transition series elements while B^{3+} cations can be Al, Ga or any trivalent first transition series elements.

Among these materials, transition elements are technologically important materials that have found many applications. The use of transition metal oxides as catalysts is the most technologically advanced and economically important. Many of the chemical processes require high selectivity for a particular product, and many involve oxidation of the reactant molecules. In fact, selective oxidation, ammoxidation, and selective dehydrogenation probably constitute the most important catalytic uses of transition metal oxides. The different oxidation states available in these oxides make it possible to control the selectivity in oxidation with the properties of the oxides. Some transition metal oxides can also catalyze selective hydrogenation and are used in some commercial processes.

For the zinc chromite, $ZnCr_2O_4$, as a catalyst of the ethanol conversion, the main reaction products are acetaldehyde, acetone, methylethyl ketone and ethylacetate. [1] Chromium plays a role as a promoter of butadiene selectivity in n-butane oxidative dehydrogenation on $ZnCr_xFe_{1-x}O_4$ catalyst. [2] $ZnCr_xFe_{1-x}O_4$ system has the normal spinel structure for $0 \leq x \leq 2$. The increase of chromium concentration had little effect on the selectivity of butadiene but increasing in conversion.

Table 1.1 Examples of chemical processes in which transition metal oxides are catalysts

Process	Example
Oxidation	Production of SO_3 from SO_2
	CO oxidation in emission control
Dehydrogenation (nonoxidative)	Production of styrene from ethylbenzene
Dehydrogenation (oxidative)	Production of formaldehyde from methanol and butadiene from butenes
Selective oxidation	Production of acrolein from propene, and maleic anhydride from benzene or butane
Selective ammoxidation	Production of acrylonitrile from propene
Selective reduction	Reduction of NO, selective hydrogenation of unsaturated ketones
Metathesis	Production of long chain alkenes
Water-gas shift	Production of hydrogen

Transition metal manganites are important technological materials used as negative temperature coefficient (NTC) thermistors owing to their interesting electrical properties. [3] Zinc manganite is possible candidate for high temperature applications. Some manganese-based oxides such as $ZnMn_2O_4$ and their solid solutions are known to be efficient catalysts for the selective gas-phase reduction of nitrobenzene to nitrosobenzene. [4,5] On the other hand, pure zinc manganite is an active catalyst for NO reduction by C_3H_8. [6,7] At ambient temperature, $ZnMn_2O_4$ is a normal spinel structure.

Zinc ferrite ($ZnFe_2O_4$) spinel structured is well known materials. It has been reported to be an active catalyst for the oxidative dehydrogenation of n-butane and 1-butene to butadiene [8,9], a sorbent for high-temperature desulfurization of coal gas [10], gas-sensing materials to reducing gas [11], and as a semiconductor photocatalyst for various processes [12]. The nanocrystalline powder of zinc ferrite has a normal spinel structured with a tetrahedral A site by Zn^{2+} ions and an octahedral B site by Fe^{3+} ions within the lattice of cubic close packing.

The zinc cobaltite, with normal spinel structured with Zn^{2+} ions in a tetrahedral A site and Fe^{3+} ions in an octahedral B site, is known to be catalysts, which can be used for the complete oxidation of organic substances and carbon monoxide. [13] Among the cobaltites, the highest thermal stability belongs to zinc cobaltite. It can be used as absorbents for low temperature gas desulfurization. [14]

In most of the synthetic processes, the alkoxides are hydrolyzed in an alcoholic solution yielding amorphous (or hydrated) metal oxide with large-surface area; however there surface areas are drastically decreased on calcinations at the temperatures where corresponding oxide begin to crystallize. Recently, Inoue et al. have examined the thermal reaction of metal alkoxide in glycols (glycothermal reaction) or other organic media and demonstrated that a number of novel or characteristic crystalline products can be obtained directly without bothersome procedures such as purification of the reactants or handling in inert atmosphere.

As mentioned above, the novel method for the synthesis of metal oxides in organic media may be a new route to prepare micro- and nanocrystalline metal oxides. In this work, the novel method was applied in the system of the spinel type metal oxide. The divalent cation in the tetrahedral sites would be fixed for the zinc ion, while vary the trivalent cations in the octahedral sites. The interesting trivalent cations are those trivalent ions of transition metals in the first serie. That are Ti^{3+}, V^{3+}, Cr^{3+}, Mn^{3+}, Fe^{3+}, Co^{3+} and Ni^{3+}. The purpose of the present work is to study the effect of crystalline formation and calcination temperature on the physical properties and thermal stability of spinel type metal oxides.

The present study is arranged as follow:

Chapter II presents literature reviews of the novel synthesis of several metal oxides in organic media.

The theories related to this work are described in chapter III.

Chapter IV presents the experimental systems and the spinel type metal oxide preparation.

Chapter V shows the experimental results of the characterization of samples. The X-ray diffraction (XRD) patterns, BET surface area, crystallite size, morphology and thermal decomposition of the products are explained.

In the last chapter, the overall conclusion emerged from this research is given.

Finally, the demonstration of calculation of the reagents used for the spinel type metal oxide preparation and crystallite sizes are included in the APPENDICES at the end of this thesis paperwork.

CHAPTER II

LITERATURE REVIEW

This chapter provides some background information for understanding the synthesis of metal oxide or binary metal oxide in organic media, "Glycothermal method." Since this is a new route to prepare the metal oxides, the literature reviews on the traditional preparation method that had been studied by many researchers are presented as follows. Thus all information can contribute and lead to some interesting subjects concerned in this thesis.

2.1 Glycothermal Method

Hydrothermal method has been widely applied for the synthesis of a variety of ceramic materials. However, only a few papers have dealt with the use of organic media instead of the water in hydrothermal method [15-17]. These methods have the advantage that the products consist of microcrystalline particles but are sufficiently high thermal stability; they still remain large surface areas after post-calcination at even higher temperature.

Inoue et al. [18] reported that the thermal reaction of gibbsite in ethylene glycol at 250°C yielded an ethylene glycol derivative of boehmite, in which organic moiety is incorporated covalently between the layer structures of boehmite. This reaction has been extended to the reaction of gibbsite in higher homologues of ethylene glycol, and they have found that microcrystalline χ-alumina is formed under quite mild condition [19]. By using Scanning Electron Microscope (SEM), this product had unique honeycomb-like texture. In this connection, they had examined the reaction of aluminum isopropoxide in glycol, and found the formation of the glycol derivatives of boehmite, identical compounds obtained from gibbsite [20]. The synthetic process as mentioned above, the use of glycol (organic solvent) instead of water in the synthetic system is different method from the conventional methods. This method was called "Glycothermal method".

Inoue et al. [21] also found that this reaction in inert organic solvents such as toluene, benzene and/or others, thermal decomposition of aluminum alkoxide occurred and yielded a product compose of 4 to 20 nm particles having the χ-alumina mixture. The χ-alumina was stable and maintained a surface area above 100 m^2g^{-1} until its transformation at 1150°C to be α-alumina. TEM of product showed each α-alumina particle was a single crystal hexagonal plate shape. With this result, they have applied this method for zirconia synthesis and reported that thermal decomposition of zirconium alkoxide in organic solvents yielded microcrystalline tetragonal zirconia, which had a large surface area and a fairly high thermal stability. However, zirconium isopropoxide reacted in toluene and zirconium tert-butoxide decomposed at 200°C yielding amorphous zirconia. While zirconium n-alkoxide, which decomposed into glycol, did not decompose at 300°C in inert organic solvent [22]. Therefore they tried to hydrolyze the zirconium n-alkoxide in the inert organic solvent with a limited amount of water dissolved in the solvent from the gas phase and found that this method gave microcrystalline monoclinic zirconia having a much higher thermal stability [23]. The obtained zirconia maintained large surface area even after high temperature calcination as 162 and 72 m^2/g at 500 and 900°C, respectively.

Recently, Inoue et al. [24] reported that microcrystalline binary oxide were directly formed when a mixture of two alkoxide, acetylacetonate, and/or acetate was heated in 1,4-butanediol at elevated temperature under autogeneous pressure of the glycol. An example was synthesis of gadolinium gallium garnets (GGG) by reaction of mixed gallium acetylacetonate with gadolinium acetate. This reaction has been extended to the reaction of a stoichiometric mixture of aluminium isopropoxide (AIP) and yttrium acetate, and found that crystalline yttrium aluminium garnet (YAG) is formed under similar condition. No other phases were detected. The uncalcined YAG had a large surface area (107 m^2g^{-1}) that decrease to 44 and 10 m^2g^{-1} after calcination at 1000 and 1300°C, respectively. YAG was composed of agglomerates of almost spherical particles having a relatively narrow size distribution with an average particle size of approximately 30 nm. The use of ethylene glycol instead of 1,4-butanediol in the synthetic system afforded amorphous product [25].

The reaction of aluminium isopropoxide (AIP) and other rare earth acetates have been studied. Inoue et al. [25] reported that the reaction of AIP and acetates of the lanthanide elements from Gd to Lu in 1,4-butanediol at 300°C yielded the corresponding lanthanide aluminium garnets. The reaction of AIP with samarium or europium acetate gave a mixture of the corresponding garnets phase and lanthanide acetate oxide. However, the reaction of AIP with neodymium acetate gave only neodymium acetate oxide as the sole crystalline product.

As described above, samarium and europium garnets have never been reported except as solid solutions with YAG, and this paper is the first report of the synthesis of these garnets. Because of the metastability of these garnets, thermal methods such as ceramic processes would not give these garnets. Ease in crystallization of the perovskite phase seems to be another reason for the difficulty in the synthesis of these garnets by the thermal method.

The stability of lanthanide hydroxide under the hydrothermal conditions increases in ionic size of the lanthanide element. This may be one reason for the increase in lower temperature limit for the hydrothermal synthesis of aluminium garnet with the increase in ionic size of the lanthanide element. The aluminium garnet with the large-size lanthanide ion hydrothermally prepared so far was $Tb_3Al_5O_{12}$. $Gd_3Al_5O_{12}$ could not be prepared by the hydrothermal method. Since the ionic size of samarium and europium are still larger than gadolinium, there seems to be no possibility that samarium and europium garnets could be formed by the hydrothermal method.

As mentioned above, glycothermal treatment of microcrystalline gibbsite yielded α-alumina at 280°C, a much lower temperature than the α-alumina formation temperature by the hydrothermal method. The difference between glycothermal and hydrothermal reaction was attributed to the difference in the stability of the intermediate phases, i.e. the glycol derivative of boehmite versus well-crystallized boehmite. Similarly, the success of the synthesis of samarium and europium garnets by the glycothermal method may be attributed to the instability of intermediate phases. Under glycothermal, aluminium alkoxide is easily converted to glycoxide.

Thermal decomposition of the glycoxide molecules proceeds by intra molecular participation of the remaining hydroxyl group of glycol moiety, yielding an $>Al-O^-$ anion. In the absence of RE acetate, nucleophilic attack of this aluminate ion on another glycoxide molecule takes place, finally yielding the glycol derivative of boehmite. In presence of RE acetate, this aluminate anion attacks the RE ion forming the Al-O-RE bond, which finally yields the garnets crystals under the glycothermal conditions.

For the synthesis of the catalyst and catalyst supports, metal alkoxide are widely uses as the starting materials to avoid contamination of the inorganic counter anion from the corresponding metal salts which effects the activity and selectivity of the catalyst. In a series of Inoue's studies [20-25], metal alkoxide are used as the starting materials and the effect of the structure of the alkyl group in the starting alkoxide was examined. They have found that the formation of the product requires direct cleavage of the C-O bonds in alkoxides, and therefore the thermal stability of C-O bonds maybe a decisive factor for decomposition of metal alkoxide.

Many papers as mentioned above, the synthesis of several metal oxides and binary metal oxides in organic solvents are explained. This novel method produced the products that have a large surface area and high thermal stability. This novel method may be a new route to prepare micro- and nanocrystalline metal oxides. The choice of the solvent, reaction conditions and structure of the alkyl group of the metal alkoxide can control the physical properties of the product.

2.2 Spinel type metal oxides synthesis

Generally, spinel type metal oxides are prepared by coprecipitation method, sol-gel method, or hydrothermal method. Correa Bueno et al. [1] prepared the catalysts by the coprecipitation at pH 8 from a solution of nitrates of the elements with a slight excess of $KHCO_3$. Then the precursors were washed and calcined to obtain the zinc chromite, $ZnCr_2O_4$. Armendariz et al. [2] prepared $ZnCr_xFe_{1-x}O_4$ by the coprecipitation method. A dilute solution of nitrate parents salts was neutralized with NH_4OH at constant pH. Precipitates were washed with demineralized water,

filtered and then dried in vacuo. The dried powders were dried in air in order to obtain the oxide.

Zinc manganite had been mainly prepared by solid-solid reaction between zinc oxide, ZnO, and manganese oxides, usually α-Mn_2O_3. [3] A few zinc manganites can be prepared by calcinations of hydroxides, by the sol/gel method or by coprecipitation of oxalates. Guillemet-Fritsch et al. prepared zinc manganite by the thermal decomposition in air of oxalate precursors. The precursors were obtained by the coprecipitation of an aqueous solution. The oxides were obtained after a heat treatment. On the other hand, Fierro et al. [6,7] prepared zinc manganites by thermal decomposition of carbonate precursors obtained by coprecipitation at constant pH.

Four kinds of ferrite, MFe_2O_4 (M = Cu, Zn, Cd, or Mg), had been prepared by a coprecipitation method from the nitrate of each constituent metal and iron at the designated molar ratio (M/Fe = 1:2). [11] The ferrites have high specific surface area (40-80 m^2/g) and tested for sensing properties to reducing gases of CO, H_2, LPG, C_2H_5OH and C_2H_2. Zhihao and Lide [12] had prepared zinc ferrite nanoparticles capped with a layer of dodecyl benzene sulfonic acid by the coprecipitation microemulsion method. The as-prepared nanoparticles were annealed at different temperatures in air to investigate the effect of the surfactant capping on the grain growth of the $ZnFe_2O_4$ nanoparticles during heat treatment.

Jiang et al. [26] synthesized the nanocrystalline zinc ferrite powders by high-energy ball milling in a closed container at ambient temperature from a mixture of α-Fe_2O_4 and ZnO in equimolar ratio. The phase evolution and the microstructure of the zinc ferrite prepared are studied. At room temperature, the nanocrystalline zinc ferrite shows a super paramagnetic state, indicating a higher defect concentration induced by high-energy ball milling than that in the samples prepared by the coprecipitation method.

Toledo et al. [27] carried out the hydrothermal synthesis of zinc ferrite powders. The samples were determined the importance of the preparation method through comparison of the chemical, textural and catalytic properties. The spinel structures were obtained at low temperature and having a greater BET specific surface

area than that observed in coprecipitation samples. Cabanas and Poliakoff [28] reported the continuous synthesis of nanoparticle spinel type oxide by combining hydrothermal synthesis and partial oxidation. They have been able to synthesize Fe_3O_4, $CoFe_2O_4$, $NiFe_2O_4$, $ZnFe_2O_4$ and $Ni_xCo_{1-x}Fe_2O_4$. The process is simple and clean and requires neither the addition of bases nor the use of the very high reaction temperature.

Klissurski et al. [13] had synthesized a zinc cobaltite spinel by thermal decomposition of a hydroxide-carbonate precursor obtained by coprecipitation carried out by adding a solution of Zn and Co nitrates to a sodium carbonate solution with continuous stirring. A method was proposed for the preparation of a γ-Al_2O_3-supported zinc-cobalt oxide catalyst. Similarly, Baird et al. [14] prepared the absorbent by coprecipitation at low super-saturation and a constant pH. The precursors were dried in an oven and calcined, as a finely ground powder, in a muffle oven. The finely powdered oxides were pressed into discs, crushed and sieved prior to use as absorbents.

CHAPTER III

THEORY

The basic knowledge of the spinel structure is described in the first section of this chapter, for more understanding in this unique material. In the next section, the explanation on the traditional hydrothermal method is provided. And the end of this chapter is the information of the single crystal.

3.1 Spinel structure [29-31]

Several of the commercially important magnetic oxides have the spinel structure. The parent spinel is the mineral spinel, $MgAl_2O_4$. There are well over a hundred compounds with the spinel structure reported to date. Most are oxides. Some are sulphides, selenides and tellurides. A few are halides. Many different cations may be introduced into the spinel structure and several different charge combinations are possible, namely:

2, 3	as in	$MgAl_2O_4$
2, 4	as in	Mg_2TiO_4
1, 3, 4	as in	$LiAlTiO_4$
1, 3	as in	$Li_{0.5}Al_{2.5}O_4$
1, 2, 5	as in	$LiNiVO_4$
1, 6	as in	Na_2WO_4

Similar cation combinations occur with sulphides, e.g. 2, 3: $ZnAl_2S_4$ and 2, 4: Cu_2SnS_4. With halide spinels, cations are limited to charges of 1 and 2, in order to give an overall cation: anion ratio of 3:4, e.g. Li_2NiF_4.

This structure can be described on the basis of the cubic close packing of the anions. The unit cell consists of a supercube formed by combining eight fcc units of the anions such that the edge length is doubled. This unit of 32 anions will have 64 tetrahedral and 32 octahedral voids. In the spinel structure, only eight tetrahedral and sixteen octahedral voids are occupied in an order way. This give the unit cell a

stoichiometry $A_8B_{16}X_{32}$ where A and B are the cations occupying the tetrahedral and the octahedral sites respectively and X is the anion.
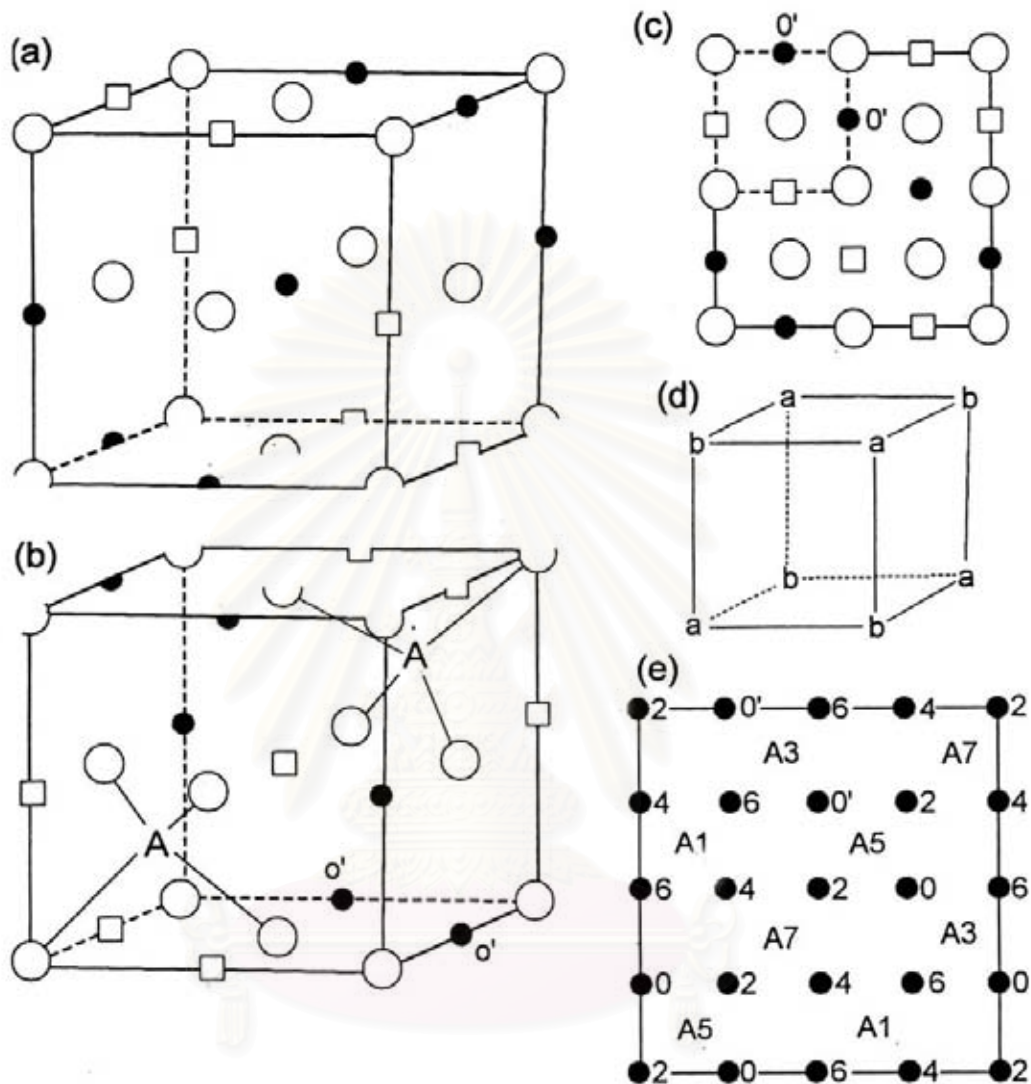
Figure 3.1 Representative parts of the spinel structure. (a) One octant of the unit cell showing oxygens at corner and face centers, empty □ and occupied ● octahedral sites. (b) A second octant, underneath the one in (a) showing in addition the occupation of two tetrahedral sites, A. (c) One face of the cubic unit cell of the spinel structure. The dashed part coincides with the base of the subcell shown in (b). (d) Alternating arrangement of the two types of octant (a) and (b). (e) Cation positions in spinel. Numbers refer to fractional heights, as multiples of c/8. Octahedral sites, 0', are also shown in (b, c) [30]
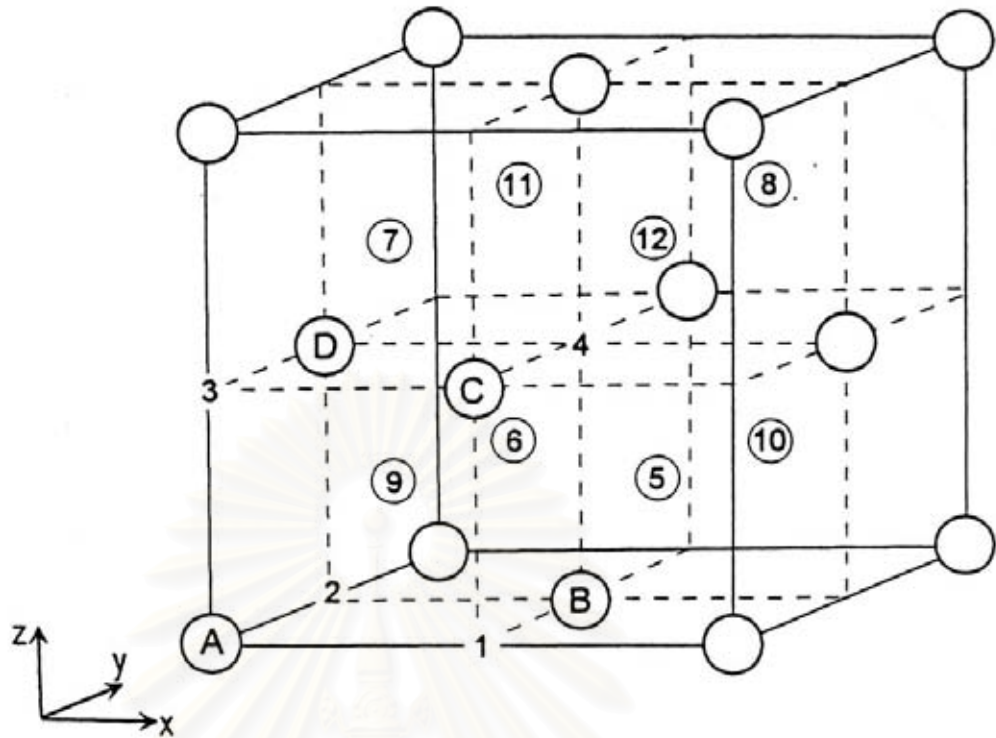
Figure 3.2 Available cation sites, 1-12, in an fcc anion array [30]

Writing the general formula of a normal spinel as $A^{tet}B_2^{oct}O_4$, first consider the $B_2^{oct}O_4$ part. This is a rock salt structure with ccp O^{2-} ions but with only alternate octahedral sites occupied by B cations. Two rock salt-derivative subcells are shown in Figure 3.1(a, b). The bottom face of the subcell in (a) is the same as the top face of the subcell in (b). Oxygens are shown at corners and face centers. Some octahedral positions are occupied (solid circles) but alternate ones in any of the three unit cell directions are empty (small squares). The base of the spinel unit cell is shown in (c) formed by the base of (b), dashed, and that of three adjacent subcells. The alternating, empty-occupied-empty sequence of octahedral sites is clearly seen and also occurs similarly in the third dimension (a, b).

To complete the structure, need to locate the tetrahedral A cations. In a fcc anion array (Figure 3.2), the eight tetrahedral sites, 5-12, are located as shown. These tetrahedral sites are equidistant from oxygen atoms but also from the octahedral cation sites. Cation-cation repulsion does not allow adjacent tetrahedral and octahedral sites to be occupied simultaneously. Therefore need to find those tetrahedral sites for

which all four neighboring octahedral sites are empty. In Figure 3.1(a), all of the tetrahedral sites have at least one neighboring octahedral cation and none of the tetrahedral sites in this octant is occupied. The octant immediately below (or above) that in (a) is shown in (b), note that its top face is the same as the bottom face in (a). In this octant, two of the tetrahedral sites have no octahedral cation neighbors and therefore, both of these contain an A cation. Taking the spinel structure as a whole, the eight octants fall into two structural groups, as represented by (a) and (b). The A cations are located in the four octants of type (b).

The two types of octant are arranged such that they alternate in any of the three unit cell directions. They are arranged in the same way as anions and cations in the rock salt structure, Figure 3.1(d). Figure 3.1(e) show a projection of the unit cell onto one face, showing cation positions only. The orientation is exactly the same as in (b) and (c) but now atom heights, above the plane of the paper, are given as multiples of c/8. Octahedral positions are solid circles, which occupied tetrahedral positions that represented by A.

Two extreme types of behavior may be distinguished. In normal spinels, the cations are in the sites that would be expected from the formula AB_2O_4, with A in tetrahedral sites and B in octahedral sites. Examples of normal spinels are $MgAl_2O_4$ and $MgTi_2O_4$. In inverse spinels, half of the B ions are in tetrahedral sites, leaving the remaining B ions and the A ions to occupy the octahedral sites. Usually, the occupancy of these octahedral sites is disordered. Examples of inverse spinels are $MgFe_2O_4$ and Mg_2TiO_4.

The formulae of spinels may be expanded in order to distinguish between normal and inverse:

Normal: $[A]^{tet}[B_2]^{oct}O_4$

Inverse: $[B]^{tet}[A, B]^{oct}O_4$

The structure of spinel is based on the structure of diamond, which has the same high symmetry. The position of the A ions is nearly identical to the positions occupied by carbon atoms in the diamond structure. This could explain the relatively high hardness and high density typical of this group. The arrangement of the other ions in the structure conforms to the symmetry of the diamond structure. But, they

disrupt the cleavage, as there is no cleavage direction in any member of this group. The arrangement of the ions also favors the octahedral crystal habit, which is predominant crystal form and is in fact the trademark of the spinels. All members of this group that share the spinel structure show the same type of twinning that is named after spinel.

A representative selection of normal and inverse spinels is listed in Table 3.1.

Table 3.1 Structure of some spinels [30, 31]

Crystal	Type	Structure
$MgAl_2O_4$	2, 3	Normal
$CoAl_2O_4$	2, 3	Normal
$CuCr_2S_4$	2, 3	Normal
$CuCr_2Se_4$	2, 3	Normal
$CuCr_2Te_4$	2, 3	Normal
$MgTi_2O_4$	2, 3	Normal
Co_2GeO_4	2, 4	Normal
Fe_2GeO_4	2, 4	Normal
$MgFe_2O_4$	2, 3	Inverse
$NiFe_2O_4$	2, 3	Inverse
$MgIn_2O_4$	2, 3	Inverse
$MgIn_2S_4$	2, 3	Inverse
Mg_2TiO_4	2, 4	Inverse
Zn_2SnO_4	2, 4	Inverse
Zn_2TiO_4	2, 4	Inverse
$LiAlTiO_4$	1, 3, 4	Li in 8a
$LiMnTiO_4$	1, 3, 4	Li in 8a
$LiZnSbO_4$	1, 2, 5	Li in 8a
$LiCoSbO_4$	1, 2, 5	Li in 8a

3.2 Hydrothermal method [30,31]

The method involves heating the reactants in water/steam at high pressures and temperatures. The water performs two roles, as a pressure-transmitting medium and as a solvent, in which the solubility of the reactants is P, T-dependent. In addition, some or all of the reactance are partially soluble in the water under pressure and this enables reaction to take place in, or with the aid of, liquid and/or vapor phases. Under these conditions, reactions may occur that, in the absence of water, would occur only at much high temperatures. The method is therefore particularly suited for the synthesis of phases that are unstable at higher temperatures. It is also a useful technique for growth of single crystals; by arranging for a suitable temperature gradient to be present in the reaction vessel, dissolution of the starting material may occur at the hot end and reprecipitation at the cooler end.

The design of hydrothermal equipment is basically a tube, usually of steel, closed at one end. The other end has a screw cap with a gasket of soft copper to provide a seal. Alternatively, the 'bomb' may be connected directly to and independent pressure source, such as a hydraulic ram; this is known as the 'cold seal' method. The reaction mixture and an appropriate amount of water are placed inside the bomb, which then sealed and placed inside an oven at the required temperature, usually at a temperature in the range 100-500°C. Pressure is controlled either externally or by the degree of filling in a sealed bomb. By making use of the P/T 'phase diagram', Figure 3.3(a); curve AB is the saturated steam curve and separates water (above) from steam (below); at temperatures above 374°C, point B, the water is in the supercritical condition and there is no distinction between liquid and vapor states.

The applications of the hydrothermal method is:

(a) Synthesis of new phases: calcium silicate hydrate.

Hydrothermal methods have been used successfully for the synthesis of many materials. A good example is the family of calcium silicate hydrates, many of which are important components of set cement and concrete. Typically, lime, CaO

and quartz, SiO_2, are heated with water at temperatures in the range 150 to 500°C and pressure of 0.1 to 2 kbar. Each calcium silicate hydrate has, for its synthesis, optimum preferred conditions of composition of starting mix, temperature, pressure and time. For example, xonolite, $Ca_6Si_6O_{17}(OH)_2$, may be prepared by heating equimolar mixtures of CaO and SiO_2 at saturated stream pressures in the range150 to 350°C.

(b) Growth of single crystals.

For the growth of single crystals by hydrothermal methods it is often necessary to add a mineralizer. A mineralizer is any compound added to the aqueous solution that speeds up its crystallization. It usually operates by increasing the solubility of the solute through the formation of soluble species that would not usually be present in the water. For instance, the solubility of quartz in water at 400°C and 2 kbar is too small to permit the recrystallization of quartz, in a temperature gradient, within a reasonable space of time. On addition of NaOH as a mineralizer, however, large quartz crystals may be readily grown. Using the following conditions, crystals of kilogram size have been grown: quartz and 1.0 M NaOH solution are held at 400°C and 1.7 kbar; at this temperature some of the quartz dissolves. A temperature gradient is arranged to exist in the reaction vessel and at 360°C the solution is supersaturated with respect to quartz, which precipitates onto a seed crystal. In summary, therefore, quartz dissolves in the hottest part of the reaction vessel, is transported throughout the vessel via convection currents and is precipitated in cooler parts of the vessel where its solubility in water is lower. Quartz single crystals are use in many devices in radar and sonar, as piezoelectric transducers, as monochromators in X-ray diffraction, etc. Annual world production of quartz single crystals, using hydrothermal and other methods, is currently a staggering 600 tons.

Using similar methods, many substances have been prepared as high quality single crystals, e.g. corundum (Al_2O_3) and ruby (Al_2O_3 doped with Cr^{3+}).
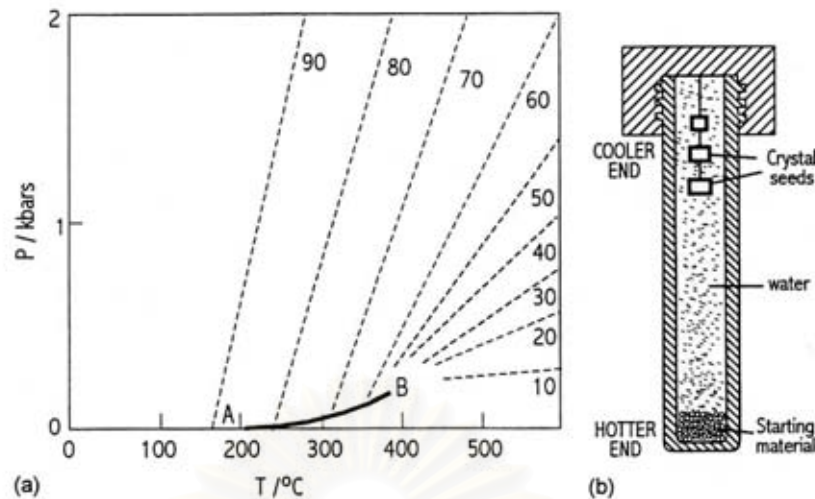
Figure 3.3 (a) Pressure-temperature relations for water at constant volume, dashed curves represent pressures developed inside a close vessel; numbers represent the percentage degree of filling of the vessel by water at ordinary P, T. (b) Schematic hydrothermal bomb used for crystal growth. [30]

3.3 Single crystal [32]

In crystalline solids the atoms or molecules are stacked in a regular manner, forming a three-dimensional pattern, which may be obtained by a three-dimensional repetition of a certain pattern unit called a unit cell. When the periodicity of the pattern extends throughout the certain piece of material, one speaks of a single crystal. A single crystal is formed by the growth of a crystal nucleus without secondary nucleation or impingement on other crystal.

3.3.1 Growth techniques

Among the most common methods of growing single crystals are those of P. Bridgeman and J. Czochralski. In the Bridgeman method the material is melted in a vertical cylindrical vessel, which tapers conically to a point at the bottom. The vessel then is lowered slowly into a cold zone. Crystallization begins in the tip and continues usually by growth from the first formed nucleus. In the Czochralski method a small single crystal (seed) is introduced into the surface of the melt and then drawn slowly upward into a cold zone. Single crystals of ultrahigh purity have been grown

by zone melting. Single crystals are also often grown by bathing a seed with a supersaturated solution, the supersaturation being kept lower than necessary for sensible nucleation.

When grown from a melt, single crystals usually take the form of their container. Crystals grown from solution (gas, liquid, or solid) often have a well-defined form, which reflects the symmetry of the unit cell. For example, rock salt or ammonium chloride crystals often grow from solutions in the form of cubes with faces parallel to the 100 planes of the crystal, or in the form of octahedrons with faces parallel to the 111 planes. The growth form of crystals is usually dictated by kinetic factors and does not correspond necessarily to the equilibrium form.

3.3.2 Physical properties

Ideally, single crystals are free from internal boundaries. They give rise to a characteristic x-ray diffraction pattern. For example, the Laue pattern of a single crystal consists of a single characteristic set of sharp intensity maxima.

Many types of single crystal exhibit anisotropy, that is, a variation of some of their physical properties according to the direction along which they are measured. For example, the electrical resistivity of a randomly oriented aggregate of graphite crystallites is the same in all directions. The resistivity of a graphite single crystal is different, however, when measured along crystal axes. This anisotropy exist both for structure-sensitive properties, which are strongly affected by crystal imperfections (such as cleavage and crystal growth rate), and structure-insensitive properties, which are not affected by imperfections (such as elastic coefficients).

Anisotropy of a structure-insensitive property is described by a characteristic set of coefficients, which can be combined to give the macroscopic property along any particular direction in the crystal. The number of necessary coefficients can often be reduced substantially by consideration of the crystal symmetry, whether anisotropy, with respect to a given property, exists depends on crystal symmetry. The structure-sensitive properties of crystals (for example, strength and diffusion coefficients) seem governed by internal defects, often on an atomic scale.

CHAPTER IV

EXPERIMENTAL

This chapter explained the experimental system and the experimental procedures that were used in this work. The chemicals used in the preparation of the spinel type metal oxides are shown in section 4.1. The preparation apparatus are shown in section 4.2. In sections 4.3 and 4.4, the spinel type metal oxide preparation and characterization are presented respectively.

4.1 Chemicals

The lists of chemicals used in this work are shown in the following:

1) Zinc acetate (99.9%), $(CH_3COO)_2Zn$, Aldrich Chemical Company, USA.

2) Chromium (III) acetylacetonate (97%), $[CH_3COCH=C(O-)CH_3]_3Cr$, Aldrich Chemical Company, USA.

3) Manganese (III) acetylacetonate (tech.), $[CH_3COCH=C(O-)CH_3]_3Mn$, Aldrich Chemical Company, USA.

4) Iron (III) acetylacetonate (97%), $[CH_3COCH=C(O-)CH_3]_3Fe$, Aldrich Chemical Company, USA.

5) Cobalt (III) acetylacetonate (98%), $[CH_3COCH=C(O-)CH_3]_3Co$, Aldrich Chemical Company, USA.

6) 1,4-Butanediol (99%), $HO(CH_2)_2OH$, Aldrich Chemical Company, USA.

7) Ultra high purity nitrogen gas (99.99%vol.), Thai Industrial Gas Co. Ltd.

Table 4.1 Reagents used for the synthesis of the spinel type metal oxides

Spinel type metal oxide	Reagents	Weight or Volume
Zinc chromite	Zinc acetate	5.00 g
	Chromium (III) acetylacetonate	19.5913 g
	Organic solvents: 1,4-butanediol	
	In the inner glass	100 cm^3
	In the gap	30 cm^3
Zinc manganite	Zinc acetate	5.00 g
	Manganese (III) acetylacetonate	19.1635 g
	Organic solvents: 1,4-butanediol	
	In the inner glass	100 cm^3
	In the gap	30 cm^3
Zinc ferrite	Zinc acetate	5.00 g
	Iron (III) acetylacetonate	19.8072 g
	Organic solvents: 1,4-butanediol	
	In the inner glass	100 cm^3
	In the gap	30 cm^3
Zinc cobaltite	Zinc acetate	5.00 g
	Cobalt (III) acetylacetonate	19.7761 g
	Organic solvents: 1,4-butanediol	
	In the inner glass	100 cm^3
	In the gap	30 cm^3

4.2 Instruments and apparatus

The schematic diagram of the reaction apparatus for the synthesis of the spinel type metal oxides is shown in Figure 4.1.
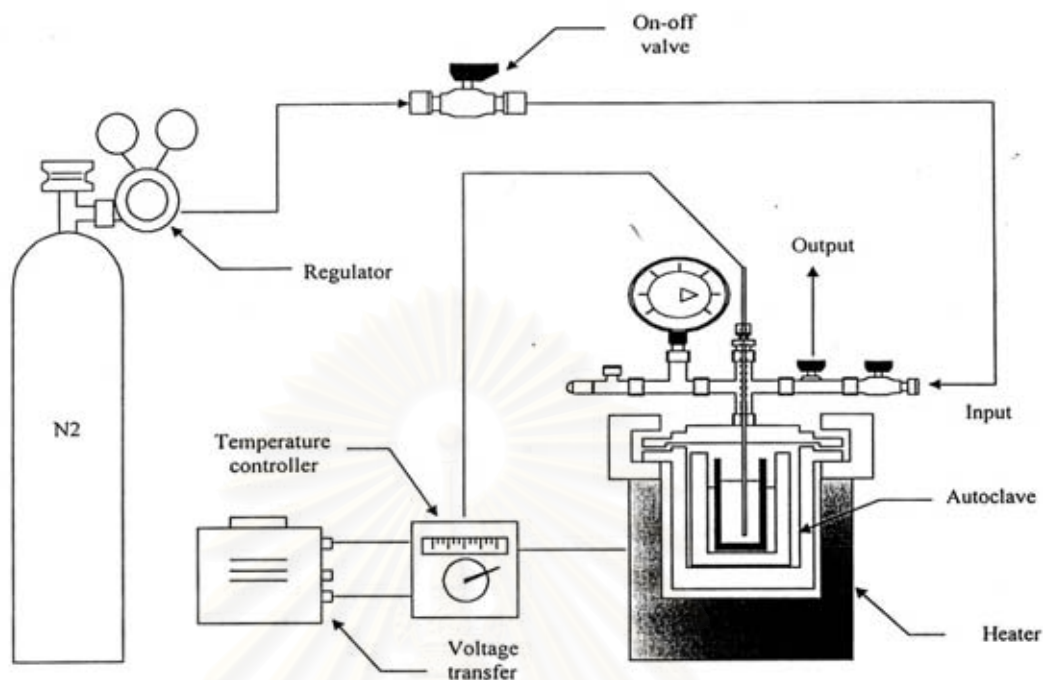
Figure 4.1 Schematic diagram of the reaction apparatus

Autoclave reactor: The autoclave is made of stainless steel with 1000 cm^3 volume and 10 cm inside diameter. This consists of a pressure gauge within the range of 0 to 140 bar and a relief valve, which used to control pressure in the autoclave. This autoclave can be operated at high pressure and high temperature. The reaction was carried out under the autogeneous pressure, which gradually increased as the temperature was raised.

Automatic temperature controller: This consists of a magnetic switch connected to a variable voltage transfer and a RKC temperature controller connected to a thermocouple with 0.5 mm in diameter attached to the synthesis mixtures in autoclave. A dial setting establishes a set point at any temperature within the range of 0 to 400ºC.

Electrical furnace (Heater): This supplied the required heated to the autoclave for the reaction. Autoclave can be operated from room temperature up to 300ºC at voltage of 200 volts.
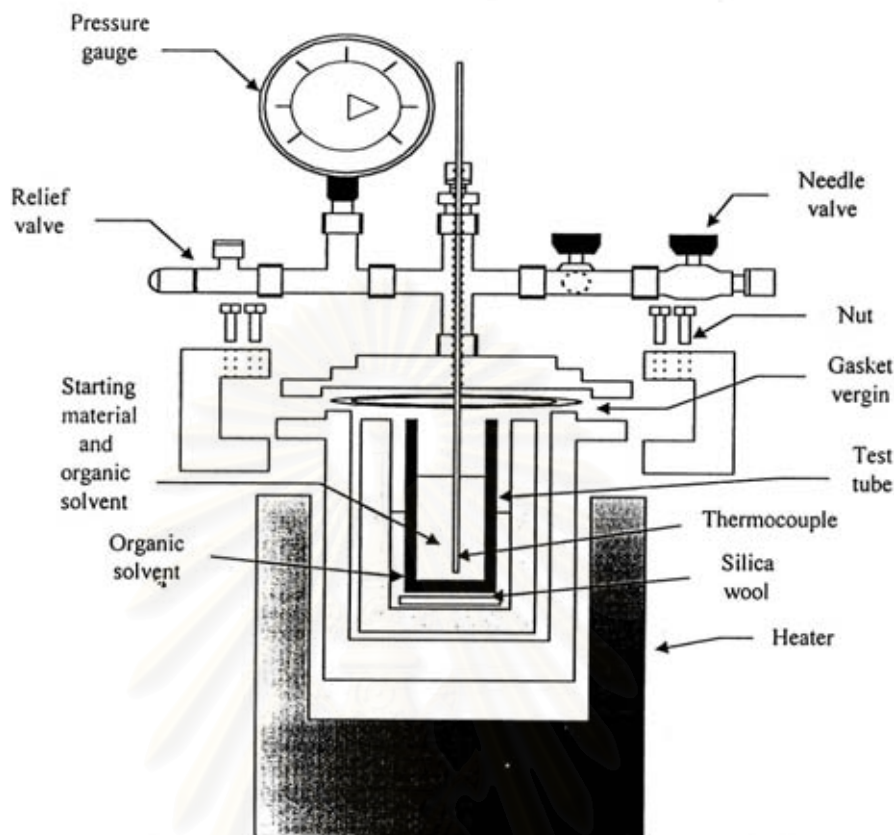
Figure 4.2 Autoclave reactor

Gas controlling system: Ultra high purity nitrogen gas is equipped with a pressure regulator (0-150 bar), and needle valves were used to release gas from autoclave.

4.3 Catalyst preparation

The synthesis of zinc ferrite, 5 g of zinc acetate and an appropriate amount of iron (III) acetylacetonate (Zn/Fe atomic ratio is 0.5) were dissolved in 100 cm^3 of organic media: 1,4-butanediol; in a test tube which was then set in an autoclave. 30 cm^3 of the 1,4-butanediol was added in the gap between the test tube and the autoclave wall. The autoclave was purged with nitrogen, heated to a desired temperature that was 300°C at a desired rate of 2.5 and 1.0°C/min, and held at this temperature for 2 hours. Autogeneous

pressure gradually increased as the temperature was raised in which depended on the kind of an organic media. After the autoclave was cooled, the resulting products were washed repeatedly with methanol by centrifugation and air-dried. Part of the product was calcined in a box furnace, heated at a rate of 10°C/min to the desire temperature and held at that temperature for 1 hour.

For the synthesis of the other spinel type metal oxides were doing the same procedure with the used of 5 g of zinc acetate and an appropriate amount of metal acetylacetonate, as shown in Table 4.1, in order to control the atomic ratio of Zn/Metal equal to 0.5.

4.4 Characterization of the catalyst samples

4.4.1 X-ray Diffraction (XRD)

In X-ray diffraction (XRD) a collimated beam of X rays, with wavelength $\lambda \approx 0.5\text{-}2$ Å; is incident on a specimen and is diffracted by the crystalline phases in the specimen according to Bragg's law ($\lambda = 2d\sin\theta$, where d is the spacing between atomic planes in the crystalline phase). The intensity of the diffracted X rays is measured as a function of the diffraction angle 2θ and the specimen's orientation. This diffraction pattern is used to identify the specimen's crystalline phases and to measure its structural properties, including strain (which is measured with accuracy), epitaxy, and the size and orientation of crystallites (small crystalline regions).

XRD patterns of the catalyst samples were determined by using Ni-filtered Cu Kα radiation. A scan rate of 0.04°/s was used to record the patterns in the 2θ range of 10-80° (SIEMENS XRD D5000, Petrochemical Engineering Research Laboratory, Chulalongkorn University). The crystallite size was estimated from line broadening according to the Scherer equation. The value of the shape factor, K, was taken to be 0.89 and α-Al$_2$O$_3$ was used to be internal standard to eliminate the broadening effect attributed to the equipment.

4.4.2 Morphology

In Transmission Electron Microscopy (TEM) method, a thin solid specimen (≤ 200 nm thick) is bombarded in vacuum with highly focused monoenergetic beam of electrons. The beam is of sufficient energy to propagate through the specimen. A series of electrons are observed in the form of a diffraction pattern beneath the specimen. This information is used to determine the atomic structure of the material in the sample. Transmitted electrons form the images from small regions of sample that contain contrast, due to several scattering mechanisms associated with interactions between electron images yields information about atomic structure and about defects present in the materials.

The morphology of the catalyst samples was observed by a JEOL TEM-200cx transmission electron microscope, which operated at 100 kV at the Scientific and Technological Research Equipment Center, Chulalongkorn University.

4.4.3 BET surface area measurement

Physical adsorption isotherms are measured near the boiling point of a gas (e.g., nitrogen, at 77 K). From these isotherms the amount of gas needed to form a monolayer can be determined. If the area occupied by each adsorbed gas molecule is know, then the surface area can be determined for all finely divided solids, regardless of their chemical composition.

Table 4.2 Operation condition of gas chromatograph (GOW-MAC)

Model	GOW-MAC
Detector	TCD
Helium flow rate	30 ml. min^{-1}
Detector temperture	80 °C
Detector current	80 mA

The specific surface area of the samples were calculated using the Brunauer-Emmett-Teller single point method on the basis of nitrogen uptake measured at liquid-nitrogen boiling point temperature equipped with a gas chromatograph.

4.4.3.1 BET apparatus

The reaction apparatus of BET surface area measurement consisted of two feed lines of helium and nitrogen. The flow rate of the gas was adjusted by means of fine-metering valve on the gas chromatograph. The sample cell made from pyrex glass. The schematic diagram of the reaction apparatus was shown in Figure 4.3 and the operation condition of gas chromatograph (GOW-MAC) is shown in Table 4.2.

4.4.3.2 Measurement

The mixture gases of helium and nitrogen flowed through the system at the nitrogen relative pressure of 0.3. The catalyst sample was placed in the sample cell, ca. 0.3-0.5 g, which was then heated up to 160 °C and held at that temperature for 2 hours. Then the catalyst sample was cooled down to room temperature and was measured the specific surface area. There were three steps to measure the specific surface area.

Adsorption step: The catalyst sample that set in the sample cell was dipped into the liquid nitrogen. Nitrogen gas that flowed through the system was adsorbed on the surface of the catalyst sample until equilibrium was reached.

Desorption step: The sample cell with nitrogen gas-adsorbed catalyst sample was dipped into the water at room temperature. The adsorbed nitrogen gas was desorbed from the surface of the catalyst sample. This step was completed when the indicator line was back in the position of the base line.

Calibration step: 1 ml of nitrogen gas at atmospheric pressure was injected through the calibration port of the gas chromatograph and the area was measured. The area was the calibration peak. The calculation method is explained in Appendix C.
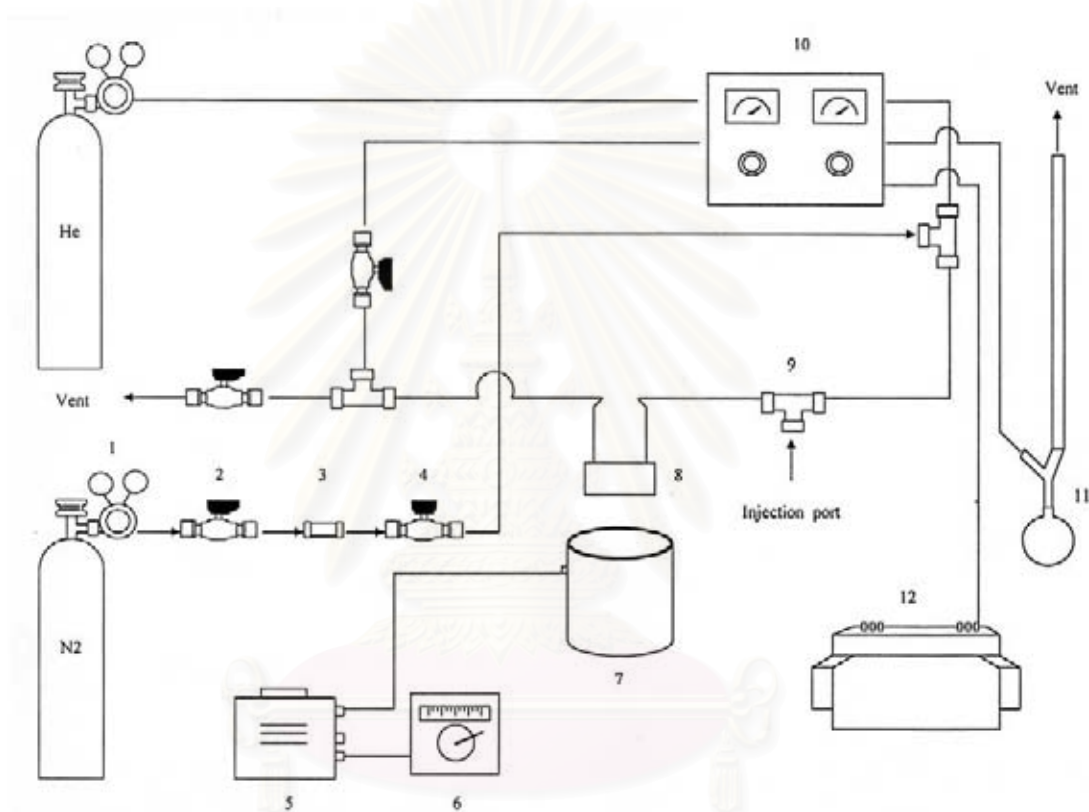
1. Pressure regulator   2. On-off valve   3. Gas filter

4. Needle valve   5. Voltage transformer   6. Temperature controller

7. Heater   8. Sample cell   9. Three-way

10. Gas chromatograph with TCD   11. Bubble flow meter   12. Indicator

Figure 4.3 Schematic diagram of the BET specific surface area measurement

4.4.4 Thermogravimetric analysis

Shimadzu TA-50 thermal analyzer (Japan) was used in this work. The catalyst was load in a Pt pan then placing in the furnace. Air was used as a purging gas. The furnace temperature was raised from room temperature up to the desired temperature at a constant heating rate of 10ºC/min and held at that temperature for 1 hour. The data were displayed and recorded by using a computer. The data were used to study the decomposition of the catalyst during the heating.

CHAPTER V

RESULTS AND DISCUSSION

The glycothermal method was applied for the synthesis of the spinel type metal oxide. The studied spinel structures were fixed the zinc ion in the tetrahedral sites while varied the trivalent cations in the octahedral sites. The interesting trivalent cations were the trivalent ions of transition metals in the first serie. That are Ti^{3+}, V^{3+}, Cr^{3+}, Mn^{3+}, Fe^{3+}, Co^{3+} and Ni^{3+}.

In order to control the variables in the study, the starting reagents were fixed for zinc acetate and metal (III) acetylacetonates. The used metal (III) acetylacetonate in the study were vanadium (III) acetylacetonate, chromium (III) acetylacetonate, manganese (III) acetylacetonate, iron (III) acetylacetonate and cobalt (III) acetylacetonate, which were provided by Aldrich Chemical Company, USA. The effect of trivalent cations of Ti^{3+} and Ni^{3+} in octahedral sites were not studied, since there was not any provided of titanium (III) acetylacetonate and nickel (III) acetylacetonate. After the glycothermal reaction of zinc acetate and metal (III) acetylacetonate in 1,4-butanediol at 300ºC for 2 hours under autogeneous pressure, zinc chromite and zinc ferrite were directly crystallized while zinc manganite and zinc cobaltite were formed via the undetermined intermediate product. The glycothermal reaction of zinc acetate and vanadium (III) acetylacetonate yielded the undetermined intermediate product, which melted after calcined at the temperature 600ºC. That made the obtained product impossible to study at higher calcination temperature. Therefore, zinc vanadate was not studied. In conclusion, the studied spinel type metal oxides were zinc chromite, zinc manganite, zinc ferrite and zinc cobaltite.

The formations of the spinel type metal oxides, zinc chromite, zinc manganite, zinc ferrite and zinc cobaltite, were respectively described in the first section of the chapter. The crystallite sizes observed by X-ray diffraction and particle size observed by transmission electron microscopy are provided in this section, as well as the BET surface area. The second section exhibits the proposed mechanisms of spinel formation and the comparative thermal stability of the spinel type metal oxides.

5.1 Formation of pure zinc chromite

      The reaction of zinc acetate and chromium (III) acetylacetonate in the glycol solvent of 1,4-butanediol at 300ºC for 2 hours under autogeneous pressure yielded nanocrystalline zinc chromite. The X-ray diffraction patterns of the products obtained by all reactions show that the spinel phases were directly crystallized. Both of the crystallite size and the BET surface area of zinc chromite depended on the reaction heating rate.

      The X-ray diffraction (XRD) patterns of the as-synthesized products of zinc chromite obtained from glycothermal reaction of starting mixtures at 300ºC and held at that temperature for 2 hours are given in Figure 5.1. The figure indicated that the spinel phase was formed without any contamination with other phases such as ZnO and Cr_2O_3. [2] The broadening diffraction peaks confirmed the rather small crystallite size of the products as clearly exhibited in the XRD patterns. The crystallite sizes of the products, which calculated by the line broadening of XRD using Scherrer equation, were 4.97 and 4.74 nm. The average particle sizes determined from the transmission electron micrograph (TEM) of the products were 5.33 and 4.67 nm, which were in good agreement with the crystallite size obtained from XRD, indicated that each primary particle observed by TEM is a single crystal of spinel type zinc chromite. The BET surface area of the products obtained from the reaction heating rate of 2.5 and 1.0ºC/min were 192.39 and 185.99 m^2 g^{-1} respectively.

      Parts of the product were calcined at various temperatures of 600 to 1000ºC. The XRD patterns and BET surface area of the calcined products were investigated. Table 5.1 shows the BET surface area and crystallite size of the products after calcined. The XRD patterns of the calcined products were nearly identical to that before calcined despite the fact that the XRD peaks were sharper and narrower (Figures 5.2 and 5.3). As expected from the patterns, these products still preserved the spinel structure even after calcined at 1000ºC. Figures 5.4(a) to (d) and 5.5(a) to (d) show the TEM photographs of the zinc chromite products before and after calcined at various temperatures.

Table 5.1 Crystallite size and BET surface area of the as-synthesized and calcined products zinc chromite prepared at different reaction heating rates, (a) 2.5ºC/min and (b) 1.0ºC/min

Calcination temperature	$d_{XRD}^{(1)}$, nm		$d_{TEM}^{(2)}$, nm		$S_{BET}^{(3)}$, m^2g^{-1}	
	(a)	(b)	(a)	(b)	(a)	(b)
As-syn	4.97	4.74	5.33	4.67	192.39	185.99
600ºC	11.62	12.52	11.67	12.67	62.91	57.56
700ºC	13.95	15.15	14.07	15.33	48.17	41.04
800ºC	17.26	21.94	17.33	22.00	41.64	34.88
900ºC	24.14	30.88	24.00	30.67	29.87	22.12
1000ºC	41.29	38.95	41.80	38.67	14.52	14.23

[1] Crystallite size of the products estimated by the Scherrer equation

[2] Particle size of the products observed by TEM

[3] Specific surface area of the products estimated by BET single point method
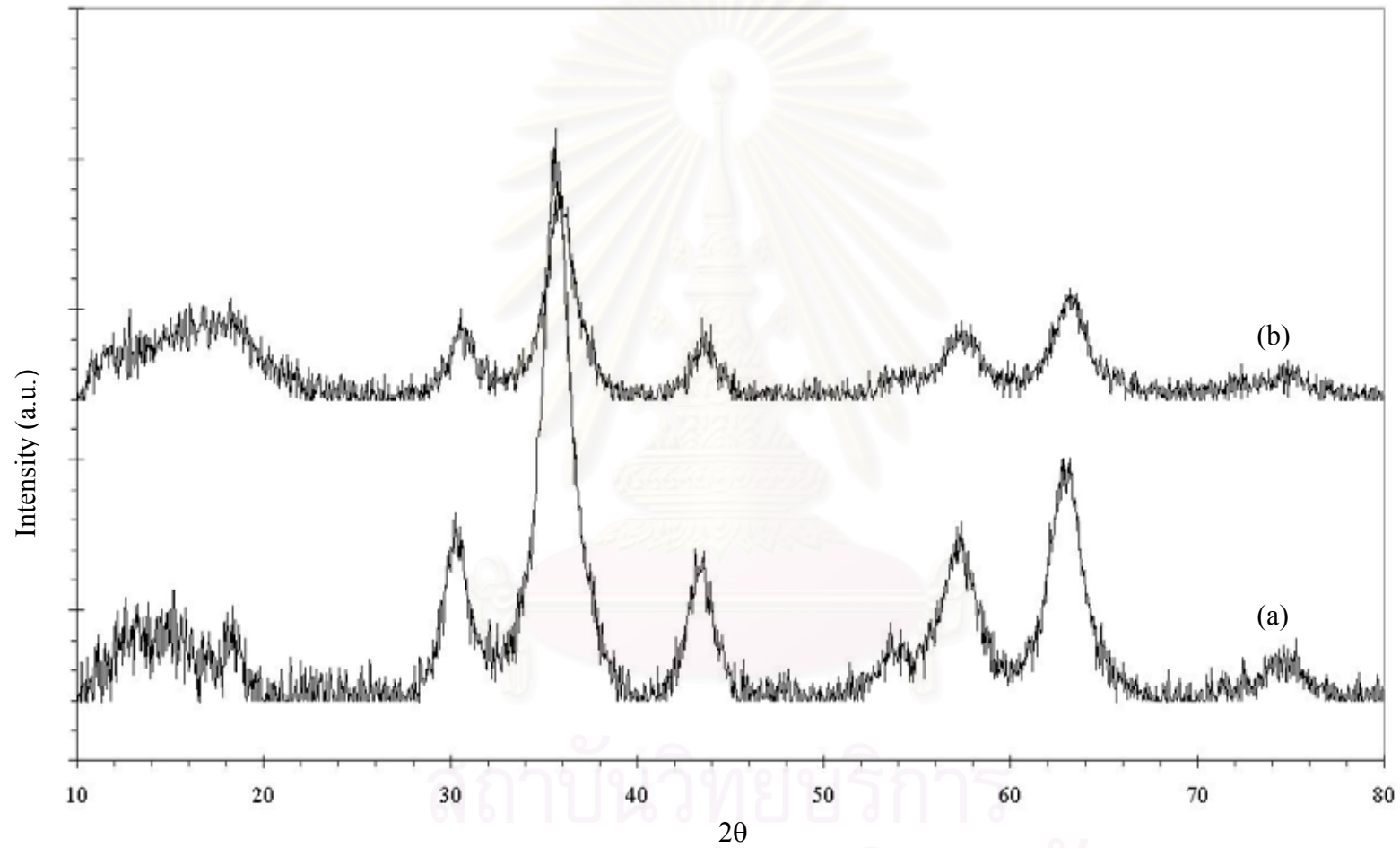
Figure 5.1 The XRD patterns of the as-synthesized zinc chromite prepared at different reaction heating rates, (a) 2.5ºC/min and (b) 1.0ºC/min
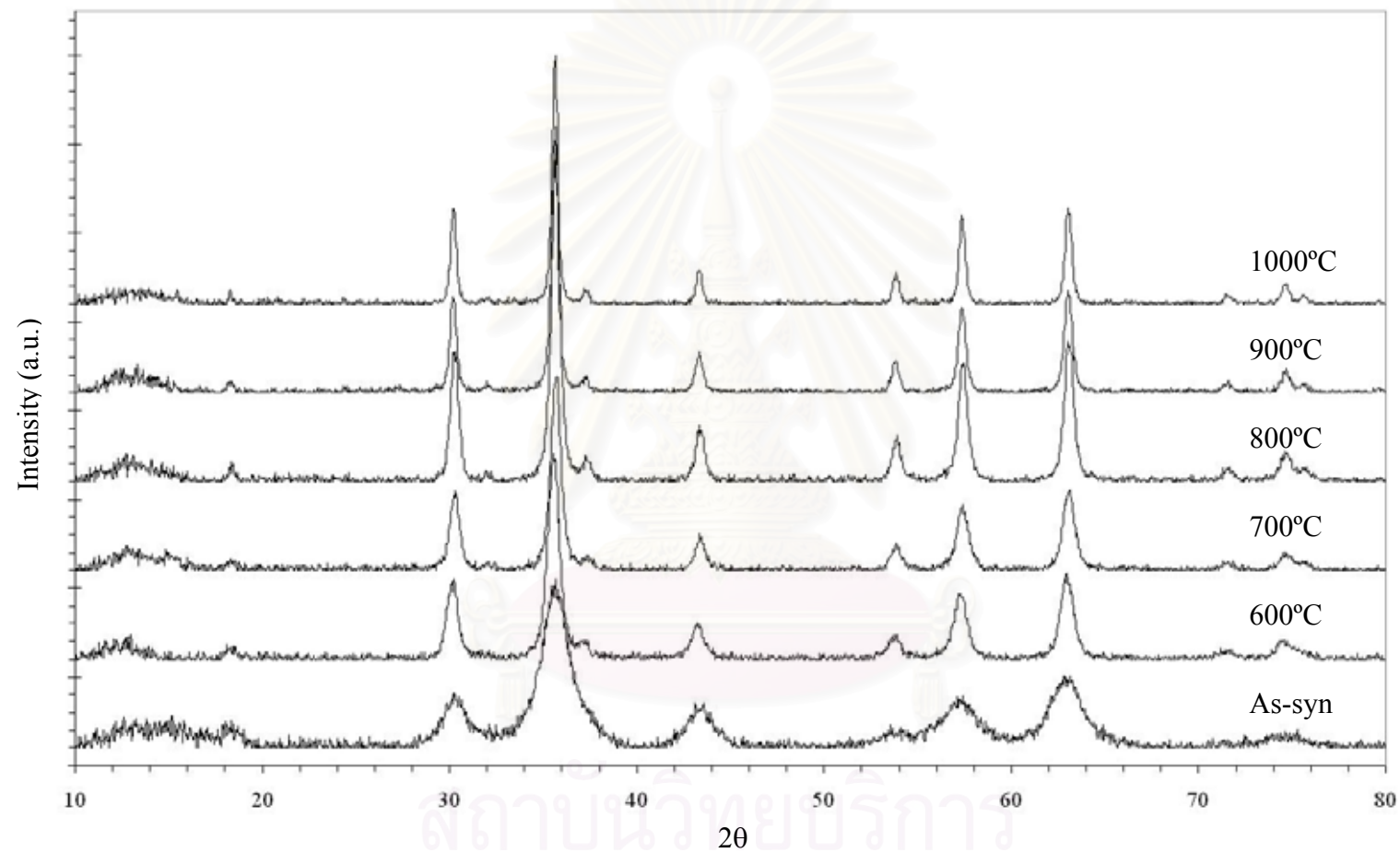
Figure 5.2 The XRD patterns of zinc chromite prepared at reaction heating rate of 2.5ºC/min in 1,4-butanediol and products after calcined at 600, 700, 800, 900 and 1000ºC
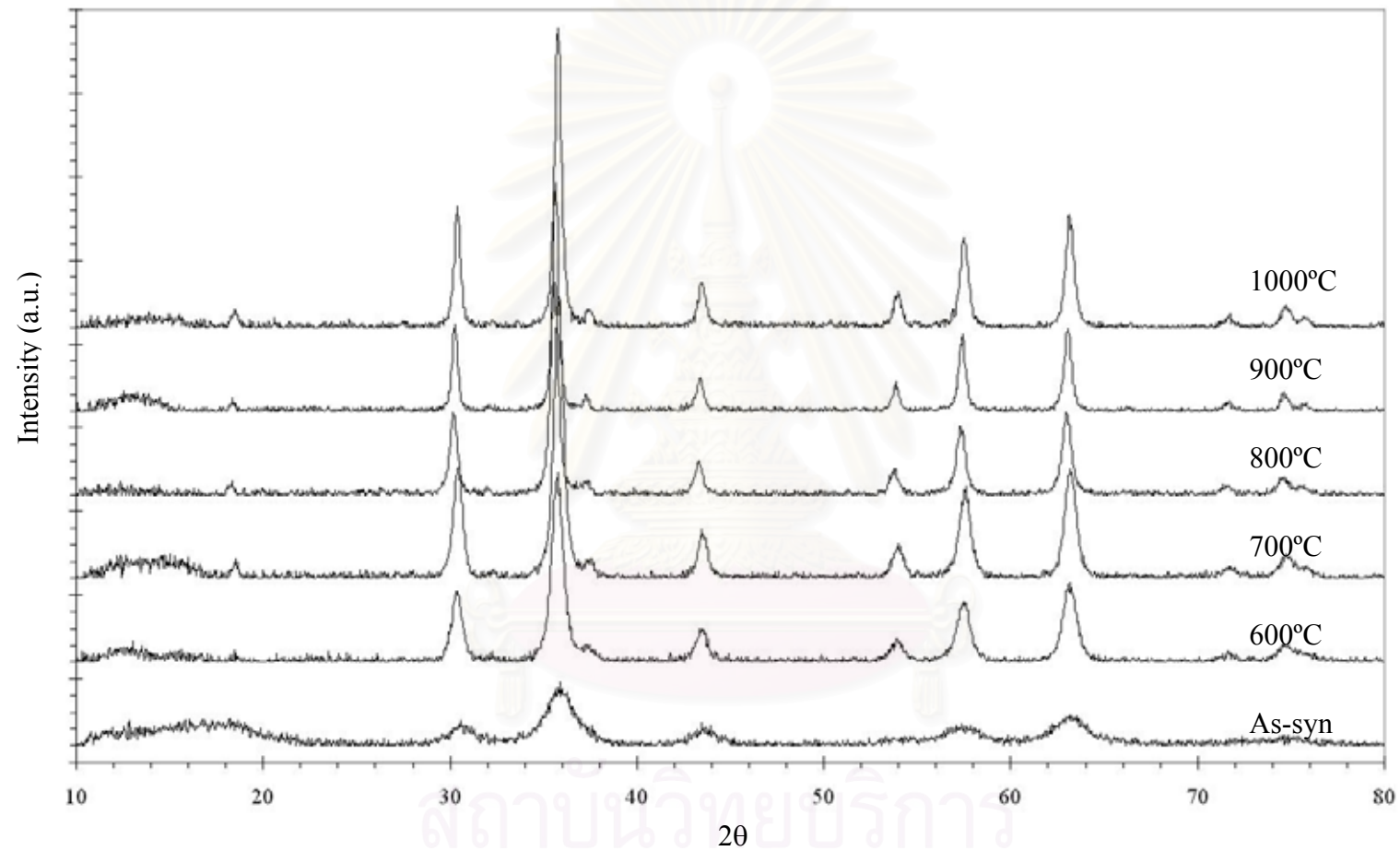
Figure 5.3 The XRD patterns of zinc chromite prepared at reaction heating rate of 1.0ºC/min in 1,4-butanediol and products after calcined at 600, 700, 800, 900 and 1000ºC
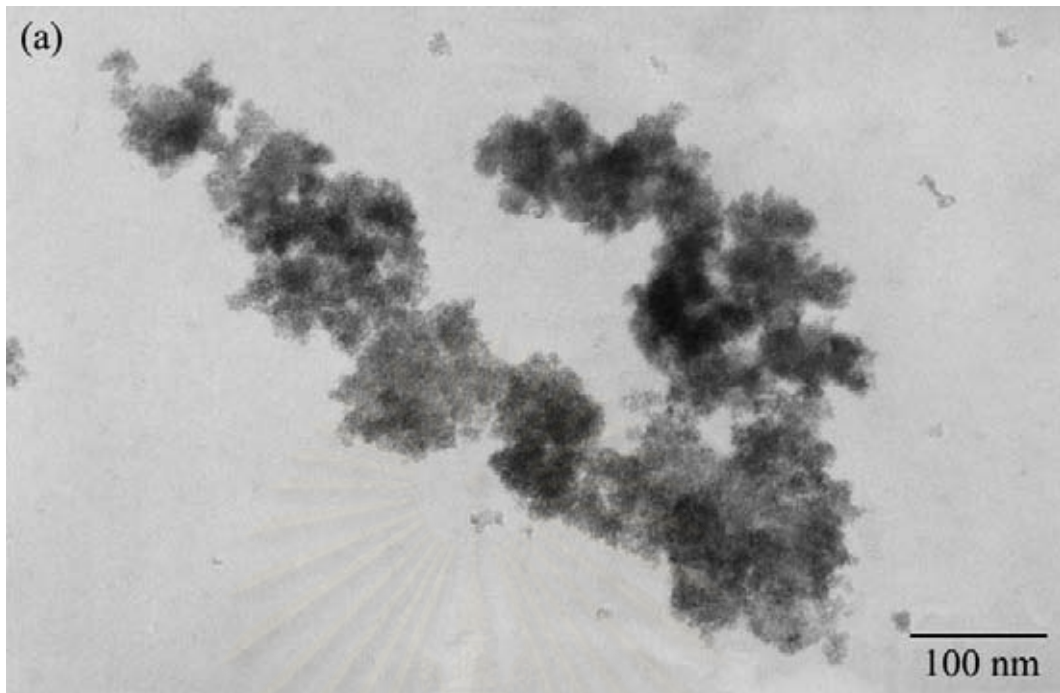
Figure 5.4(a) TEM photograph of the as-synthesized zinc chromite product prepared at reaction heating rate of 2.5ºC/min (x150000)
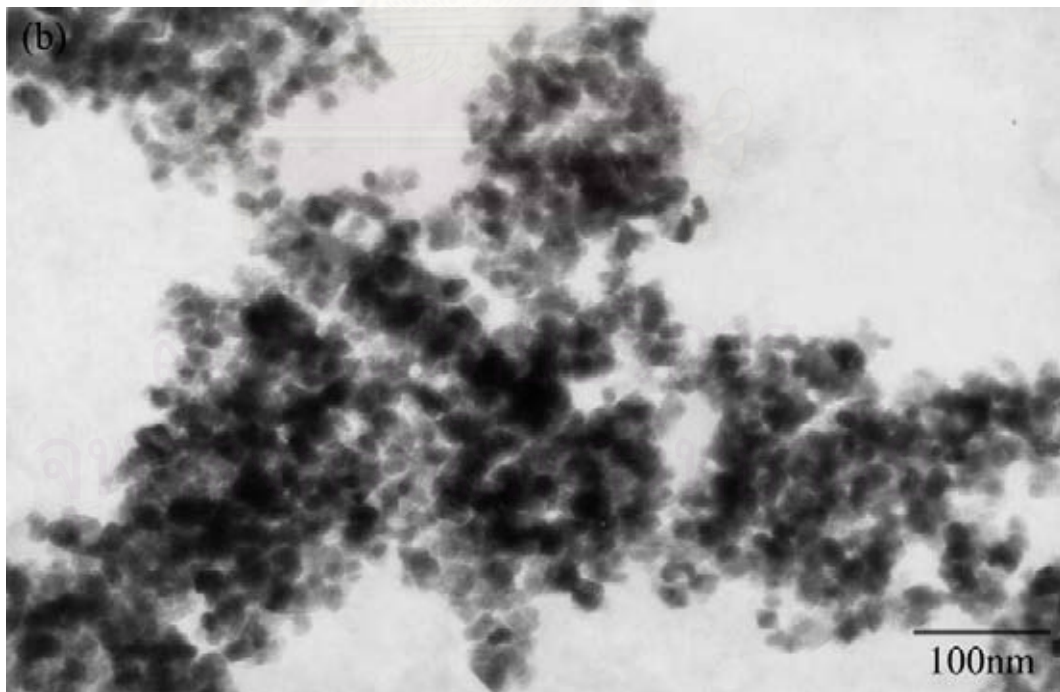
Figure 5.4(b) TEM photograph of the zinc chromite product prepared at reaction heating rate of 2.5ºC/min after calcined at 600ºC (x150000)
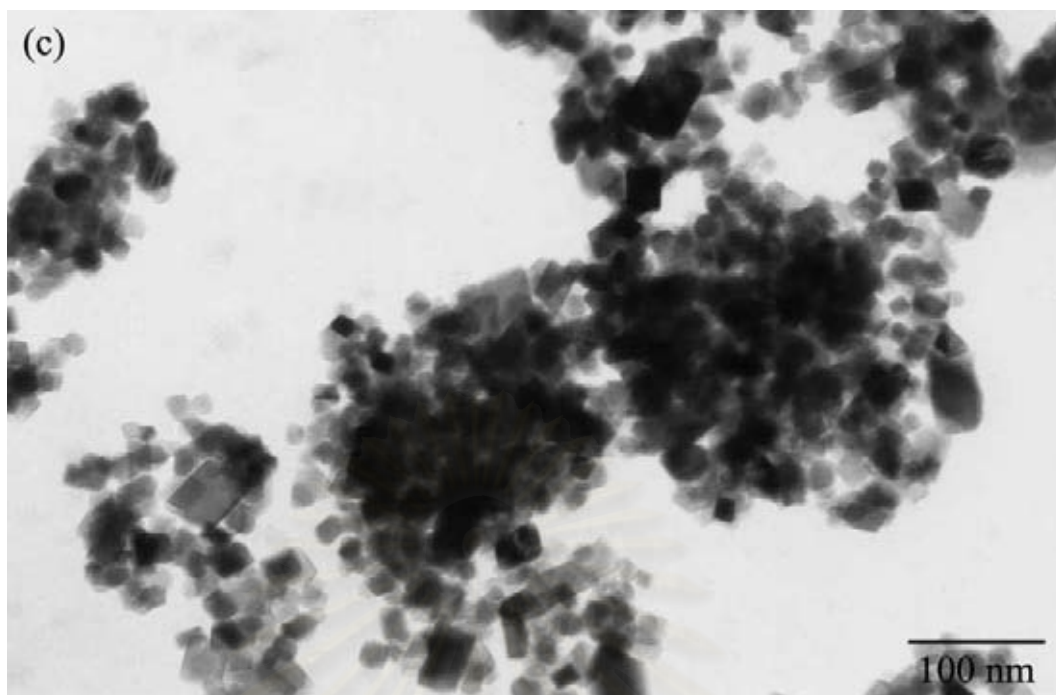
Figure 5.4(c) TEM photograph of the zinc chromite product prepared at reaction heating rate of 2.5ºC/min after calcined at 800ºC (x150000)

Figure 5.4(d) TEM photograph of the zinc chromite product prepared at reaction heating rate of 2.5ºC/min after calcined at 1000ºC (x150000)
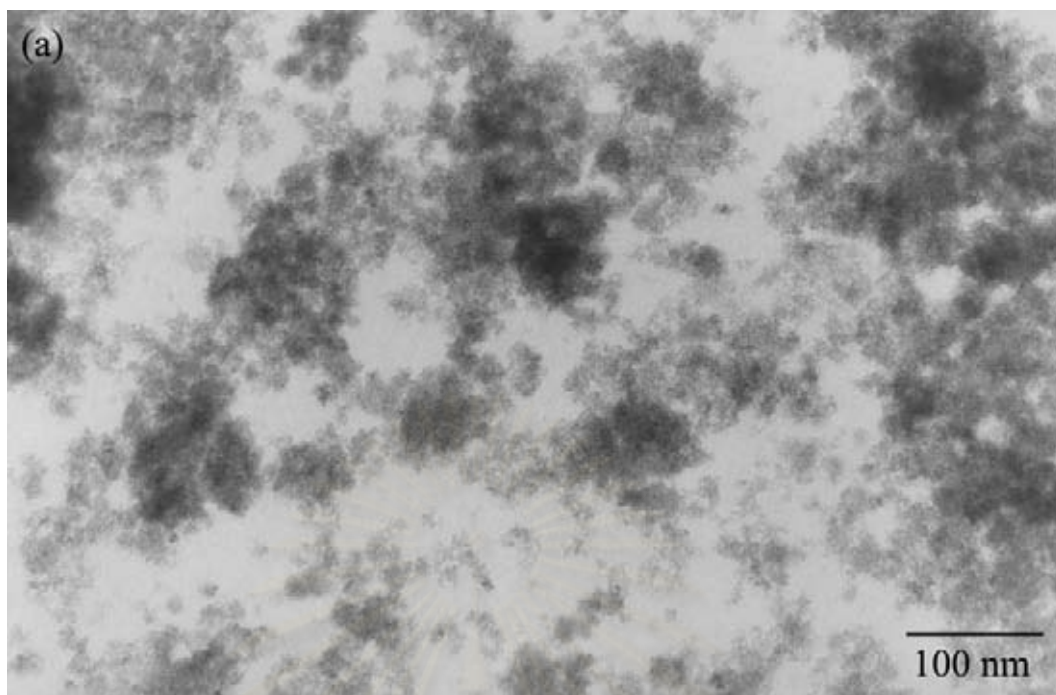
Figure 5.5(a) TEM photograph of the as-synthesized zinc chromite product prepared at reaction heating rate of 1.0ºC/min (x150000)
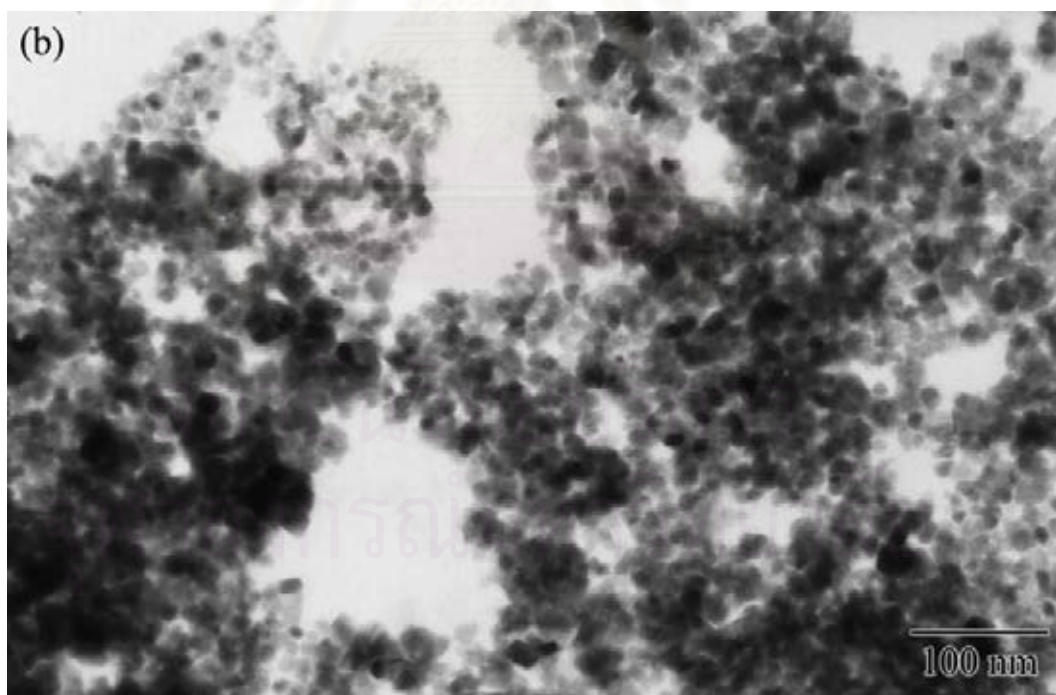
Figure 5.5(b) TEM photograph of the zinc chromite product prepared at reaction heating rate of 1.0ºC/min after calcined at 600ºC (x150000)

Figure 5.5(c) TEM photograph of the zinc chromite product prepared at reaction heating rate of 1.0ºC/min after calcined at 800ºC (x150000)

Figure 5.5(d) TEM photograph of the zinc chromite product prepared at reaction heating rate of 1.0ºC/min after calcined at 1000ºC (x150000)

5.2 Formation of pure zinc manganite

Unlike zinc chromite, both the glycothermal reaction of zinc acetate and manganese (III) acetylacetonate in 1,4-butanediol 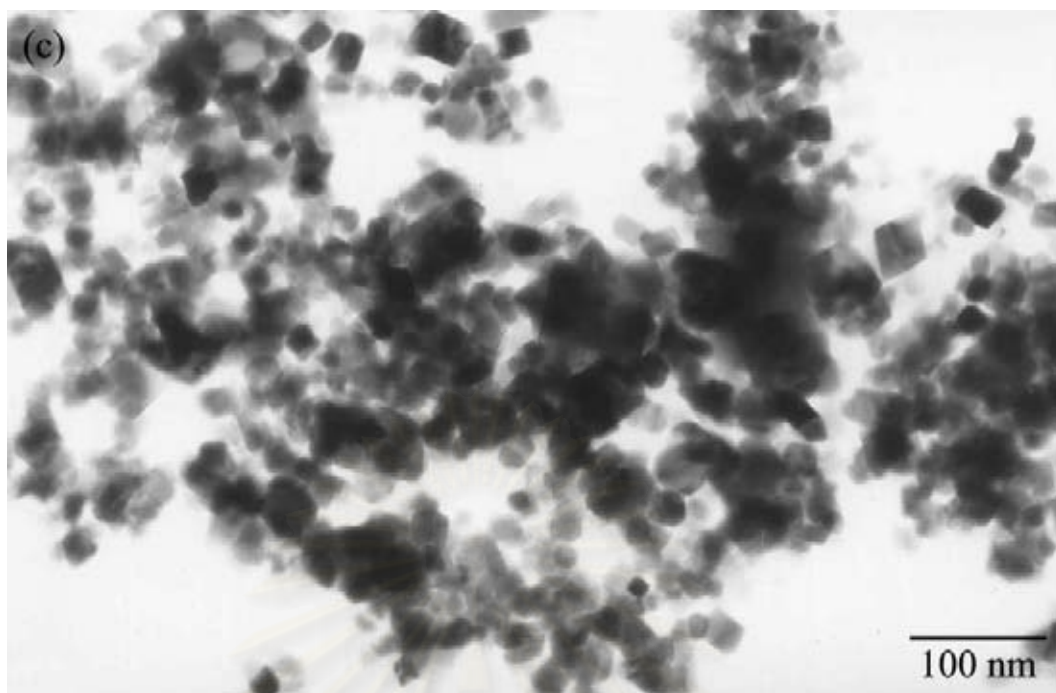at 300ºC under autogeneous pressure with the reaction heating rate of 2.5 and 1.0ºC/min did not yield the spinel zinc manganite. But obtained the product that could not be identified, which assigned to be the undetermined intermediate product (UIP). The XRD patterns of the as-synthesized UIPs are shown in Figure 5.6, compare to the characteristic XRD patterns of zinc manganite. In Figure 5.7, TEM photograph of the UIP, prepared at the reaction heating rate of 2.5ºC/min, is exhibited. By the thermogravimetric analysis method, the thermal decomposition of UIP was studied. From thermogravimetric analysis graph (Figure 5.8), the decomposition of UIP occurs in two stages. The first decomposition occurred at 350 to 360ºC, giving the second intermediate product (Product I). For the second step, the decomposition was completed by 600ºC, yielded the ultimate product (Product II).

From the result of TGA, both the UIPs obtained from glycothermal reaction with reaction heating rate of 2.5 and 1.0ºC/min were calcined at 600ºC to yield the ultimate products. The XRD patterns of the calcined ultimate products show that the zinc manganite spinel phase was formed after calcined without any contaminated phase. (Figure 5.9) [6,7] The products were attributed to be the as-synthesized zinc manganite.

The crystallite size of the products prepared from the reaction heating rate 2.5 and 1.0ºC/min calculated by the Scherrer equation from the XRD broadening were 28.80 and 21.72 nm, respectively. These results are in good agreement with the particle size observed by TEM, which were 28.67 and 22.00 nm, respectively. Therefore, it can be indicated that the product is a single crystal zinc manganite. The BET surface areas of the products were measured. The as-synthesized products had rather small surface area of 20.39 and 23.91 m^2g^{-1}.

Parts of the products were calcined at various temperatures of 700 to 1000ºC The XRD patterns and the BET surface area of the calcined products were investigated. The XRD patterns were almost identical to the as-synthesized products

except that the XRD peaks were sharper, as shown in Figures 5.10 and 5.11. As expected from the XRD patterns, the products still preserved the spinel structure even after calcined at 1000ºC. Figures 5.12(a) to (d) and 5.13(a) to (d) show the TEM photograph of the zinc manganite products before and after calcined at various temperatures. The BET surface area of the products after calcined were shown in Table 5.2, as well as both crystallite sizes and particle size obtained from Scherrer equation and observed by TEM, respectively.

Table 5.2 Crystallite size and BET surface area of the as-synthesized and calcined products zinc manganite prepared at different reaction heating rates, (a) 2.5ºC/min and (b) 1.0ºC/min

Calcination temperature	$d_{XRD}^{(1)}$, nm		$d_{TEM}^{(2)}$, nm		$S_{BET}^{(3)}$, m^{2}g^{-1}	
	(a)	(b)	(a)	(b)	(a)	(b)
As-syn	28.80	21.72	28.67	22.00	20.39	23.91
700ºC	35.05	25.10	34.67	25.33	10.95	11.02
800ºC	40.34	34.44	40.00	34.67	9.58	9.70
900ºC	45.73	36.13	46.00	36.00	7.13	5.70
1000ºC	55.01	49.33	54.67	49.33	4.44	4.57

[1] Crystallite size of the products estimated by the Scherrer equation

[2] Particle size of the products observed from TEM

[3] Specific surface area of the products estimated by BET single point method
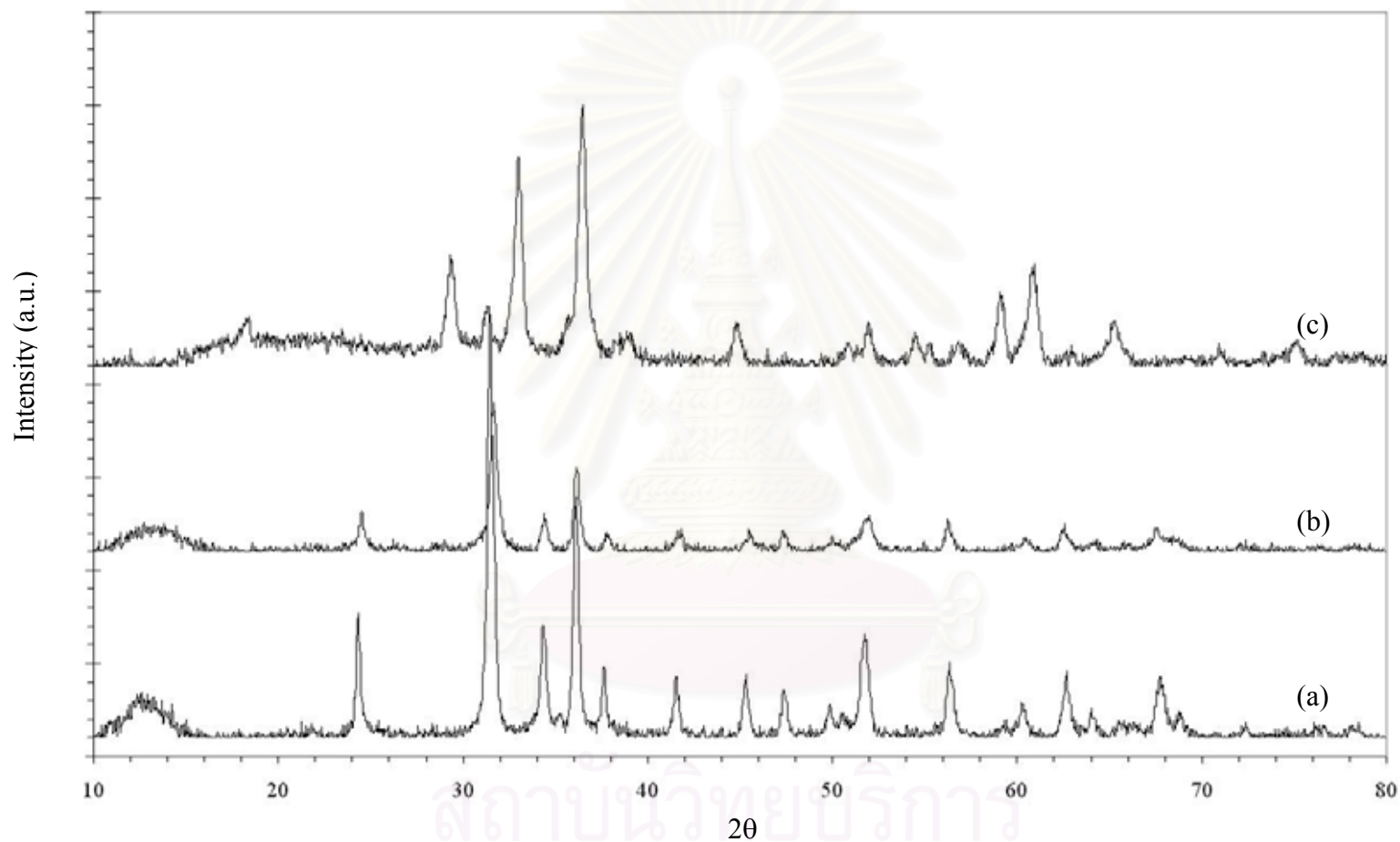
Figure 5.6 The XRD patterns of the undetermined intermediate product prepared at different reaction heating rates, (a) 2.5ºC/min and (b) 1.0ºC/min, compare to the characteristic XRD patterns of (c) zinc manganite

Figure 5.7 TEM photograph of the undetermined intermediate product prepared at reaction heating rate of 2.5ºC/min (x150000)
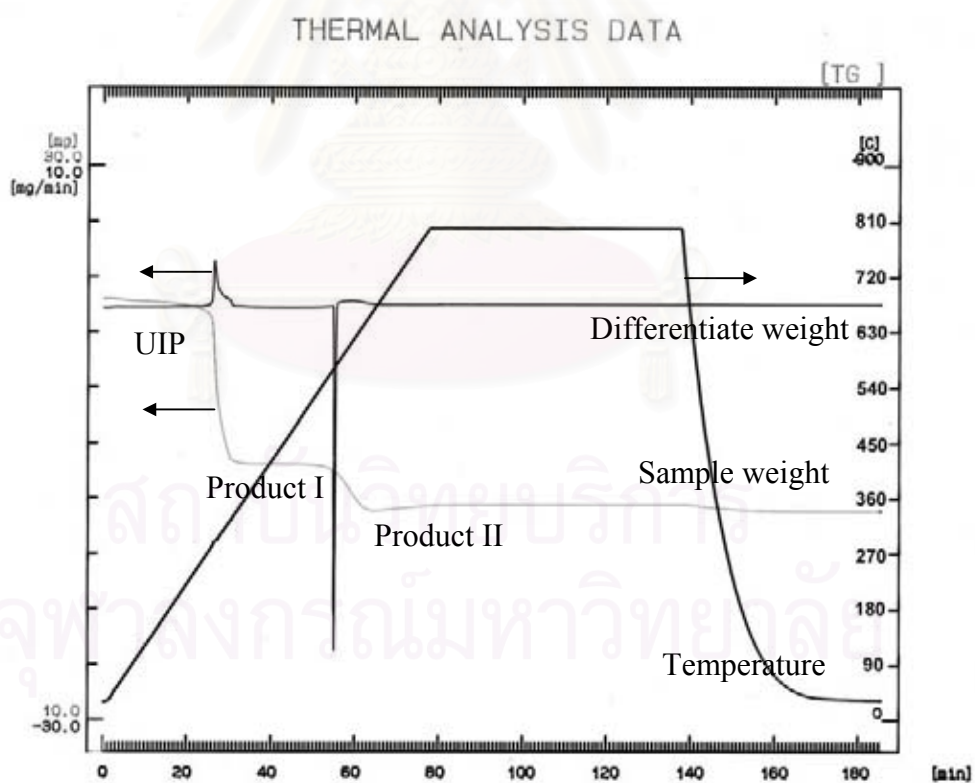
Figure 5.8 The thermogravimetric graph of the undetermined intermediate product obtained from glycothermal reaction of zinc acetate and manganese (III) acetylacetonate at reaction heating rate 2.5ºC/min
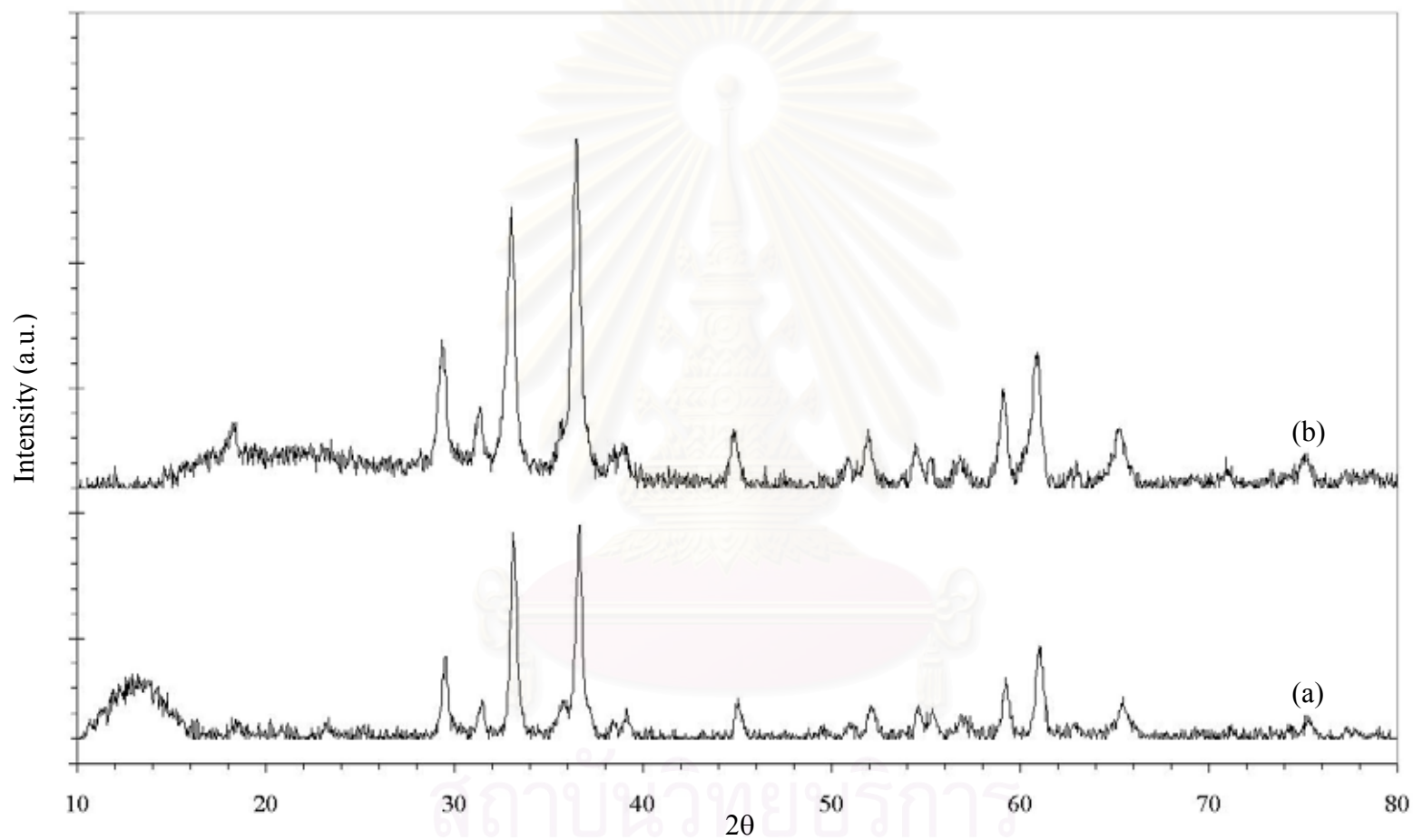
Figure 5.9 The XRD patterns of the as-synthesized zinc manganite prepared at different reaction heating rates, (a) 2.5ºC/min and (b) 1.0ºC/min
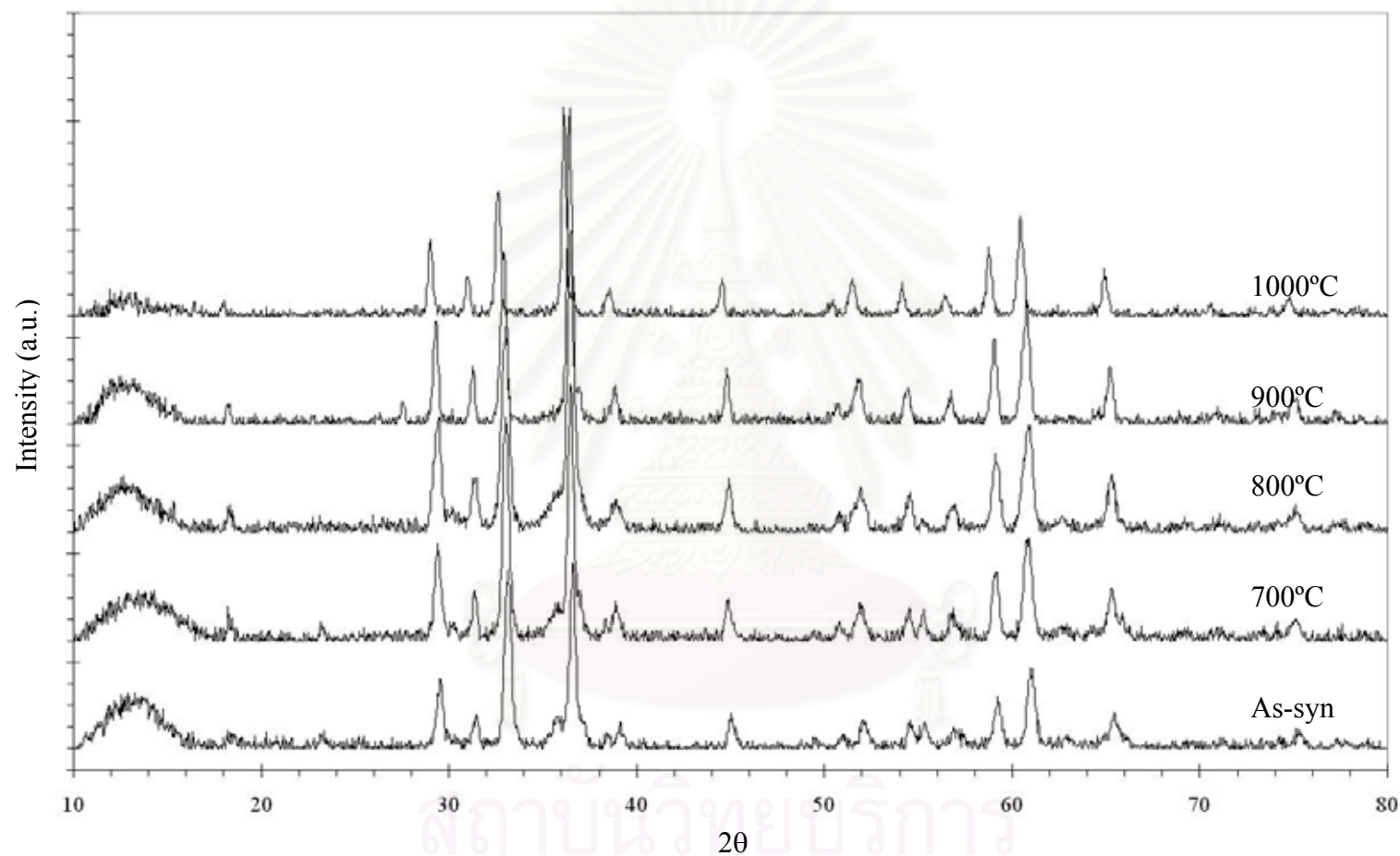
Figure 5.10 The XRD patterns of zinc manganite prepared at reaction heating rate of 2.5ºC/min in 1,4-butanediol and products after calcined at 700, 800, 900 and 1000ºC
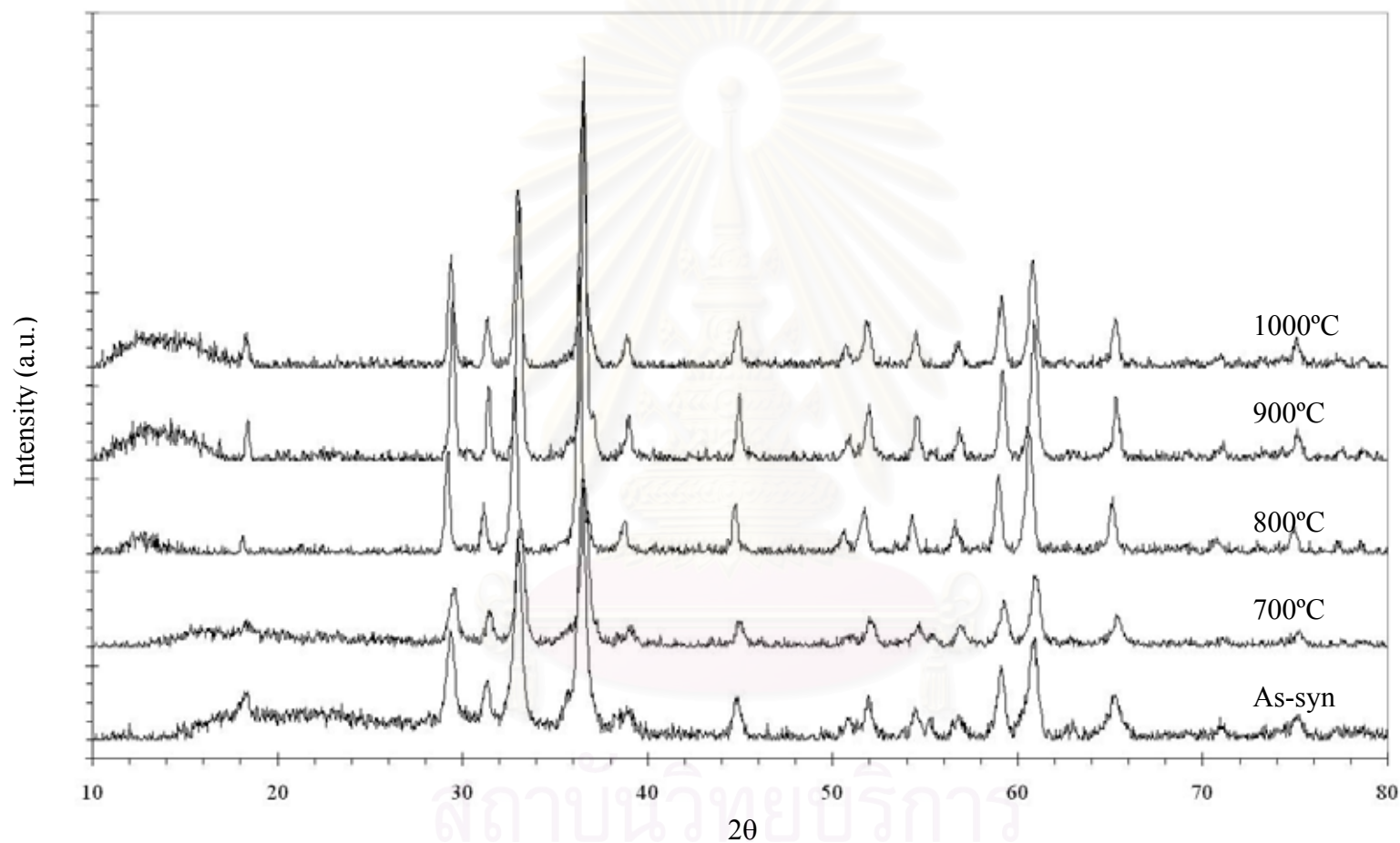
Figure 5.11 The XRD patterns of zinc manganite prepared at reaction heating rate of 1.0ºC/min in 1,4-butanediol and products after calcined at 700, 800, 900 and 1000ºC
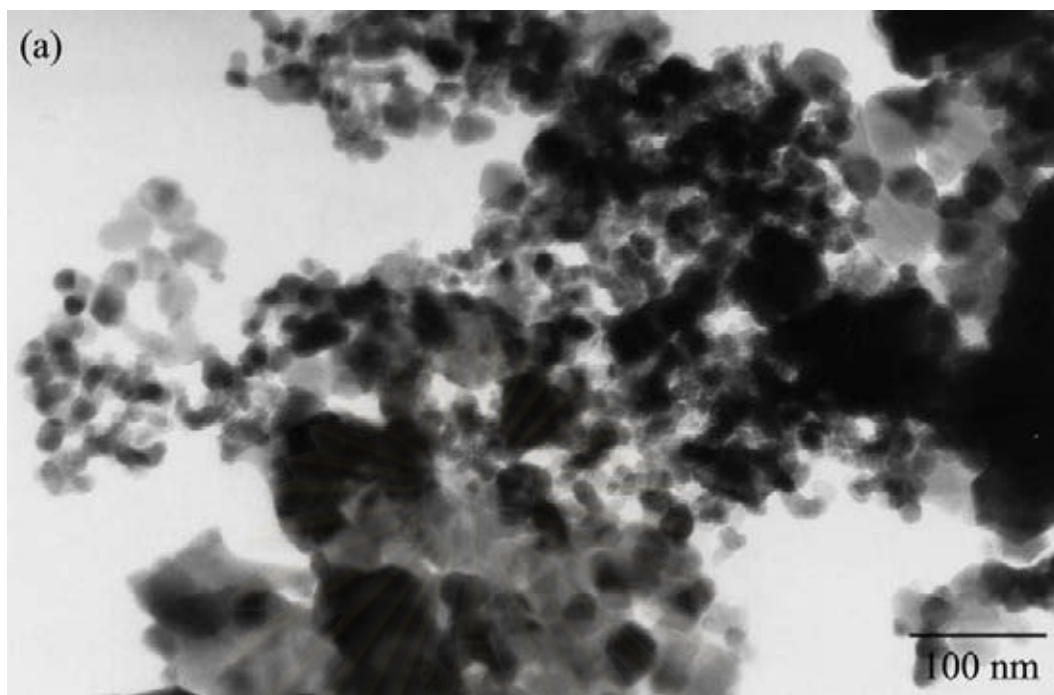
Figure 5.12(a) TEM photograph of the as-synthesized zinc manganite product prepared at reaction heating rate of 2.5ºC/min (x150000)
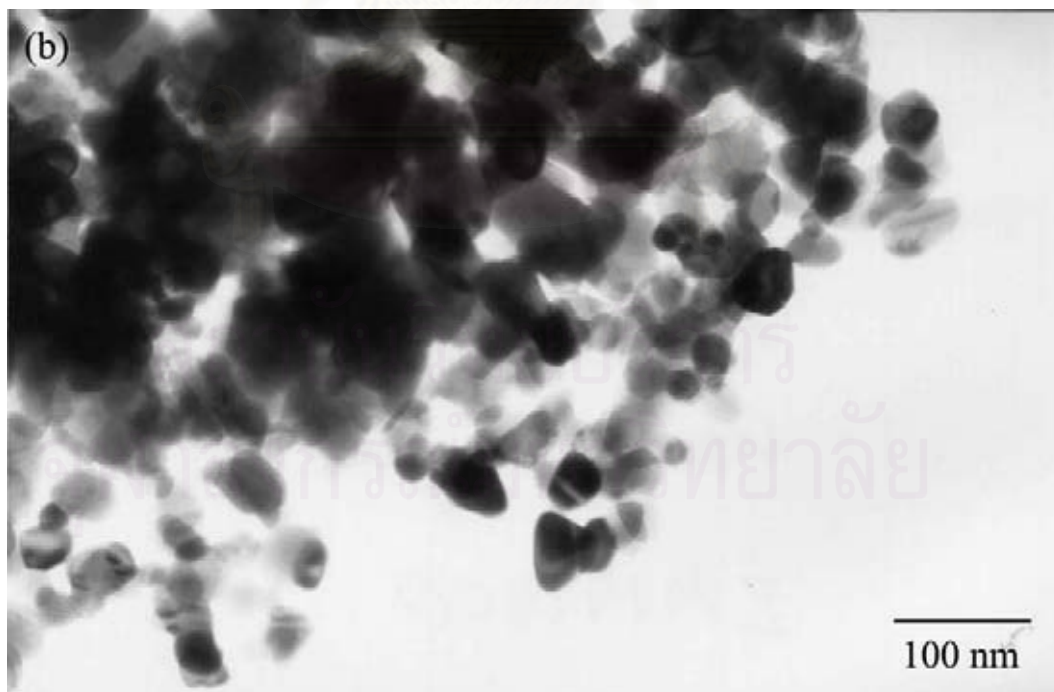
Figure 5.12(b) TEM photograph of the zinc manganite product prepared at reaction heating rate of 2.5ºC/min after calcined at 800ºC (x150000)
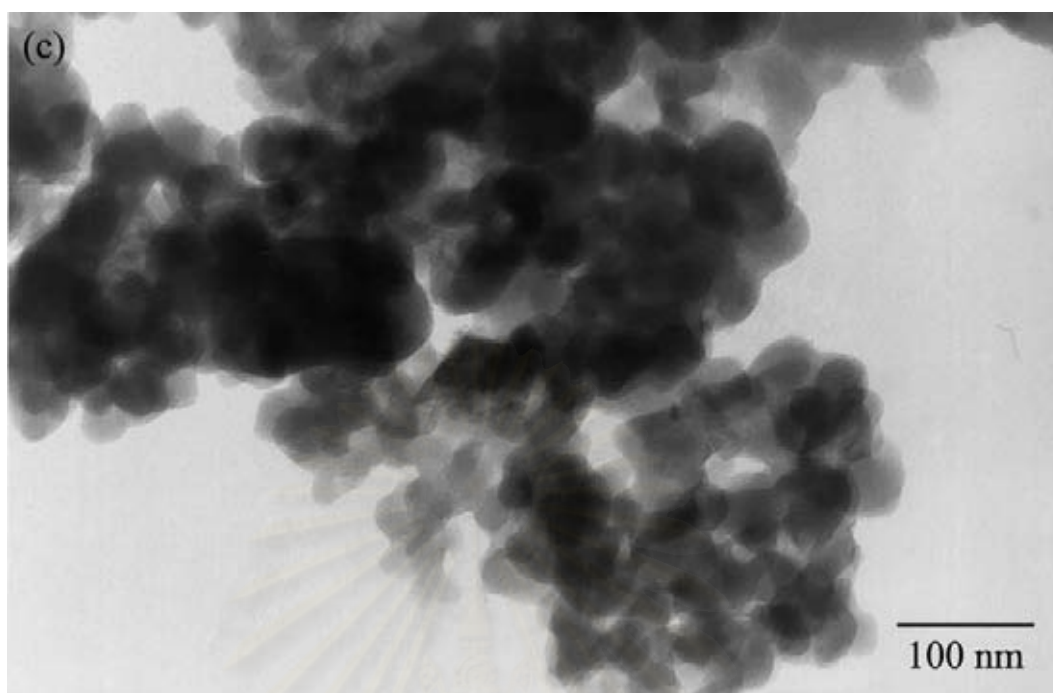
Figure 5.12(c) TEM photograph of the zinc manganite product prepared at reaction heating rate of 2.5ºC/min after calcined at 1000ºC (x150000)
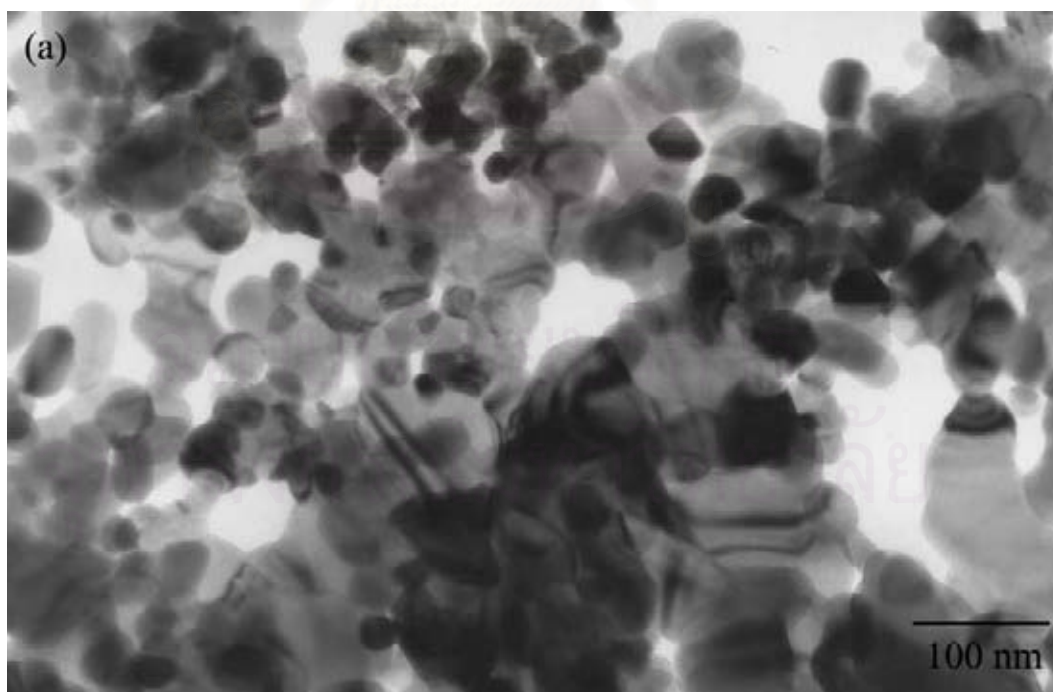
Figure 5.13(a) TEM photograph of the as-synthesized zinc manganite product prepared at reaction heating rate of 1.0ºC/min (x150000)
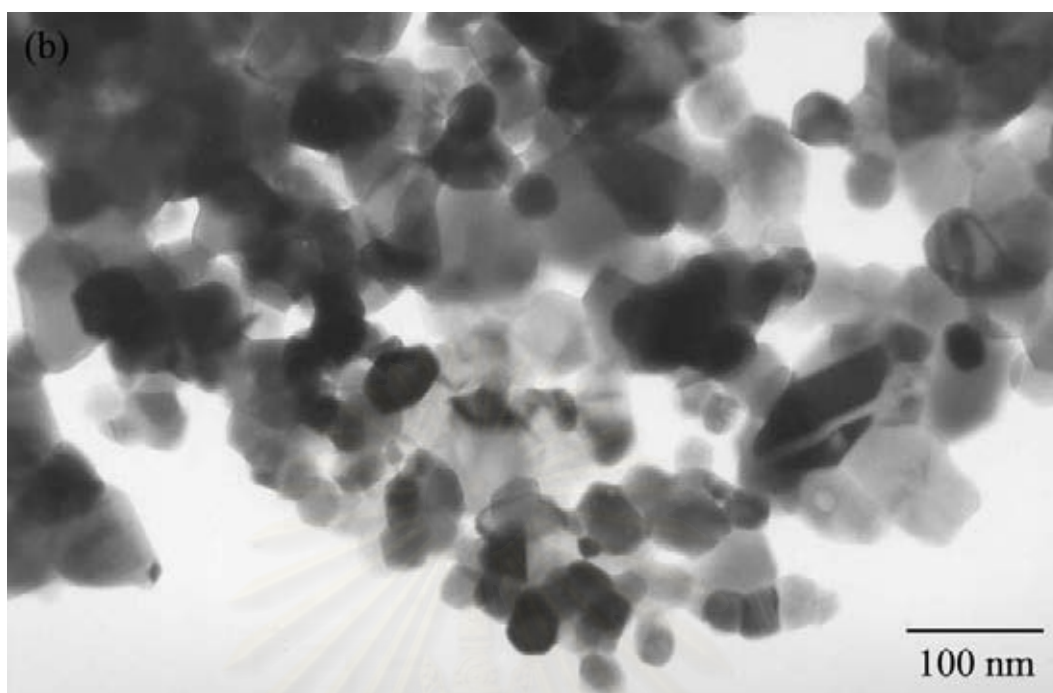
Figure 5.13(b) TEM photograph of the zinc manganite product prepared at reaction heating rate of 1.0ºC/min after calcined at 800ºC (x150000)
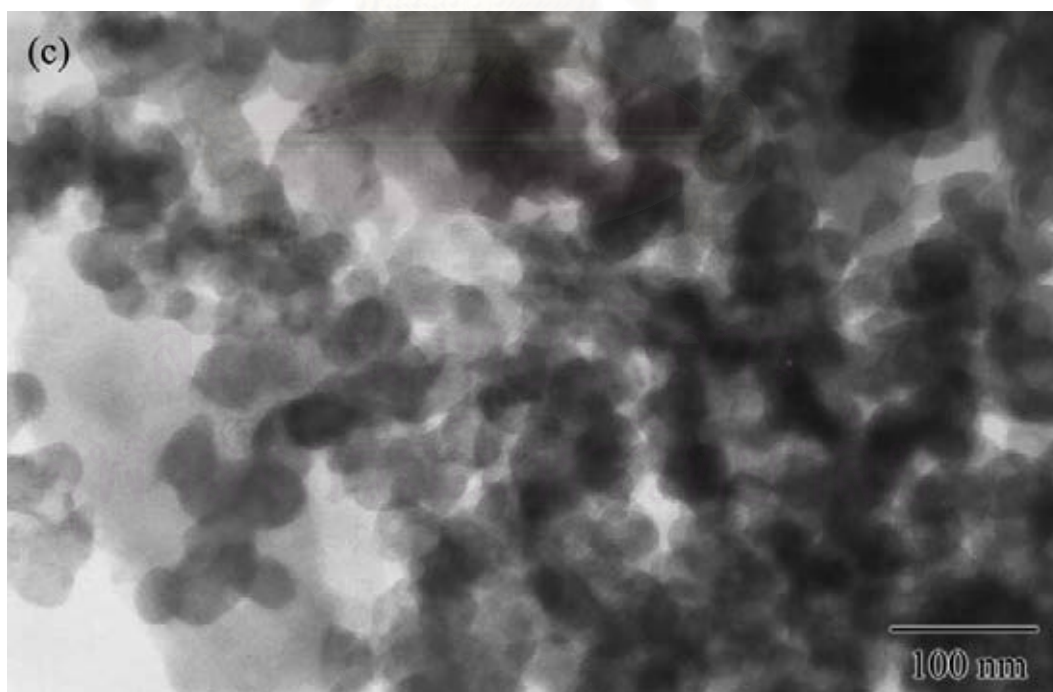
Figure 5.13(c) TEM photograph of the zinc manganite product prepared at reaction heating rate of 1.0ºC/min after calcined at 1000ºC (x150000)

5.3 Formation of pure zinc ferrite

The glycothermal reaction of zinc acetate and iron (III) acetylacetonate, as the same conditions of preparing zinc chromite, directly yielded nanocrystalline zinc ferrite. The XRD patterns of the as-synthesized products obtained from the reaction at 300ºC with the reaction heating rates of 2.5 and 1.0ºC/min were shown in Figure 5.14. It had been found that the products exhibited the completely similar XRD characteristic peaks to the normal spinel phase. [10] The crystallite sizes calculated by Scherrer equation from the XRD broadening of products at the reaction heating rate 2.5 and 1.0ºC/min were 31.40 and 35.01 nm, respectively. The average particle size determine from TEM photographs of the products were 31.67 and 35.00 nm, which are in good agreement with the XRD crystallite sizes. Indicating that the as-synthesized products of zinc ferrite were single crystal of spinel. The BET surface area of the as-synthesized products at the reaction heating rate of 2.5 and 1.0ºC/min were 21.45 and 20.49 m^2g^{-1}, respectively.

The as-synthesized zinc ferrites were calcined at various temperatures from 600 up to 1000ºC. The XRD patterns and the BET surface areas of the products after calcined were investigated as shown in Figure 5.15 and 5.16. Both the XRD patterns of the calcined products were almost identical to the pattern of the as-synthesized products except the sharper peaks. As expected from the patterns, the products still preserved the spinel structure even after calcined at high temperature of 1000ºC.

The BET surface area and the crystallite sizes calculated from XRD broadening and the particle sizes observed by TEM were shown in Table 5.3. The TEM photographs of the as-synthesized zinc ferrites and calcined products at 600, 800 and 1000ºC were shown in Figures 5.17(a) to (d) for the products prepared at reaction heating rate of 2.5ºC/min while Figures 5.18(a) to (d) for the reaction heating rate of 1.0ºC/min.

Table 5.3 Crystallite size and BET surface area of the as-synthesized and calcined products zinc ferrite prepared at different reaction heating rates, (a) 2.5ºC/min and (b) 1.0ºC/min

| Calcination temperature	$d_{XRD}^{(1)}$, nm		$d_{TEM}^{(2)}$, nm		$S_{BET}^{(3)}$, m^{2}g^{-1}	
	(a)	(b)	(a)	(b)	(a)	(b)
As-syn	31.40	35.01	31.67	35.00	21.45	21.12
600ºC	35.54	42.47	36.00	42.67	11.03	11.15
700ºC	44.28	48.28	44.67	48.00	4.44	4.47
800ºC	45.80	53.05	46.00	53.33	2.78	2.69
900ºC	50.91	77.78	50.67	78.00	2.11	2.15
1000ºC	102.51	104.93	102.67	105.33	0.90	0.86

[1] Crystallite size of the products estimated by the Scherrer equation

[2] Particle size of the products observed by TEM

[3] Specific surface area of the products estimated by BET single point method
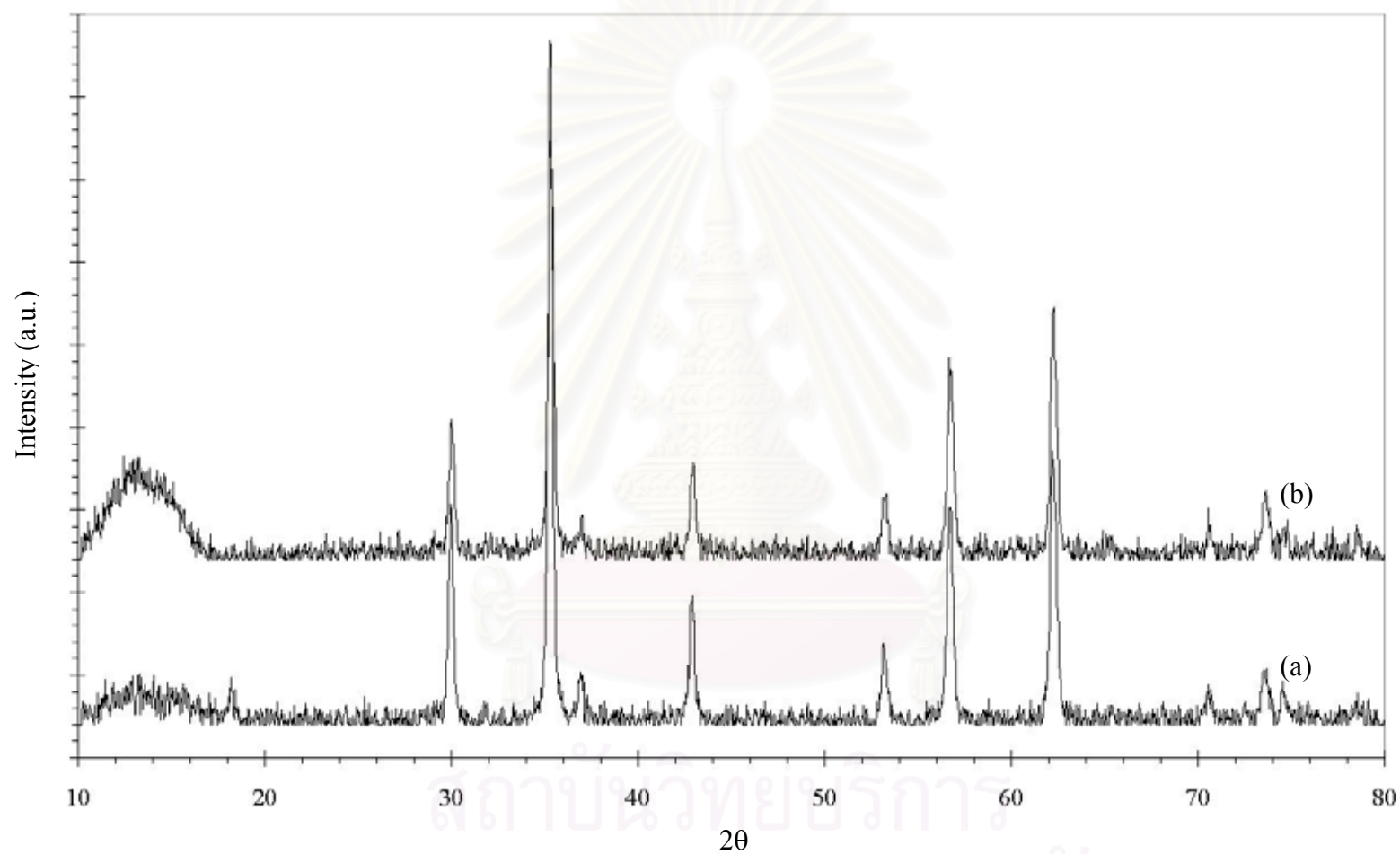
Figure 5.14 The XRD patterns of the as-synthesized zinc ferrite prepared at different reaction heating rates, (a) 2.5ºC/min and (b) 1.0ºC/min
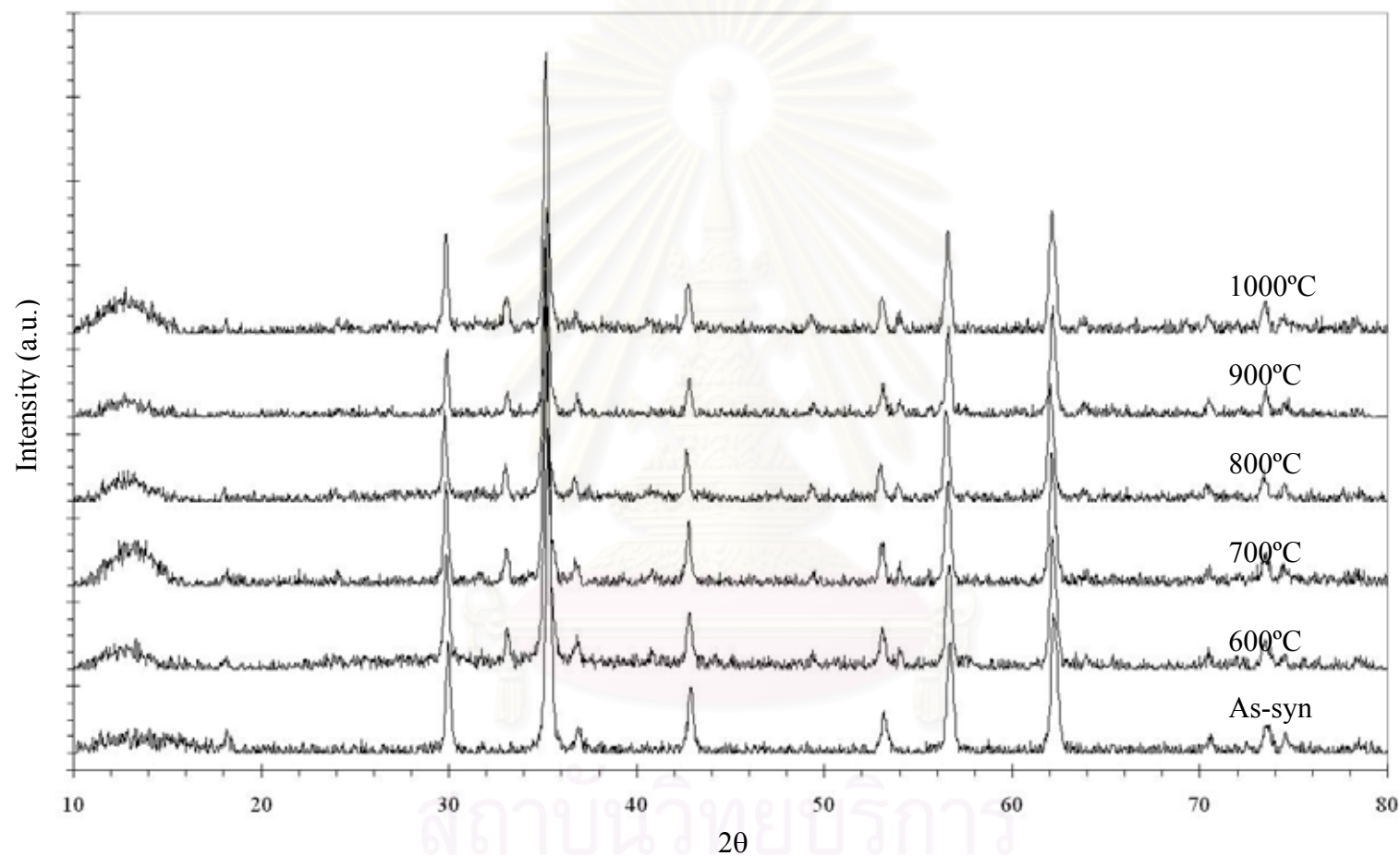
Figure 5.15 The XRD patterns of zinc ferrite prepared at reaction heating rate of 2.5ºC/min in 1,4-butanediol and products after calcined at 600, 700, 800, 900 and 1000ºC
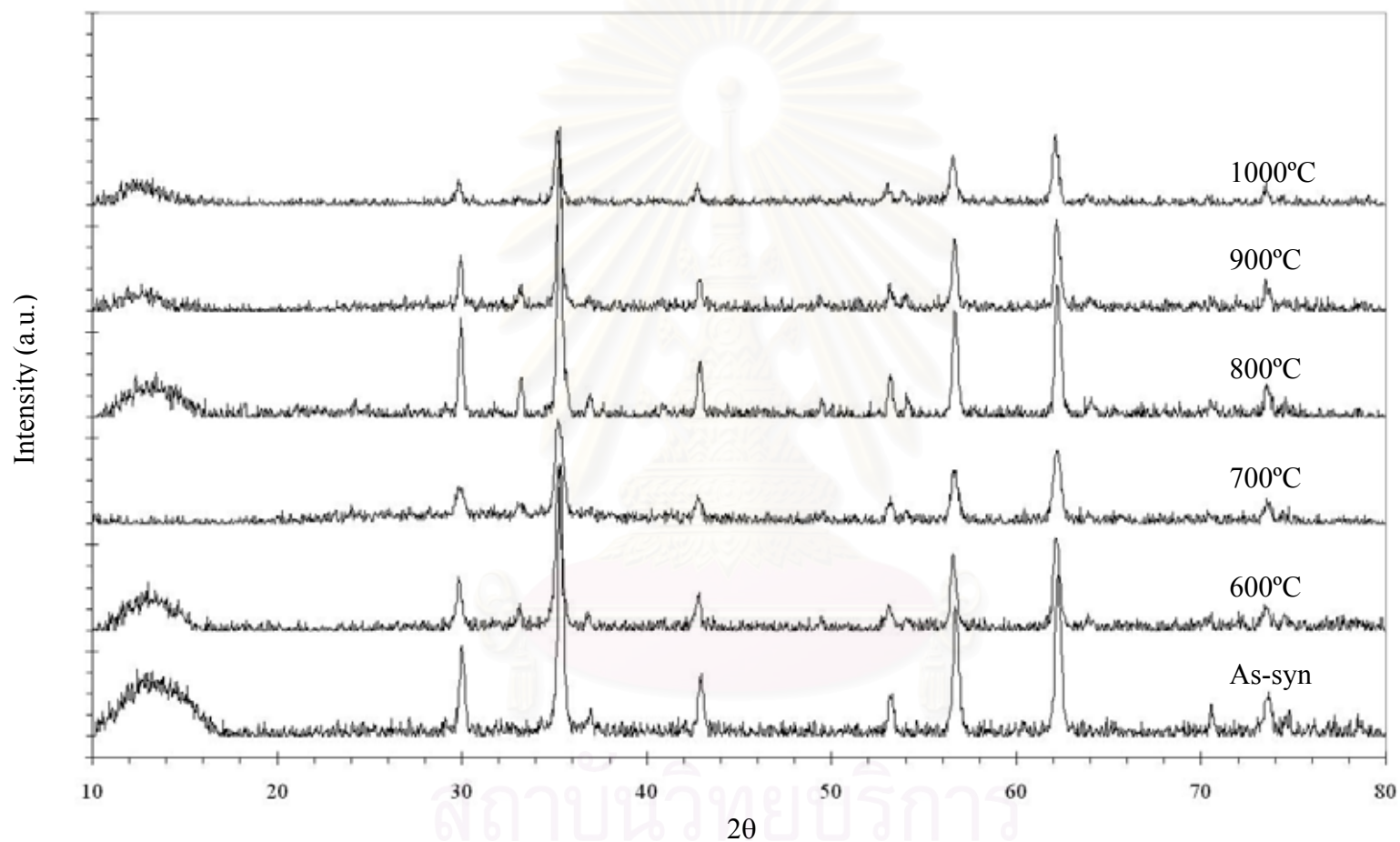
Figure 5.16 The XRD patterns of zinc ferrite prepared at reaction heating rate of 1.0ºC/min in 1,4-butanediol and products after calcined at 600, 700, 800, 900 and 1000ºC
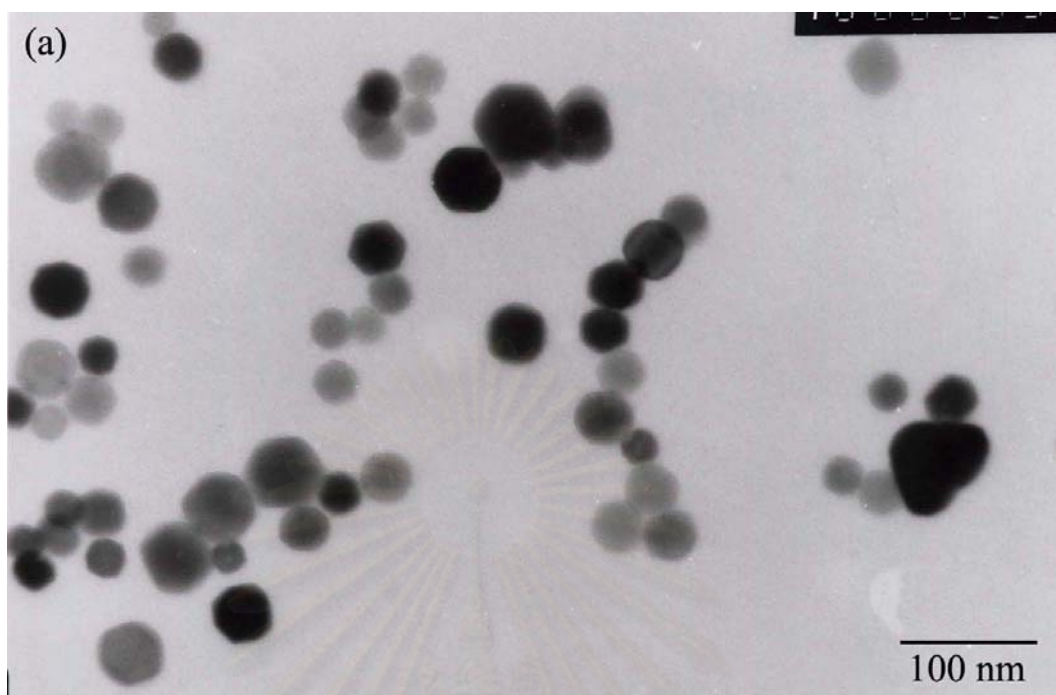
Figure 5.17(a) TEM photograph of the as-synthesized zinc ferrite product prepared at reaction heating rate of 2.5ºC/min (x150000)

Figure 5.17(b) TEM photograph of the zinc ferrite product prepared at reaction heating rate of 2.5ºC/min after calcined at 600ºC (x150000)
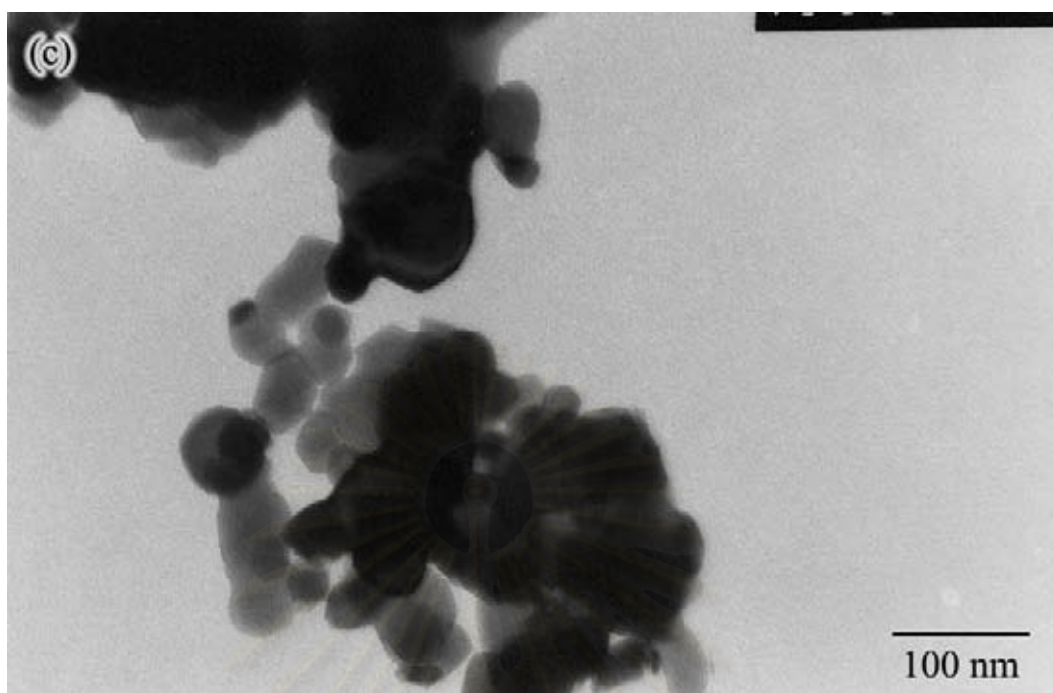
Figure 5.17(c) TEM photograph of the zinc ferrite product prepared at reaction heating rate of 2.5ºC/min after calcined at 800ºC (x150000)
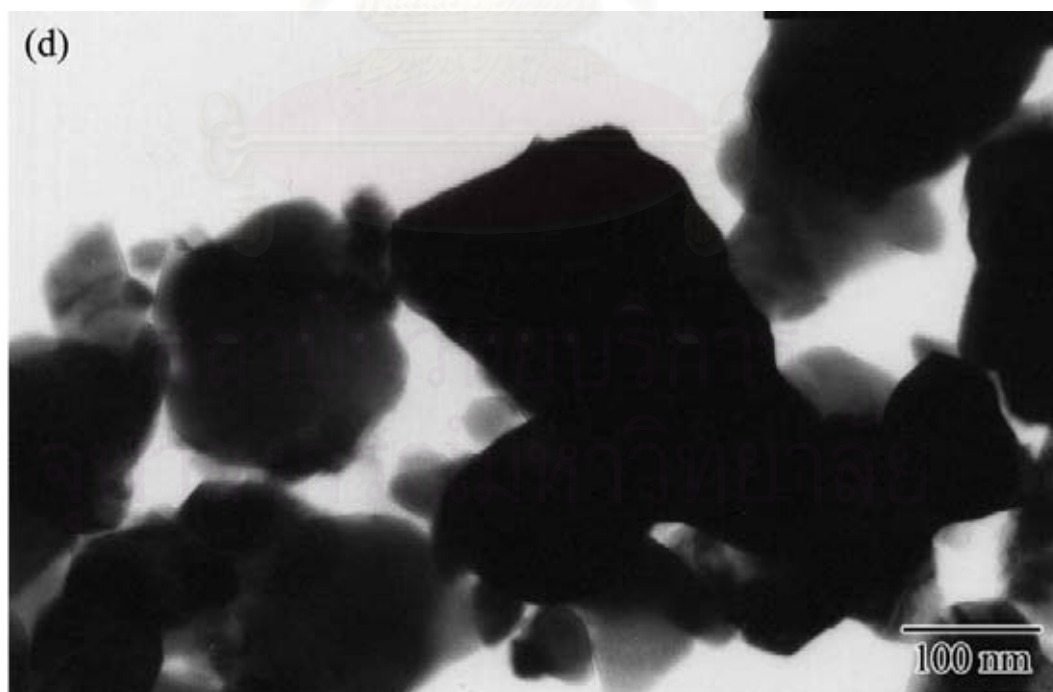
Figure 5.17(d) TEM photograph of the zinc ferrite product prepared at reaction heating rate of 2.5ºC/min after calcined at 1000ºC (x150000)
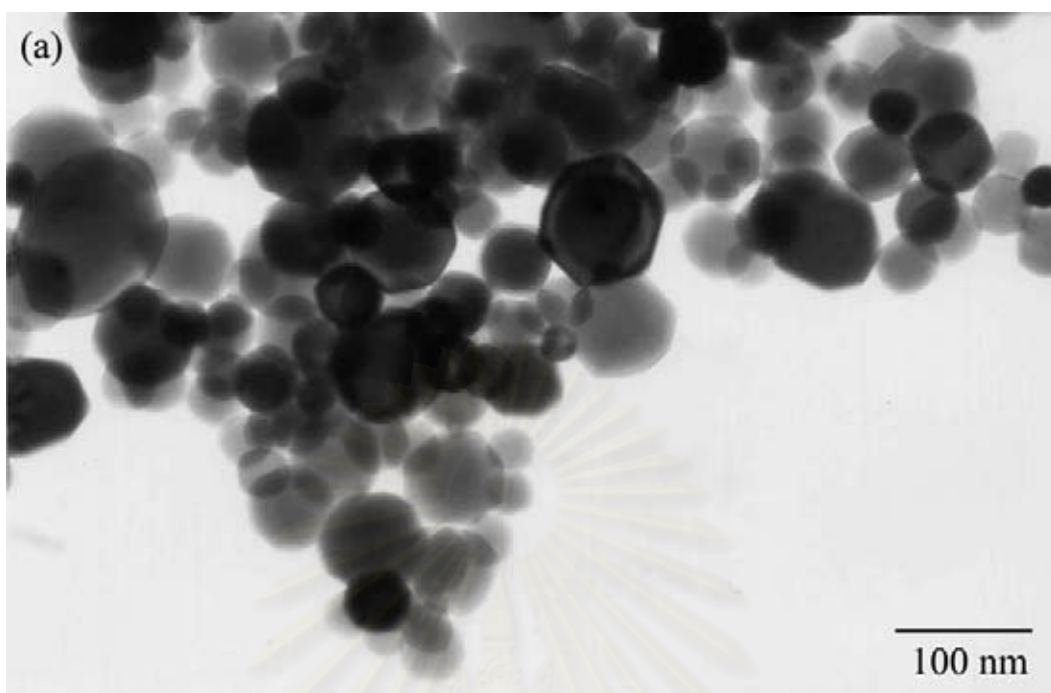
Figure 5.18(a) TEM photograph of the as-synthesized zinc ferrite product prepared at reaction heating rate of 1.0ºC/min (x150000)
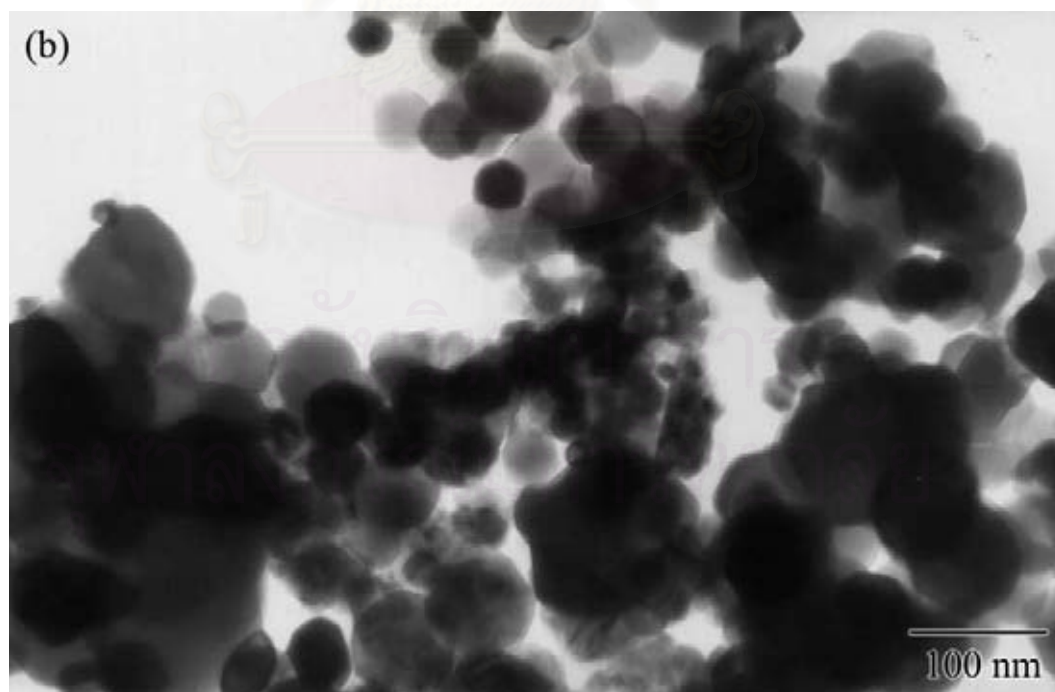
Figure 5.18(b) TEM photograph of the zinc ferrite product prepared at reaction heating rate of 1.0ºC/min after calcined at 600ºC (x150000)
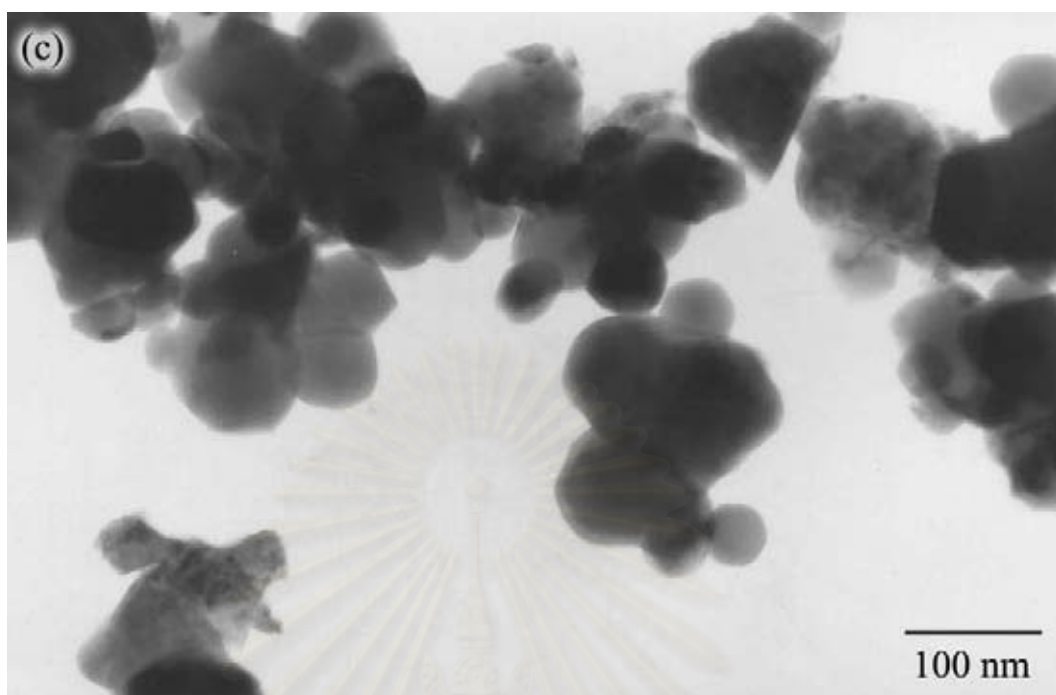
Figure 5.18(c) TEM photograph of the zinc ferrite product prepared at reaction heating rate of 1.0ºC/min after calcined at 800ºC (x150000)
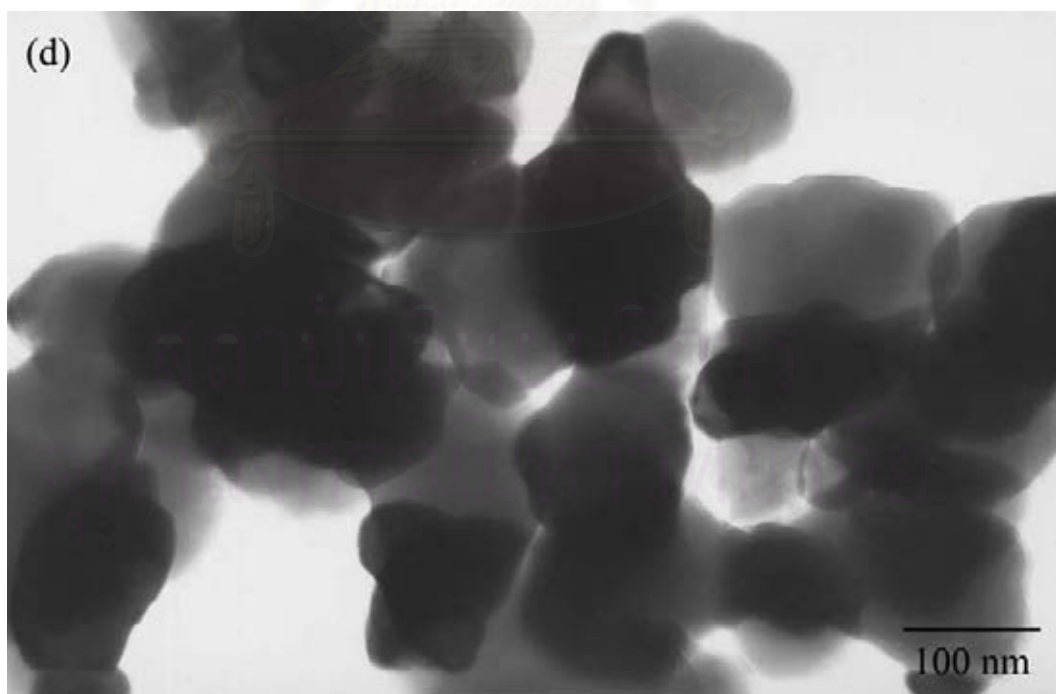
Figure 5.18(d) TEM photograph of the zinc ferrite product prepared at reaction heating rate of 1.0ºC/min after calcined at 1000ºC (x150000)

5.4 Formation of pure zinc cobaltite

Similar to zinc manganite, both the glycothermal reaction of zinc acetate with cobalt (III) acetylacetonate at reaction heating rate 2.5 and 1.0ºC/min gave the undetermined intermediate products (UIPs). The XRD patterns of the as-synthesized products prepared in 1,4-butanediol at 300ºC under autogeneous pressure with different reaction heating rate of 2.5 and 1.0ºC/min are shown in Figure 5.19, compare to the characteristic XRD atterns of zinc cobaltite. Thermogravimetric analysis method was used to investigate the thermal decomposition of the UIP obtained from glycothermal reaction at reaction heating rate 2.5ºC/min. The temperature was heated from room temperature, with the heating rate of 10ºC/min, up to 600ºC and held at that temperature for 1 hour. The TGA graph was shown in Figure 5.21. The decomposition of UIP occurs in two connecting stages. The first step was at 210ºC and connected by the second step, 280ºC, to yield the ultimate product completely at the temperature 450ºC.

From the result of TGA, the obtained UIPs from glycothermal reaction with different reaction heating rate of 2.5 and 1.0ºC/min were calcined at 450ºC to yield the ultimate products. The XRD patterns of the calcined ultimate products show that the zinc manganite spinel phase was formed after calcined without any contaminated phase that may ascribe as ZnO or Co_2O_3. [13] The products were attributed to be the as-synthesized zinc cobaltite.

The crystallite size of the products from the reaction heating rate 2.5 and 1.0ºC/min calculated by the Scherrer equation from the XRD broadening were 29.26 and 27.24 nm, respectively. After observed by TEM, these results are in good agreement with the particle size, which were 29.33 and 26.67 nm. Therefore, it can be indicated that the product is a single crystal zinc cobaltite. The BET surface areas of the products were measured, which were 5.36 and 6.21 m^2g^{-1}, respectively.

The products were calcined at various temperatures of 600 up to 1000ºC The XRD patterns and the BET surface areas of the calcined products were investigated. The XRD patterns were almost identical to the as-synthesized products except that the XRD peaks were sharper. As expected from the patterns of the products that still

preserved the spinel structure even after calcined at 1000ºC. The BET surface area of the products after calcined were shown in Table 5.4, as well as both crystallite sizes obtained from Scherrer equation and the particle sizes observed by TEM.

Table 5.4 Crystallite size and BET surface area of the as-synthesized and calcined products zinc cobaltite prepared at different reaction heating rates, (a) 2.5ºC/min and (b) 1.0ºC/min

Calcination temperature	d_{XRD}[1], nm		d_{TEM}[2], nm		S_{BET}[3], m^2g^{-1}	
	(a)	(b)	(a)	(b)	(a)	(b)
As-syn	29.26	27.24	29.33	26.67	5.36	6.21
600ºC	33.58	33.65	34.00	33.33	4.63	4.62
700ºC	56.29	53.83	56.00	54.00	2.74	2.94
800ºC	75.02	75.52	75.33	76.00	2.31	2.47
900ºC	75.84	80.65	76.00	80.67	1.40	1.80
1000ºC	99.18	103.28	100.00	104.00	0.95	0.89

[1] Crystallite size of the products estimated by the Scherrer equation

[2] Particle size of the products observed from TEM

[3] Specific surface area of the products estimated by BET single point method
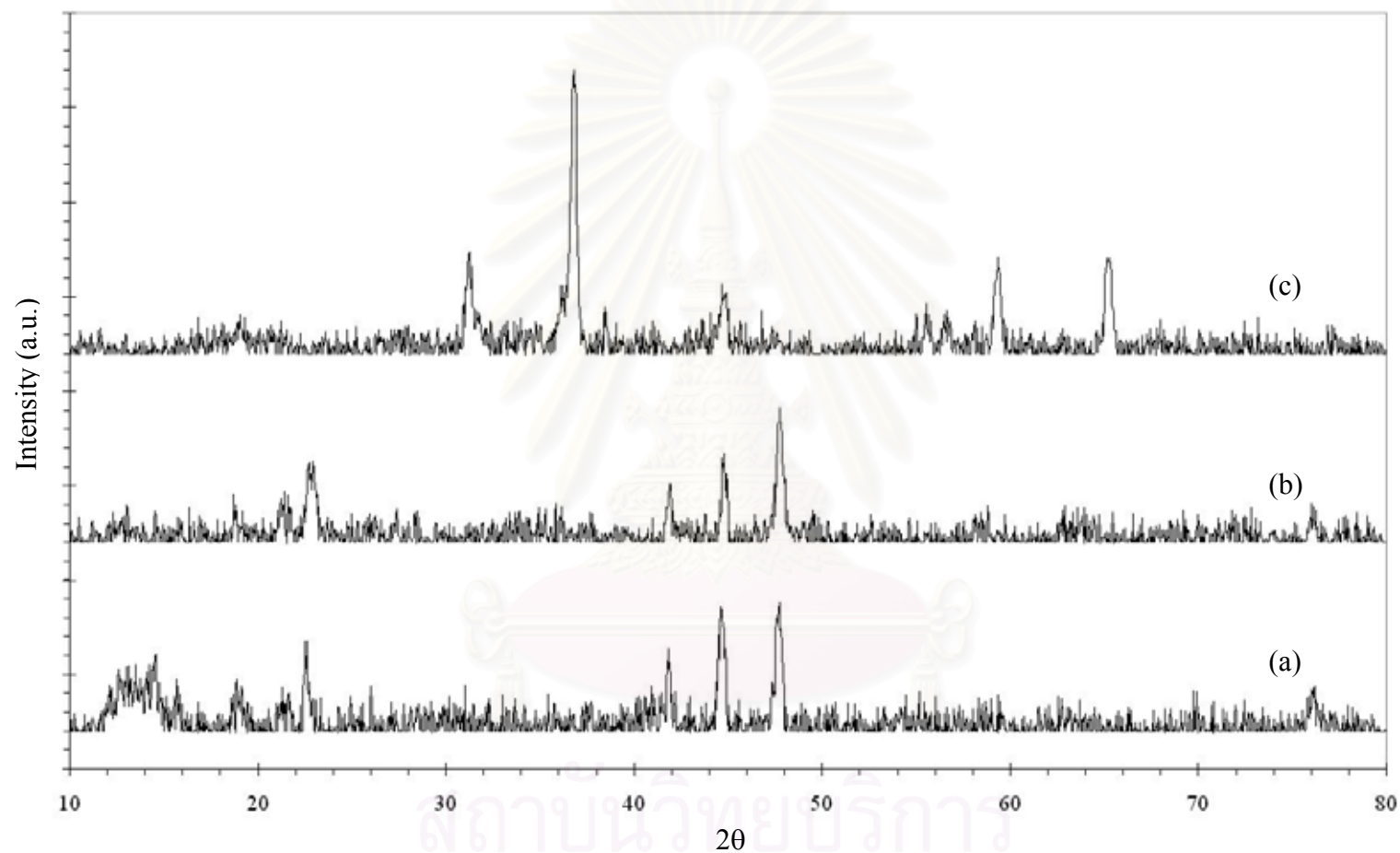
Figure 5.19 The XRD patterns of the undetermined intermediate product prepared at different reaction heating rates, (a) 2.5ºC/min and (b) 1.0ºC/min, compare to the characteristic XRD patterns of (c) zinc cobaltite
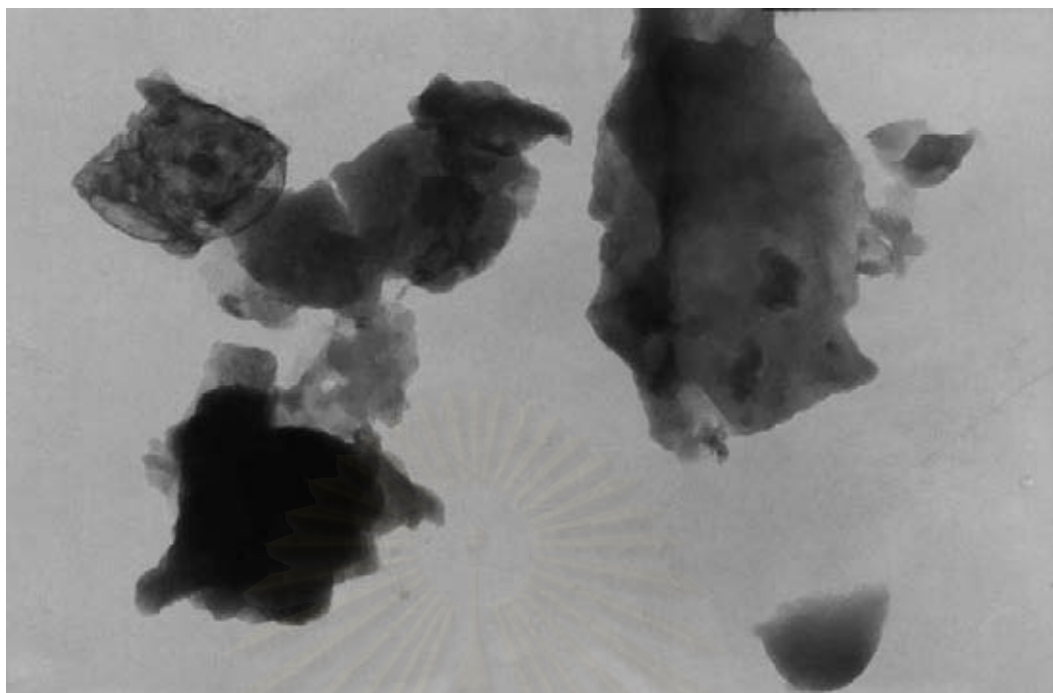
Figure 5.20 TEM photograph of the undetermined intermediate product prepared at reaction heating rate 2.5ºC/min (x150000)
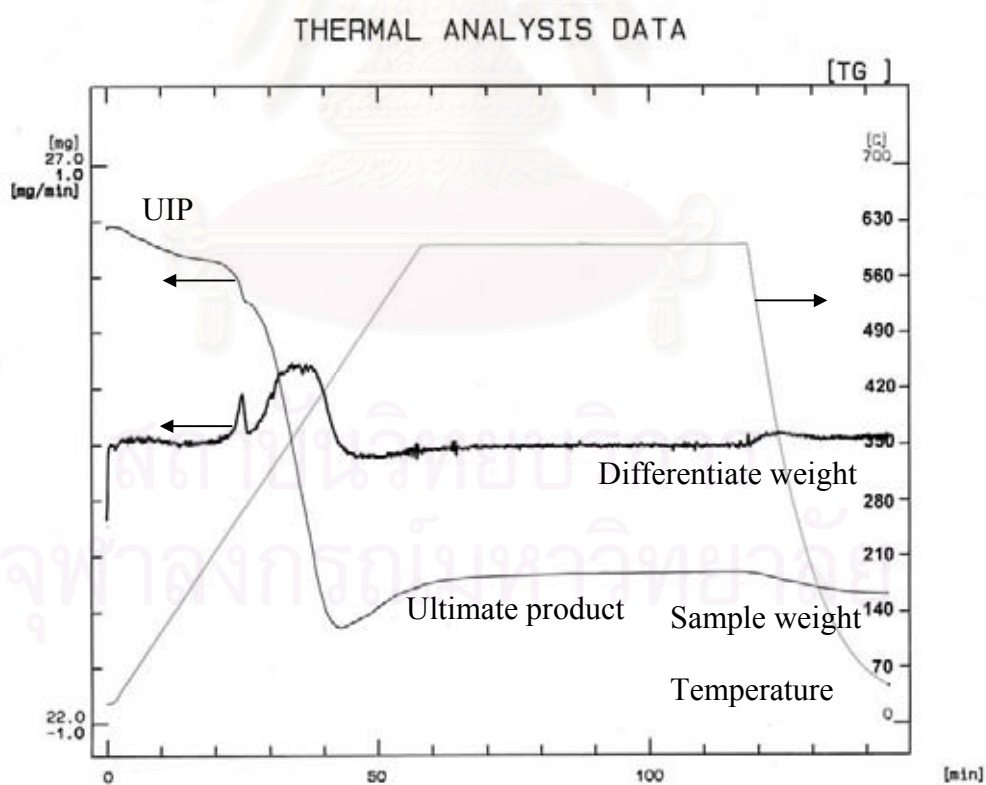
Figure 5.21 The thermogravimetric graph of the undetermined intermediate product obtained from glycothermal reaction of zinc acetate and cobalt (III) acetylacetonate at reaction heating rate 2.5ºC/min
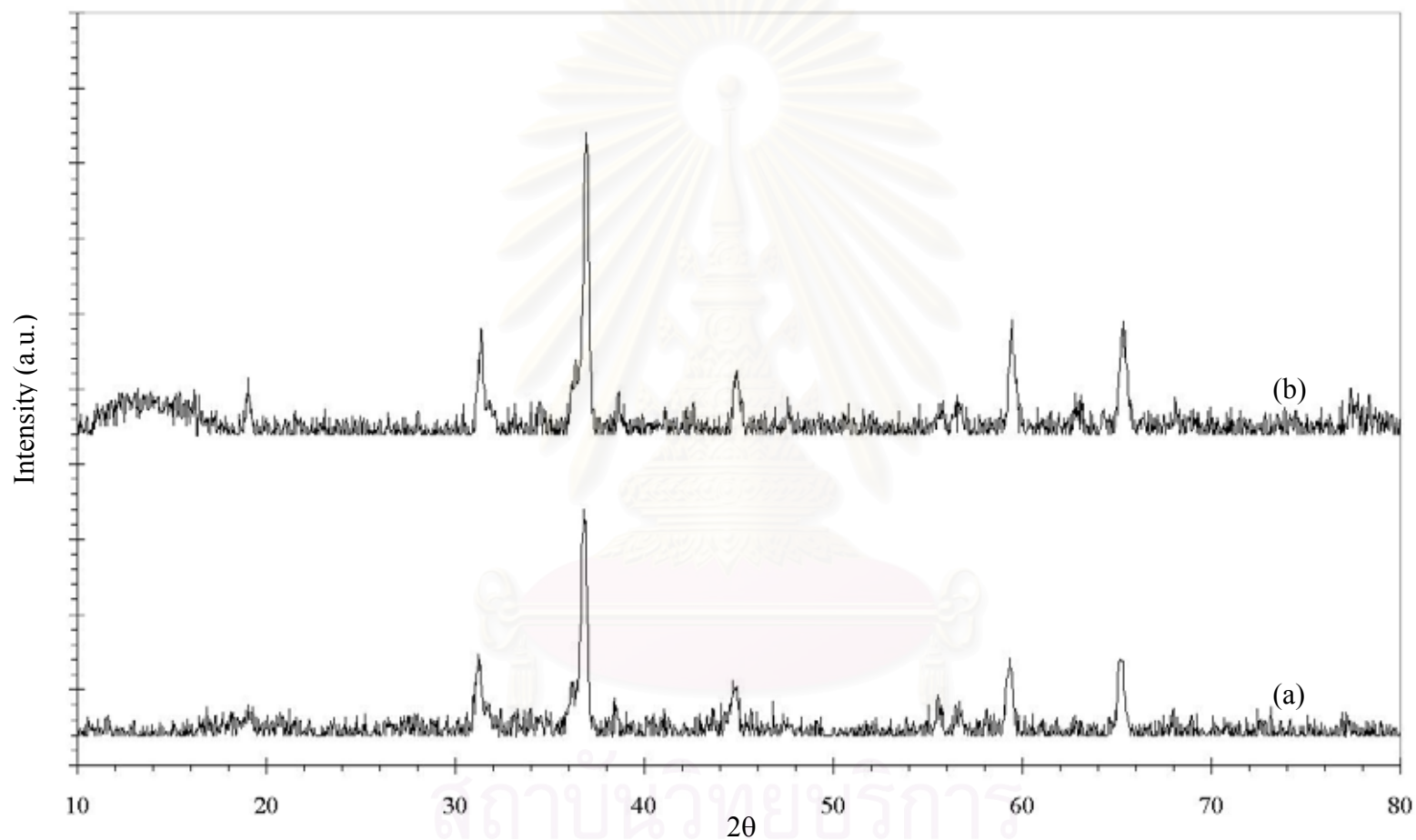
Figure 5.22 The XRD patterns of the as-synthesized zinc cobaltite prepared at different reaction heating rates, (a) 2.5ºC/min and (b) 1.0ºC/min
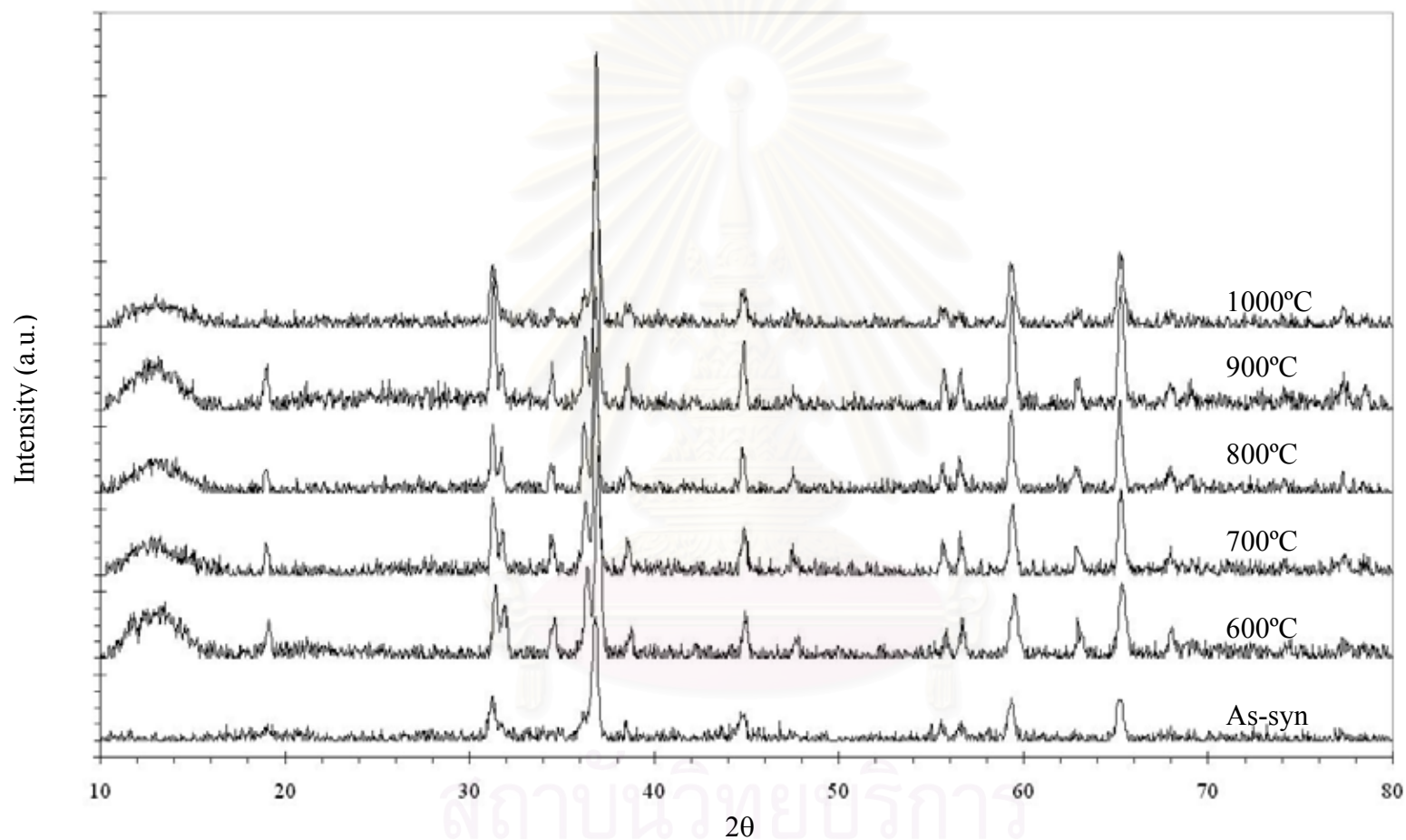
Figure 5.23 The XRD patterns of zinc cobaltite prepared at reaction heating rate of 2.5ºC/min in 1,4-butanediol and products after calcined at 600, 700, 800, 900 and 1000ºC
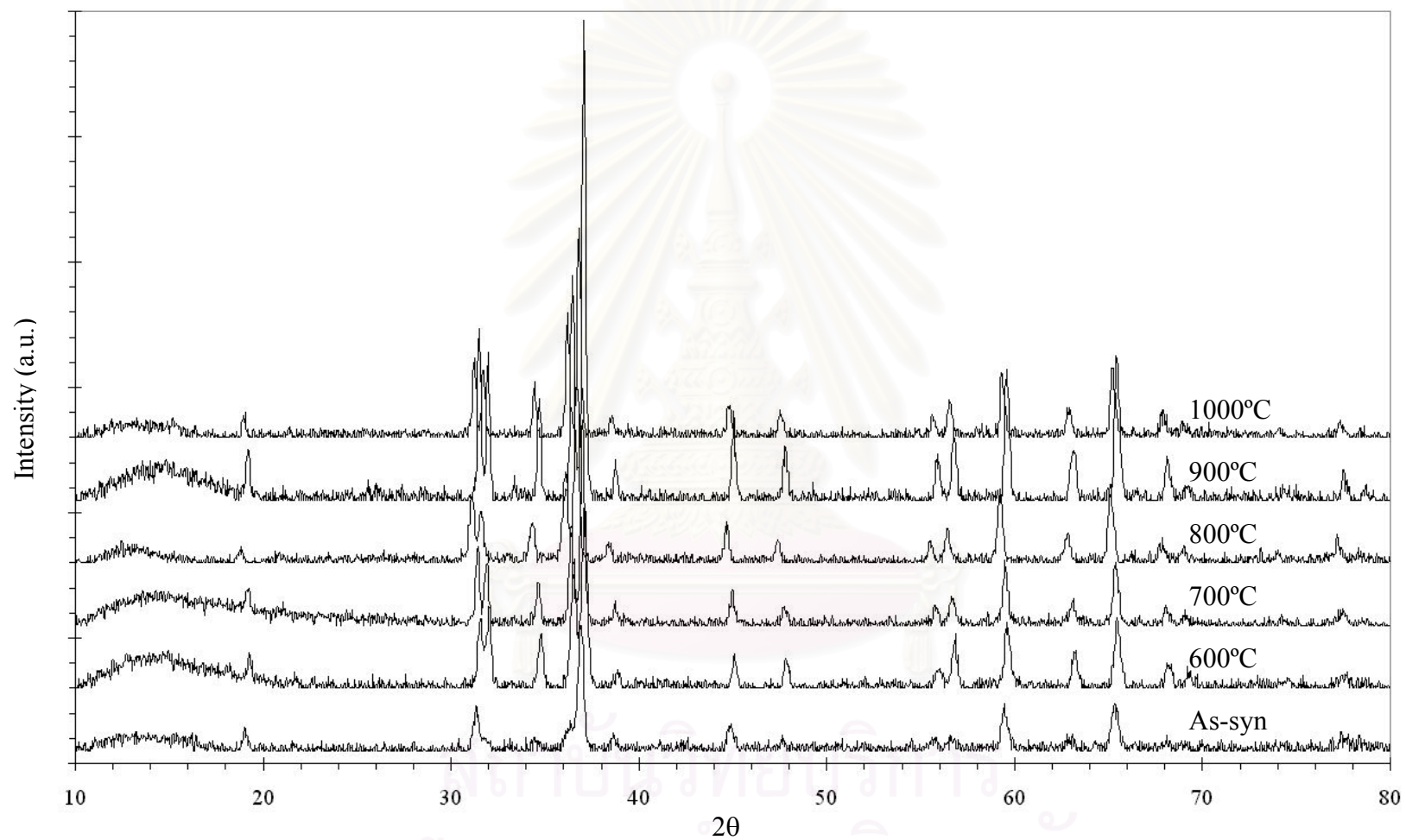
Figure 5.24 The XRD patterns of zinc cobaltite prepared at reaction heating rate of 1.0ºC/min in 1,4-butanediol and products after calcined at 600, 700, 800, 900 and 1000ºC
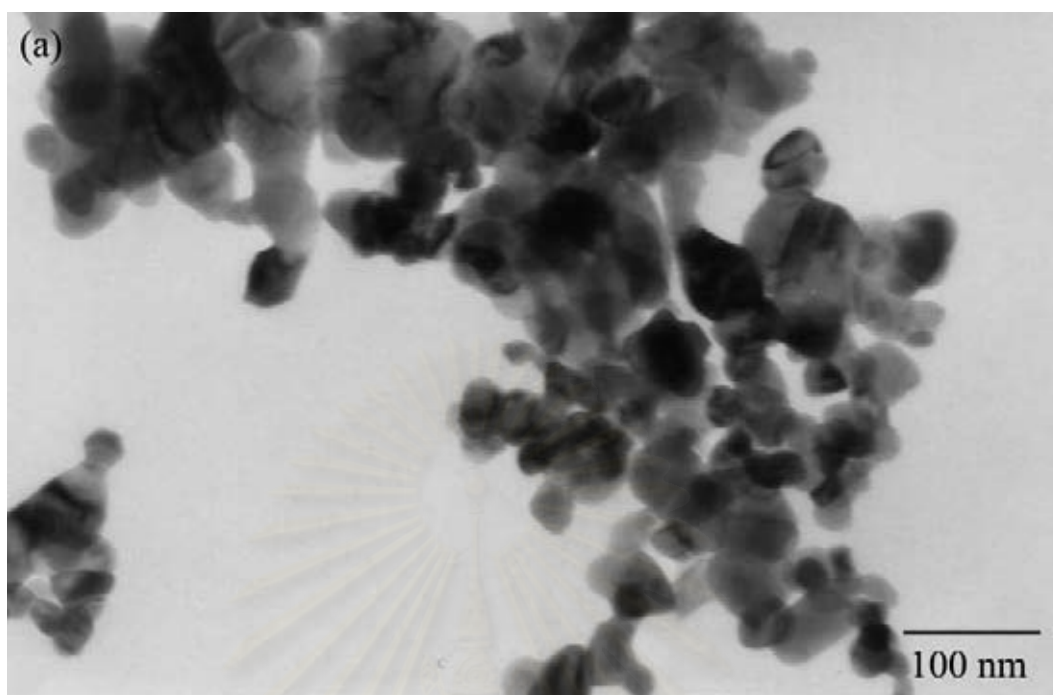
Figure 5.25(a) TEM photograph of the as-synthesized zinc cobaltite product prepared at reaction heating rate 2.5ºC/min (x150000)
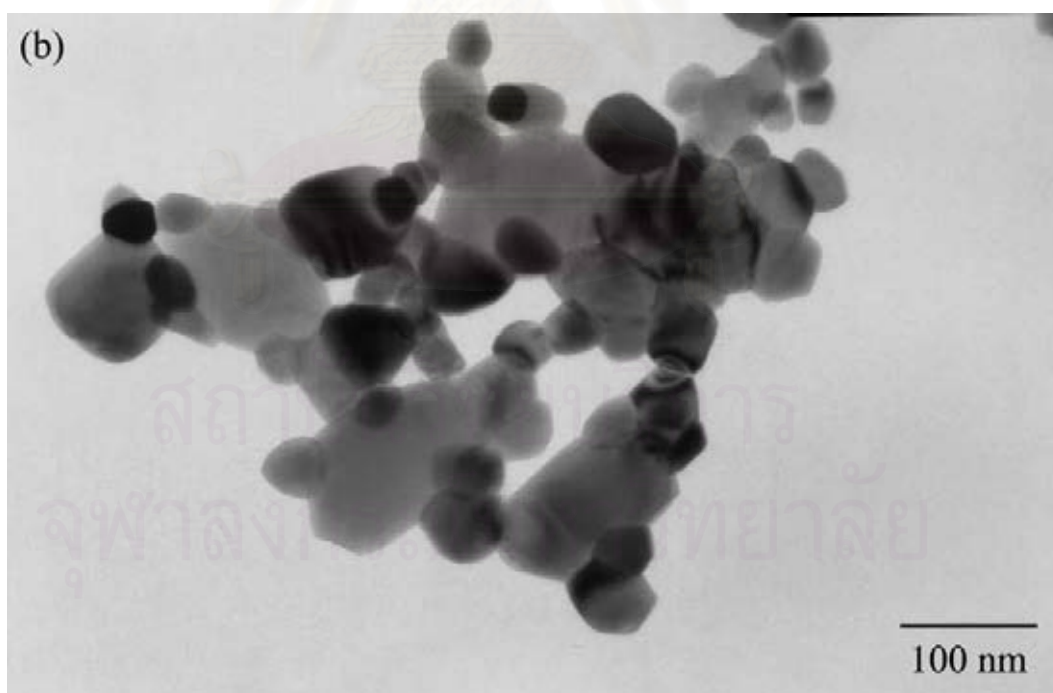
Figure 5.25(b) TEM photograph of the zinc cobaltite product prepared at reaction heating rate 2.5ºC/min after calcined at 600ºC (x150000)
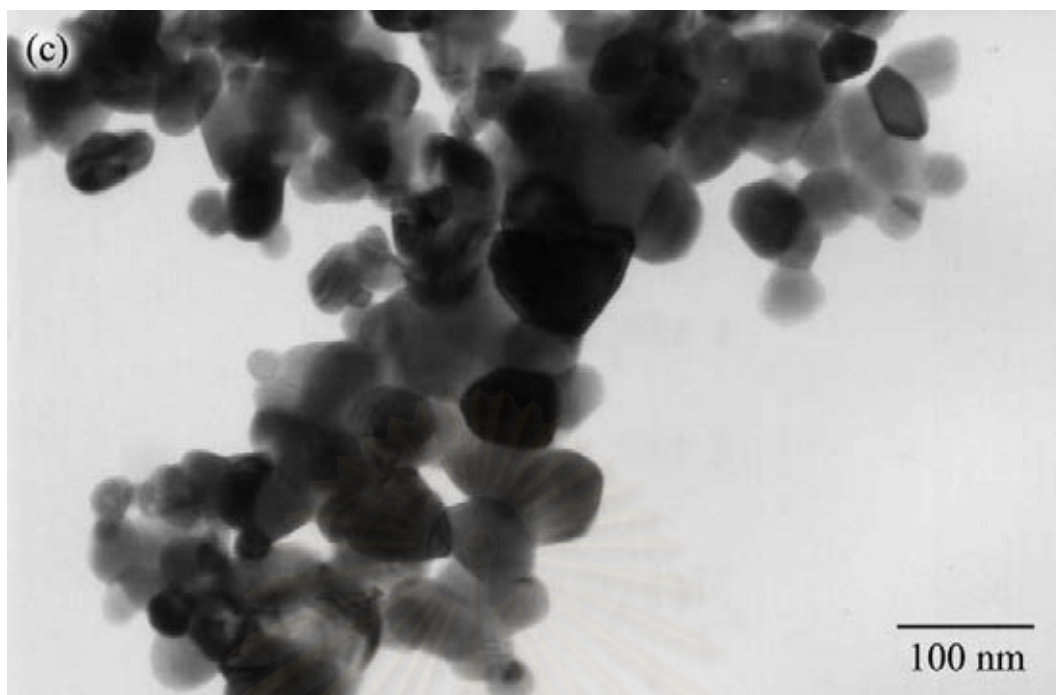
Figure 5.25(c) TEM photograph of the zinc cobaltite product prepared at reaction heating rate 2.5ºC/min after calcined at 800ºC (x150000)
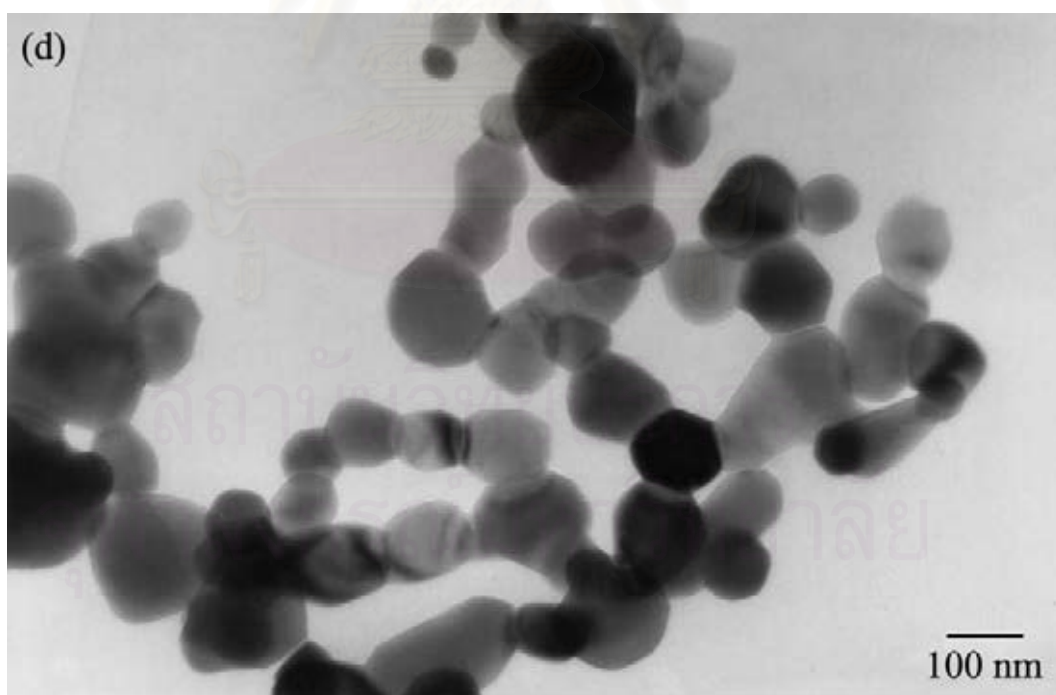
Figure 5.25(d) TEM photograph of the zinc cobaltite product prepared at reaction heating rate 2.5ºC/min after calcined at 1000ºC (x84000)
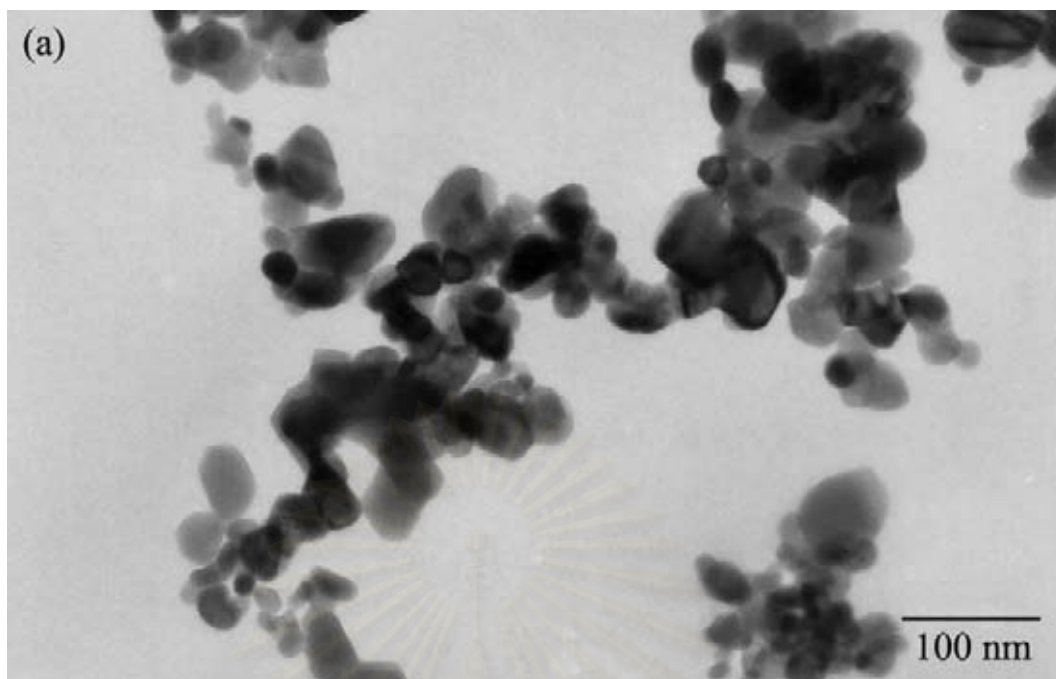
Figure 5.26(a) TEM photograph of the as-synthesized zinc cobaltite product prepared at reaction heating rate 1.0ºC/min (x150000)
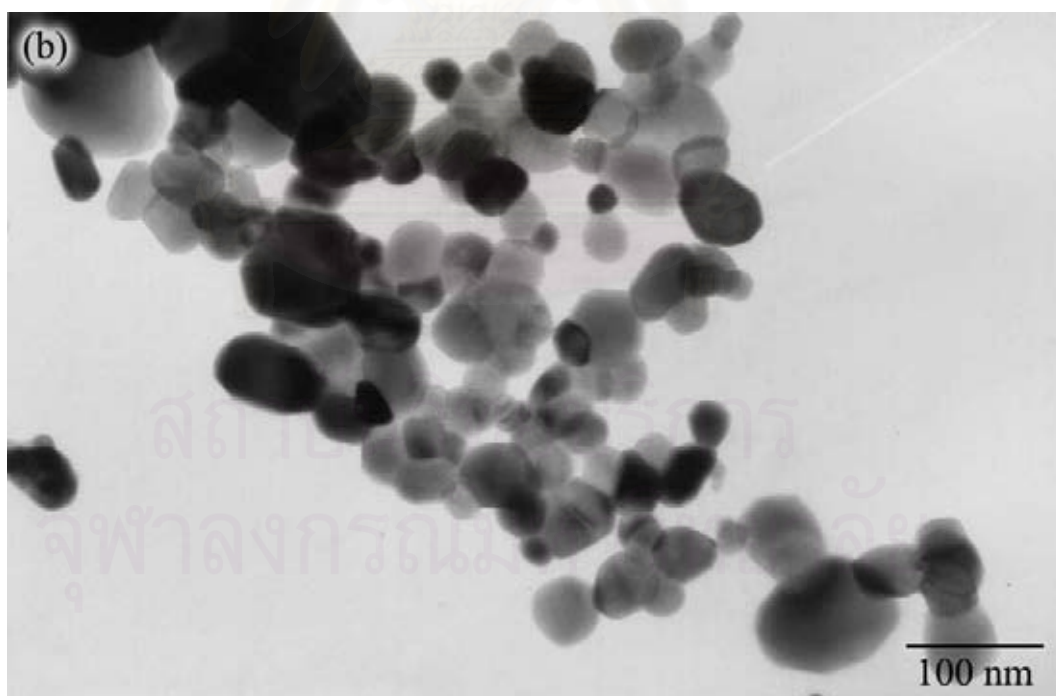
Figure 5.26(b) TEM photograph of the zinc cobaltite product prepared at reaction heating rate 1.0ºC/min after calcined at 600ºC (x150000)
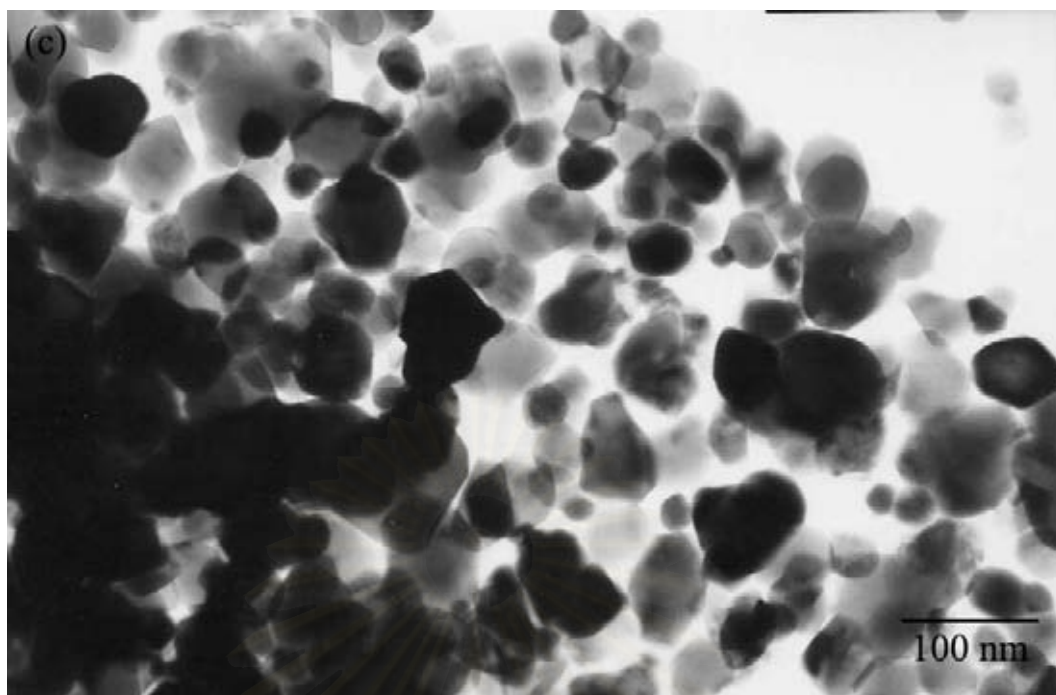
Figure 5.26(c) TEM photograph of the zinc cobaltite product prepared at reaction heating rate 1.0ºC/min after calcined at 800ºC (x150000)
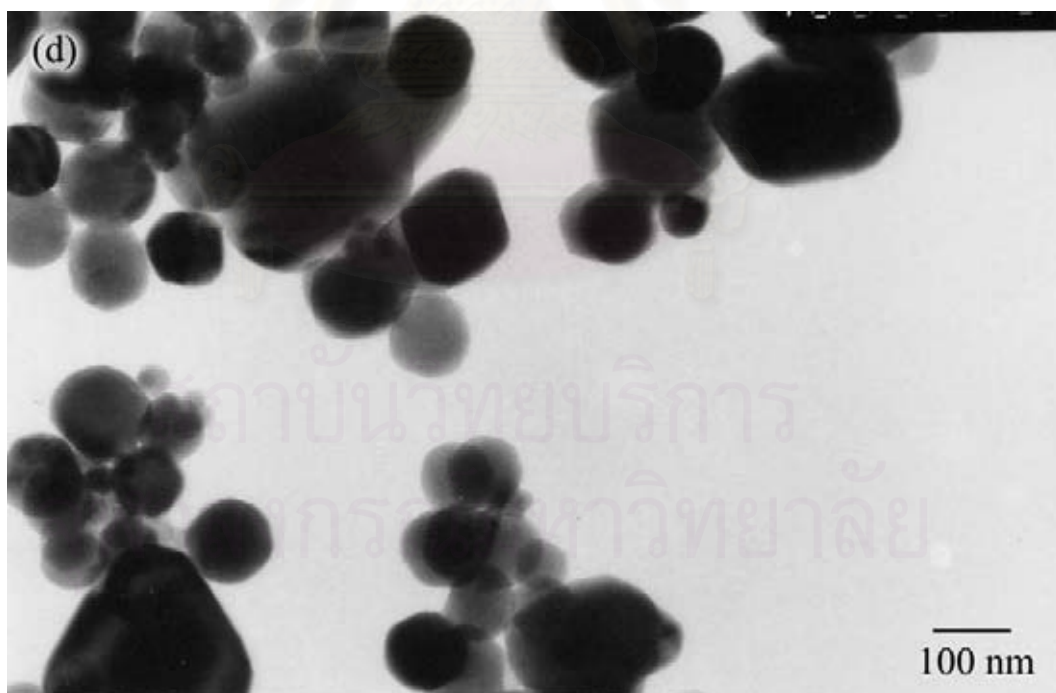
Figure 5.26(d) TEM photograph of the zinc cobaltite product prepared at reaction heating rate 1.0ºC/min after calcined at 1000ºC (x84000)

5.5 Effect of the formation of spinel on the physical properties and the thermal stability of the products

The proposed mechanism of the spinel structure formation had been previously studied. Sangthonganothai [33] had described the mechanism of the formation of spinel structure, zinc gallate and zinc aluminate, that formed under the solution reaction. This may use to explain the formation of zinc chromite and zinc ferrite. Under glycothermal reaction in 1,4-butansdiol at 300ºC for 2 hours, zinc acetate and chromium (III) acetylacetonate were converted to form glycoxides. Thermal decomposition of glycoxides proceeded by intramolecular participation of the remaining hydroxyl group of the glycol moiety, to form the anions, -Zn-O⁻ and =Cr-O⁻. Then the crystallization of spinel phase took place. The amount of zinc and chromium in the structure depended on the amount of zinc acetate and chromium (III) acetylacetonate used as the starting materials. Therefore, with the starting atomic ratio of Zn/Cr equal to 0.50, the zinc chromite spinel would form without any contaminate phases. That was confirmed by X-ray diffraction technique. The proposed mechanism of glycothermal reaction of zinc acetate and chromium (III) acetylacetonate in 1,4-butanediol can be depicted as shown in Figure 5.27.

Similarly, for zinc ferrite synthesis, iron (III) acetylacetonate can be converted to form glycoxide, as well as zinc acetate. The thermal decomposition of glycoxides took place to form the anions. And those obtained anions crystallized to form the spinel phase, zinc ferrite.

On the other hand, neither zinc manganite nor zinc cobaltite was formed under the glycothermal reaction in 1,4-butanediol at 300ºC. This may said that the glycoxides formation of manganese and cobalt did not occur. So the nucleophilic attack on zinc ion and crystallization did not take place. Finally, zinc manganite and zinc cobaltite spinel structure did not form. But both zinc manganite and zinc cobaltite were formed after calcined in the box furnace at the desired temperatures. Thus the formation of zinc manganite and zinc cobaltite must occur in another way.

After calcined the undetermined intermediate product, which obtained form glycothermal reaction of zinc acetate and manganese (III) acetylacetonate, at 600ºC

yielded zinc manganite. The XRD patterns revealed that the UIP obtained at reaction heating rate 2.5ºC/min was well crystallized and the crystallite size calculated from the XRD broadening peak was 28.05 nm. The crystallite size of UIP was close to the crystallite size of zinc manganite obtained after calcined at 600ºC, 28.67 nm. This might say that zinc manganite occur via the solid state reaction.

Not only zinc manganite, but also zinc cobaltite product occurred after calcined the UIP, which obtained from glycothermal reaction of zinc acetate and cobalt (III) acetylacetonate, at 450ºC. The crystallite size of the UIP obtained at reaction heating rate 2.5ºC/min observed from XRD broadening peak was 35.27 nm, which was close to the crystallite size of zinc cobaltite, 29.26 nm, obtained after calcined at 450ºC. This also say that zinc cobaltite occurs via the solid state reaction.
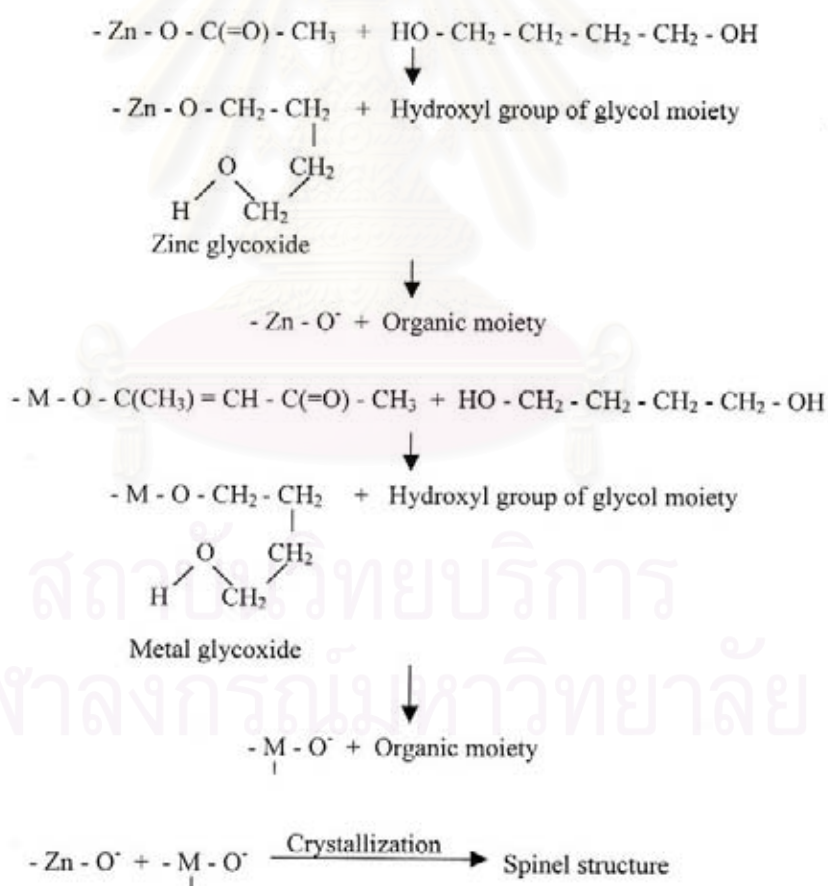
Figure 5.27 Mechanism of glycothermal reaction for the formation of spinel zinc chromite and zinc ferrite (M represents Cr or Fe)

In this work, thermal stability was defined as,

Thermal stability	=	Fractional change in crystallite size
	=	d/d_0
In which, $\quad$ d	=	Crystallite size of calcined product
d_0	=	Crystallite size of as-synthesized product

From the definition, the product with high thermal stability must change in the least in crystallite size after calcined. In Figure 5.28, the data of the products, zinc chromite, zinc manganite, zinc ferrite and zinc cobaltite, were plotted as the relation between log d/d_0 versus log $T(K)/\sqrt{d_0}$. In which, T represented the calcination temperature, and d_0 represented the as-synthesized crystallite size. The thermal stability of the products revealed that in the range of low calcination temperature, the growth of the crystallite size of the products was slowly and increasing at higher calcination temperature.

The crystallite size data of the products were plotted as the relation between d/d_0 versus d_0 in Figure 5.29. The crystallite size is subjected to change after calcined. The product with higher thermal stability would be the least change in crystallite size. As shown in the figure, zinc chromite exhibited the highest rate of the growth of crystallite size, compared to the other spinels. So, zinc chromite is more sensitive to the increasing of crystallite size than the others. All the d_0 used in the figure were the crystallite sizes of as-synthesized products and calcined products, at calcination temperature lower than 1000ºC, in order to vary the crystallite size before calcined at 1000ºC. The spinel structure products, as-synthesized and calcined products, after calcination at 1000ºC exhibited on the same line, revealed that they performed the same performance even after high temperature calcination. However, at the same d_0, zinc chromite revealed the highest thermal stability, with zinc manganite in the second place. While zinc ferrite and zinc cobaltite data lied on the same line, revealed the lowest thermal stability that close to each other. Thus, the relation exhibited the thermal stability in the order of,

$$ZnCr_2O_4 > ZnMn_2O_4 > ZnFe_2O_4 \approx Zn\,Co_2O_4 \qquad\qquad (5.1)$$

The studied spinel type binary oxide had the structure in common, except the trivalency cations in the octahedral sites that is different. These cations, Cr^{3+}, Mn^{3+}, Fe^{3+} and Co^{3+}, played an important role in the exhibition of thermal stability of the spinel products. After calcined, the surface reconstruction took place, in order to lower the surface Gibbs energy per unit surface area to attain a thermodynamically more stable system that is the sintering phenomena. [34] From the elastic interaction between small particles, the surface energy can be calculated from measurements of the contact geometry.

$$2\gamma_s - \gamma_{gb} = 0.16\frac{E\,a_0^3}{R^2} \qquad (5.2)$$

In which
γ_s = Surface energy
γ_{gb} = Grain boundary energy
E = Young's modulus
a_0 = The radius of the contact circle
R = Particle radius

From the equation, within the same product, the grain boundary energy and the Young's modulus are the properties of the product that remain constant. The radius of the contact circle is the function of the particle radius and much less than the particle radius, even in the power three. [35] Then the surface energy is strongly depended on the power two of crystallite size, the larger crystallite size become the less surface energy and more stable.

The correlation of the surface energy can be explained by Figure 5.29. Compare the small crystallite size and the large crystallite size of zinc chromite. After calcined at 1000ºC, the small crystallite size had significant change on the crystallite size more than the large crystallite size. Therefore, the large crystallite size had higher thermal stability than the small crystallite size. This confirms the correlation of the surface energy. The larger crystallite size is more stable than the smaller crystallite size, because the larger crystallite size has less surface energy than the smaller crystallite size.

The degree of coordinative unsaturation of surface cations appeared to have a reasonable correlation with thermal stability [36]. It measure the number of cations bond breaking to form the surface that because of the surface reconstruction. Therefore, the smaller the number of bonds broken, the more stable is the surface. In this case, the trivalency cations exhibited six coordinations with oxygen. Thus the stability would be involved in the chemical bond dissociation energy. The strength of chemical bond, $D^o(R-X)$, often known as the bond dissociation energy, is defined as the standard enthalpy change of the reaction, in which the bond is broken, [37]

$$R-X \rightarrow R + X \qquad (5.3)$$

It is given by the thermochemical equation,

$$D^o(R-X) = \Delta_f H^o(R) + \Delta_f H^o(X) - \Delta_f H^o(RX) \qquad (5.4)$$

In this manner, the surface reconstruction of spinel structure must involve in the bond breaking of trivalent cations and oxygen to remain stable. All the trivalent cations exhibit 6 coordinations with oxygen. Thus the thermal stability may explain by the bond dissociation energy of cations and oxygen.

Table 5.7, the bond dissociation energy of trivalent cations and oxygen were shown. Chromium has the highest bond dissociation energy, compared to another cations. Manganese is in the second place while iron and cobalt, which nearly show the bond dissociation energy in equal, are in the last place. Thus the correlation can be exhibited as,

$$Cr - O > Mn - O > Fe - O \approx Co - O \qquad (5.5)$$

This correlation affirms the correlation of the thermal stability of the spinel type metal oxides. The Cr - O bond, who has the highest bond dissociation energy, is part of the octahedral sites in the structure of zinc chromite, which shows the highest thermal stability. Therefore, when the surface reconstruction took place, the Cr - O bond need the highest energy to break bond that made zinc chromite shown the highest thermal stability. From this explanation, zinc manganite shown the thermal stability in the second place, while zinc ferrite and zinc cobaltite were in the last place.
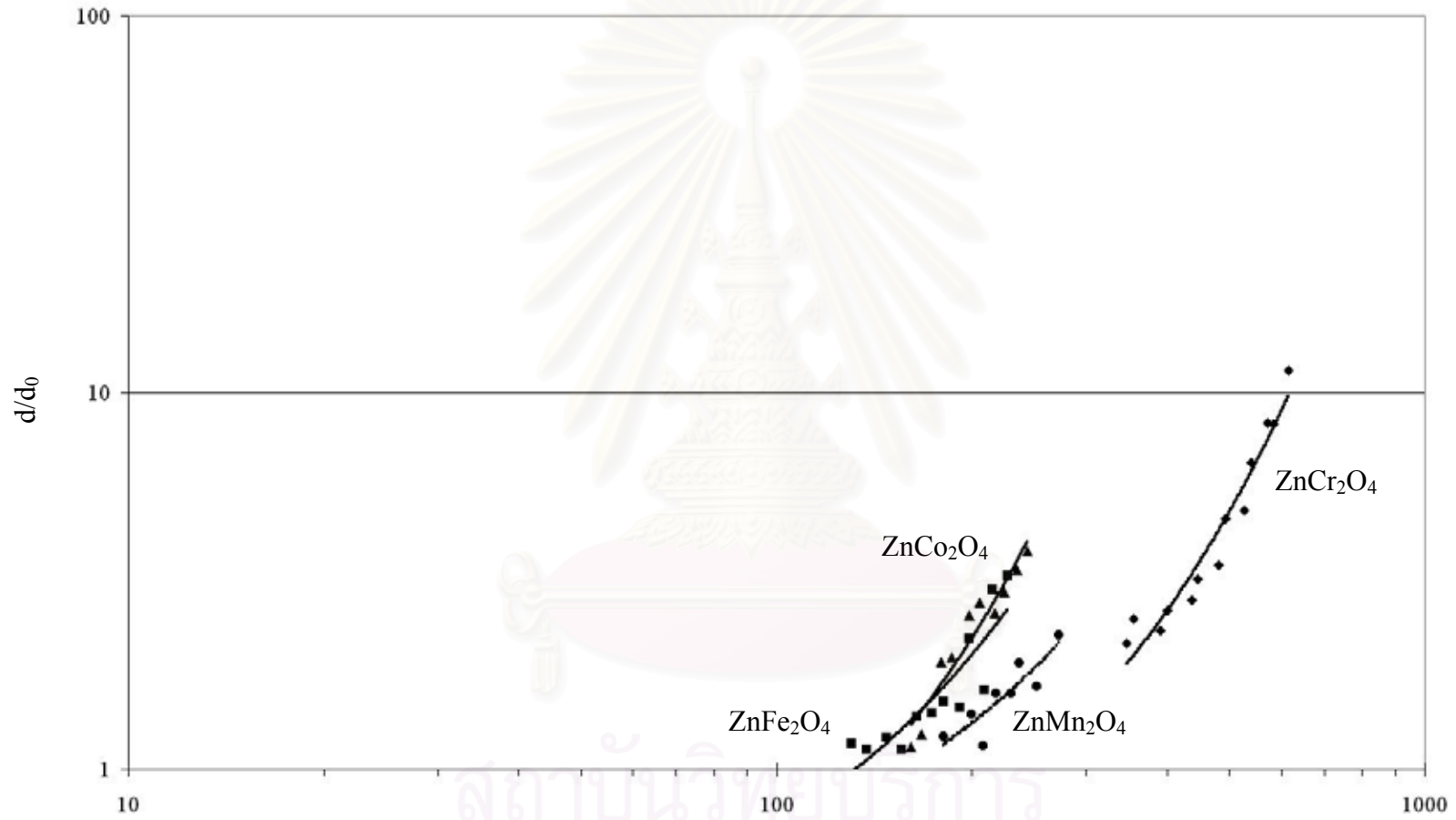
Figure 5.28 The relation between log $\Delta BET/BET_0$ versus log $T(K)/\sqrt{d_0}$ of zinc chromite, zinc manganite, zinc ferrite and zinc cobaltite

Table 5.5 Thermal stability data for the relation between log d/d_0 versus log $T(K)/\sqrt{d_0}$ of the spinel products prepared at different reaction heating rate of 2.5 and 1.0°C/min, in Figure 5.28

Product	Calcination Temperature, °C	Reaction heating rate 2.5°C/min		Reaction heating rate 1.0°C/min	
		$T(K)/\sqrt{d_0}$	d/d_0	$T(K)/\sqrt{d_0}$	d/d_0
$ZnCr_2O_4$	600	391.57	2.34	401.11	2.64
	700	436.43	2.81	447.05	3.20
	800	481.28	3.47	493.00	4.63
	900	526.14	4.86	538.94	6.52
	1000	570.99	8.31	584.89	8.22
$ZnMn_2O_4$	700	181.30	1.22	208.79	1.16
	800	199.93	1.40	230.25	1.59
	900	218.57	1.59	251.71	1.66
	1000	237.20	1.91	273.16	2.27
$ZnFe_2O_4$	600	155.79	1.13	147.55	1.21
	700	173.64	1.41	164.45	1.38
	800	191.48	1.46	181.35	1.52
	900	209.33	1.62	198.25	2.22
	1000	227.17	3.26	215.15	3.00
$ZnCo_2O_4$	600	161.38	1.15	167.25	1.24
	700	179.87	1.92	186.41	1.98
	800	198.35	2.56	205.57	2.77
	900	216.84	2.59	224.73	2.96
	1000	235.32	3.39	243.89	3.79
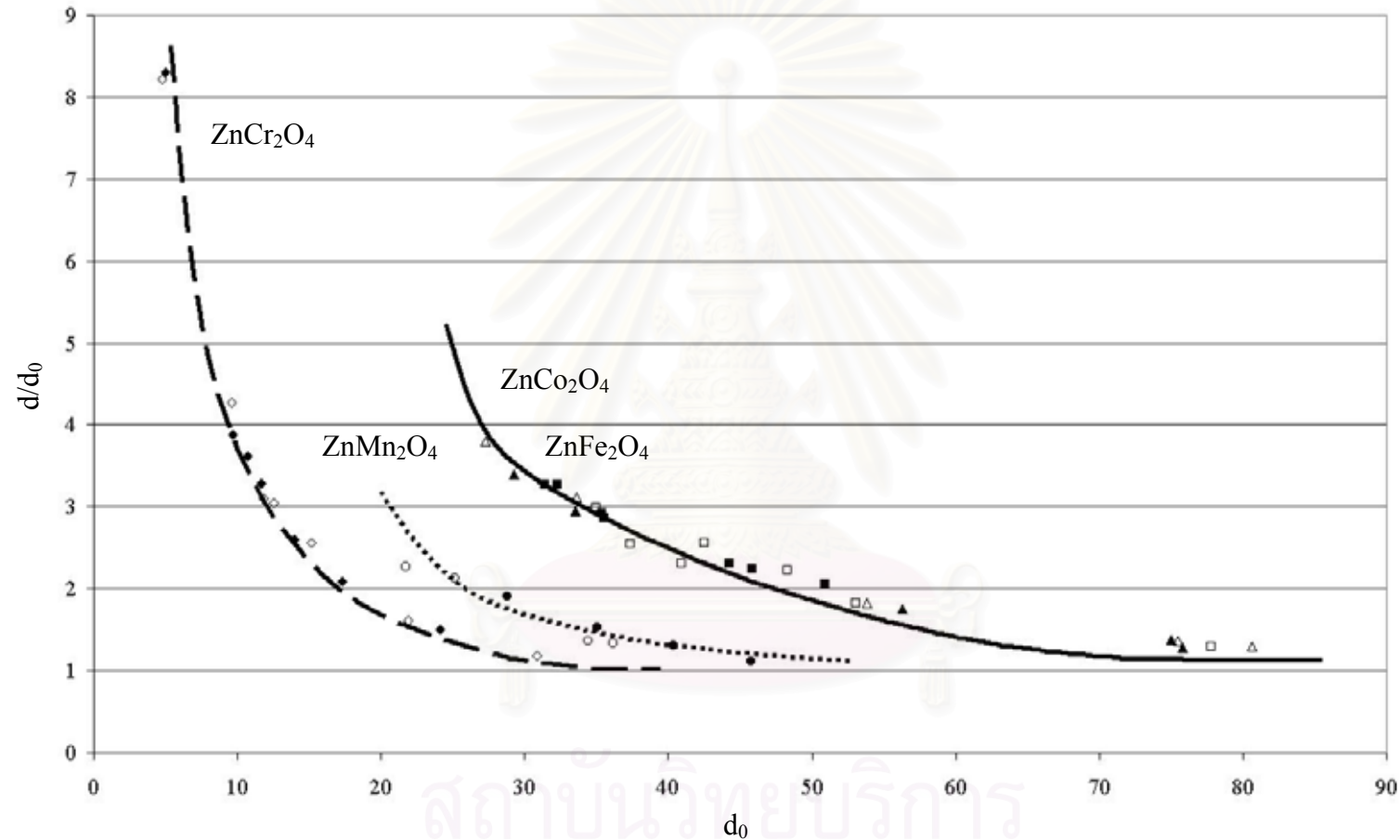
Figure 5.29 The relation between d/d_0 versus d_0 of (♦) zinc chromite, (●) zinc manganite, (■) zinc ferrite and (▲) zinc cobaltite, the solid dot exhibited the products obtained from reaction heating rate 2.5ºC/min, while the vacant dot obtained from reaction heating rate 1.0ºC/min

Table 5.6 Crystallite sizes data of as-synthesized products and calcined products, at calcination temperature lower than 1000ºC before calcined at 1000ºC (d_0) and crystallite size of product after calcined at 1000ºC (d) for the relation in Figure 5.29

Product	Reaction heating rate 2.5ºC/min		Reaction heating rate 1.0ºC/min	
	d_0	d	d_0	d
$ZnCr_2O_4$	4.97	41.29	4.74	38.95
	11.62	38.23	12.52	38.15
	13.95	36.19	15.15	38.78
	17.26	36.05	21.92	35.45
	24.14	36.34	30.88	36.63
$ZnMn_2O_4$	28.80	55.01	21.72	49.33
	35.05	53.80	25.10	53.43
	40.34	52.78	34.44	47.05
	45.73	51.21	36.14	48.06
$ZnFe_2O_4$	31.40	102.51	35.01	104.93
	35.54	101.96	42.47	108.56
	44.28	102.51	48.28	107.72
	45.80	102.51	53.05	96.62
	50.91	104.69	77.78	100.34
$ZnCo_2O_4$	29.26	99.18	27.24	103.28
	33.58	98.86	33.65	104.68
	56.29	98.42	53.83	97.99
	75.02	103.18	75.52	103.04
	75.84	97.41	80.65	104.80

Table 5.7 Bond dissociation energies of trivalent cations and oxygen [37]

Bond	Bond dissociation energy, kJ/mol
Cr - O	461 ± 9
Mn - O	402.9 ± 41.8
Fe - O	390.4 ± 17.2
Co - O	384.5 ± 13.4

CHAPTER VI

CONCLUSIONS AND RECOMMENDATION

6.1 Conclusions

The conclusion of the present research is,

The trivalent cations in the octahedral sites affected the thermal stability of spinel structures that revealed in the correlation,

$$ZnCr_2O_4 > ZnMn_2O_4 > ZnFe_2O_4 \approx ZnCo_2O_4$$
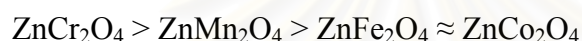
That attribute to the result of the bond dissociation energy of cations and oxygens in the octahedral coordination

6.2 Recommendation for the further studies

From the previous conclusions, the following recommendations for the further studies are proposed.

1) To study the role of the bond dissociation energy on the thermal stability of these spinel structures.

2) To study the effect of others trivalent cations in the octahedral sites on the thermal stability of spinel type metal oxide while fix the zinc cations in the tetrahedral sites

3) To study the effect of these trivalent cations, Cr^{3+}, Mn^{3+}, Fe^{3+}, and Co^{3+}, in the octahedral sites with the other divalent cations, besides Zn^{2+}, in the octahedral sites.

REFERENCES

1. J. M. Correa Bueno, M. Gazzano, M. Goncalves Coelho, A. Vaccari, Synthesis and reactivity of copper-containing nonstoichiometric spinel catalysts, *Applied Catalysis A: General* **103**, 1993: 69-78

2. H. Armendariz, J. A. Toledo, G. Aguilar-Rios, M. A. Valenzuela, P. Salas, A. Cabral, H. Jimenez, I. Schifter, Oxydative dehydrogenation of n-butane on zinc chromium ferrite catalysts, *Journal of Molecular Catalysis* **92**, 1994: 325-332

3. S. Guillemet-Fritsch, C. Chanel, J. Sarrias, S. Bayonne, A. Rousset, X. Alcobe, M. L. Martinez Sarriòn, Structure, thermal stability and electrical properties of zinc manganites, *Solid State Ionics* **128**, 2000: 233-242

4. A. Maltha, H. F. Kist, B. Brunet, J. Ziolkowski, H. Onishi, Y. Iwasawa, V. Ponec, The Active Sites of Manganese- and Cobalt-Containing Catalysts in the Selective Gas Phase Reduction of Nitrobenzene, *Journal of Catalysis* **149**, 1994: 356-363

5. A. Maltha, T. L. F. Favre, H. F. Kist, A. P. Zuur, V. Ponec, Manganese Oxides as Catalysts for the Selective Reduction of Nitrobenzene to Nitrosobenzene, *Journal of Catalysis* **149**, 1994: 364-374

6. G. Fierro, S. Morpurgo, M. Lo Jacono, M. Inversi, I. Pettiti, Preparation, characterisation and catalytic activity of Cu-Zn-based manganites obtained from carbonate precursors, *Applied Catalysis A: General* **166**, 1998: 407-417

7. G. Fierro, M. Lo Jacono, M. Inversi, R. Dragone, G. Ferraris, Preparation, characterization and catalytic activity of Co-Zn-based manganites obtained from carbonate precursors, *Applied Catalysis B: Environmental* **30**, 2001: 173-185

8. H. Armendariz, G. Aguilar-Rios, P. Salas, M. A. Valenzuela, I. Schifter, Oxidative dehydrogenation of n-butane on iron-zinc oxide catalyst, *Applied Catalysis A: General* **92**, 1992: 29-38

9. J. A. Toledo, M. A. Valenzuela, H. Armendariz, G. Aguilar-Rios, B. Zapata, A. Montaya, N. Nava, P. Salas, I. Schifter, Oxidative dehydrogenation of 1-butene to butadiene on α-Fe$_2$O$_3$/ZnAl$_2$O$_4$ and ZnFe$_x$Al$_{2-x}$O$_4$ catalysts, *Catalysis Letters* **30**, 1995: 279-288

10. W. Kim, F. Saito, Mechanochemical synthesis of zinc ferrite from zinc oxide and α-Fe$_2$O$_3$, *Powder Technology* **114**, 2001: 12-16

11. N. Chen, X. Yang, E. Liu, J. Huang, Reducing gas-sensing properties of ferrite compounds MFe_2O_4 (M = Cu, Zn, Cd, and Mg), *Sensor and actuators B: Chemical* **66**, 2000: 178-180

12. Y. Zhihao, Z. Lide, Synthesis and structural characterization of capped $ZnFe_2O_4$ nanoparticles, *Materials Research Bulletin* **33**, 1998: 1587-1592

13. D. klissurski, E. Uzonova, K Yankova, Alumina supported zinc-cobalt spinel oxide catalyst for combustion on acetone, toluene and styrene, *Applied Catalysis A: General* **95**, 1993: 103-115

14. T. Baird, K. C. Campbell, P. J. Holliman, R. W. Hoyle, M. Huxam, D. Stirling, B. P. Williams, M. Morris, Cobalt-zinc oxide absorbents for low temperature gas desulferisation, *Journal of Materials Chemistry* **9**, 1999: 599-605

15. A. J. Fanelli, J. V. Burlew, Preparation of fine alumina powder in alcohol, *Journal of the American Ceramic Society* **69**, 1986: C174-C175

16. D. M. Bibby, M. P. Dale, Synthesis of silica-sodalite from non-aqueous system, *Nature (London)* **317**, 1985: 157-158

17. J. N. Armor, E. J. Carlson, Variables in the synthesis of unusually high pore volume aluminas, *Journal of Materials Science* **22**, 1987: 2549-2556

18. M. Inoue, Y. Kondo, T. Inui, An ethylene glycol derivative of boehmite, *Inorganic Chemistry* **27**, 1988: 215-221

19. M. Inoue, H. Tanino, Y. Kondo, T. Inui, Formation of microcrystalline α-alumina by glycothermal treatment of gibbsite, *Journal of the American Ceramic Society* **72**, 1989: 352-353

20. M. Inoue, H. Kominami, T. Inui, Thermal reaction of aluminum alkoxide in glycols, *Journal of the American Ceramic Society* **73**, 1990: 1100-1102

21. M. Inoue, H. Kominami, T. Inui, Thermal tranformation of χ-alumina formed by thermal decomposition of aluminum alkoxide in organic media, *Journal of the American Ceramic Society* **75**, 1992: 2597-2598

22. M. Inoue, H. Kominami, T. Inui, Novel synthetic method for the catalytic use of thermally stable zirconia: Thermal decomposition of zirconium alkoxide in organic media, *Applied Catalysis A: General* **97**, 1993: L25-L30

23. M. Inoue, H. Kominami, T. Inui, Novel synthesis method for thermally stable monoclinic zirconia: Hydrolysis of zirconia alkoxides at high temperature with a limited amount of water dissolved in inert organic solvent from the gas phase, *Applied Catalysis A: General* **121**, 1995: L1-L5

24. M. Inoue, H. Otsu, H. Kominami, T. Inui, Synthesis of submicron spherical crystals of gadolinium gallium garnets by the glycothermal method, *Journal of Materials Science Letters* **14**, 1995: 1303-1305

25. M. Inoue, H. Otsu, T. Inui, Glycothermal synthesis of rare earth aluminium garnets, *Journal of Alloys and Compounds* **226**, 1995: 146-151

26. J. S. Jiang, X. L. Yang, L. Gao, J. K. Guo, J. Z. Jiang, Synthesis and characterization of nanocrystalline zinc ferrite, *NanoStructured Materials* **12**, 1999: 143-146

27. J. A. Toledo, M. A. Valenzuela, P. Bosch, H. Armendariz, A. Montoya, N. Nava, A. Vazquez, Effect of Al^{3+} introduction into hydrothermally prepared $ZnFe_2O_4$, *Applied Catalysis A: General* **198**, 2000: 235-245

28. A. Cabanas, M. Poliakoff, The continuous hydrothermal synthesis of nano-particulate ferrites in near critical and supercritical water, *Journal of Materials Chemistry* **11**, 2001: 1408-1416

29. D. K. Chakrabarty, *Solid state chemistry*, New Age International Limited, Publishers, New Delhi, 1996: 53-54

30. A. R. West, *Basic solid state chemistry second edition*, London, John Wiley & Sons, 1999

31. A. R. West, *Solid state chemistry and its applications*, London, John Wiley & Sons, 1997

32. *McGraw-Hill encyclopedia of science & technology*, New York, McGraw-Hill Book, 5th edition, 1982: 435

33. P. Sangthonganothai, *Solvothermal synthesis of spinel-type zinc gallate and zinc aluminate powders*, Master's thesis, Faculty of Engineering, Chulalongkorn University, 2000: 85

34. A.R. Thölén, Interaction between small particles, *Materials Science Research* **13**, 1979: 539-549

35. K.L. Johnson, K. Kendall, A.D. Roberts, Surface energy and the contact of elastic solids, *Proceedings of the Royal Society of London. Series A, Containing Papers of a Mathematical and Physical Character* **324**, 1971: 301-313

36. H. H. Kung, Transition metal oxides: surface chemistry and catalysis, *Studies in Surface Science and Catalysis* **45**, 1989: 15-20

37. D. R. Lide, *CRC handbook of chemistry and physics*, New York, CRC Press, 81st edition, 2000: 9-51 - 9-63

38. H. P. Klug, L. E. Alexander, *X-ray diffraction procedures for polycrystalline and amorphous materials*, New York, John Wiley & Sons, 1954: 491-501

39. J. R. Anderson, K. C. Pratt, *Introduction to characterization and testing of catalyst*, Sydney, Academic Press, 1985: 3-6

40. O. Mekasuvandamrong, *One pot synthesis of silica modified alumina*, Master's thesis, Faculty of Engineering, Chulalongkorn University, 1999

41. S. Theinkaew, *Synthesis of large-surface area silica modified titanium (IV) oxide ultrafine particles*, Master's thesis, Faculty of Engineering, Chulalongkorn University, 2000

APPENDICES

APPENDIX A

CALCULATION OF THE STARTING REAGENTS

In this study, the spinel type metal oxides were prepared in the organic solvent of 1,4-butanediol with the atomic ratio equal to 0.5. The prepared samples are zinc chromite, zinc manganite, zinc ferrite and zinc cobaltite.

A.1 Zinc chromite

Zinc acetate and chromium (III) acetylacetonate are used as the reactants.
1. Zinc acetate, 99.99%, molecular weight 183.46 g/mol.
   Zinc atomic weight 65.39 g/mol.
2. Chromium (III) acetylacetonate, 97%, molecular weight 349.33 g/mol.
   Chromium atomic weight 51.996 g/mol.

Zinc acetate 5 g is used for preparation of zinc chromite. The reagent 5 g is consisted of zinc equal to:

$$\text{Zinc} = \frac{65.39}{183.46} \times 5 \text{ g}$$
$$= 1.7821 \text{ g}$$
$$\text{Zinc} = \frac{1.7821}{65.39} \text{ mol} = 0.0272 \text{ mol}$$

From the atomic ratio 0.5, the used of chromium is equal to:
$$\text{Chromium} = 2 \times 0.0272 \text{ mol}$$
$$= 0.0544 \text{ mol}$$

Chromium 0.0544 mol is used in the preparation, which the used of chromium (III) acetylacetonate equal to:

Chromium (III) acetylacetonate $= \dfrac{349.33}{0.97} \times 0.0544$ g

$= 19.5913$ g

A.2 Zinc manganite

Zinc acetate and manganese (III) acetylacetonate are used as the reactants.

1. Zinc acetate, 99.99%, molecular weight 183.46 g/mol.
   Zinc atomic weight 65.39 g/mol.
2. Manganese (III) acetylacetonate, tech., molecular weight 352.27 g/mol.
   Manganese atomic weight 54.938 g/mol.

Zinc acetate 5 g is used for preparation of zinc manganite. The reagent 5 g is consisted of zinc equal to:

Zinc $= \dfrac{65.39}{183.46} \times 5$ g

$= 1.7821$ g

Zinc $= \dfrac{1.7821}{65.39}$ mol $= 0.0272$ mol

From the atomic ratio 0.5, the used of manganese is equal to:

Manganese $= 2 \times 0.0272$ mol

$= 0.0544$ mol

Manganese 0.0544 mol is used in the preparation, which the used of manganese (III) acetylacetonate equal to:

Manganese (III) acetylacetonate $= 352.27 \times 0.0544$ g

$= 19.1635$ g

A.3 Zinc ferrite

Zinc acetate and iron (III) acetylacetonate are used as the reactants.

1. Zinc acetate, 99.99%, molecular weight 183.46 g/mol.

   Zinc atomic weight 65.39 g/mol.

2. Iron (III) acetylacetonate, 97%, molecular weight 353.18 g/mol.

   Iron has atomic weight 55.847 g/mol.

Zinc acetate 5 g is used for preparation of zinc ferrite. The reagent 5 g is consisted of zinc equal to:

$$\text{Zinc} = \frac{65.39}{183.46} \times 5 \text{ g}$$

$$= 1.7821 \text{ g}$$

$$\text{Zinc} = \frac{1.7821}{65.39} \text{ mol} = 0.0272 \text{ mol}$$

From the atomic ratio 0.5, the used of iron is equal to:

$$\text{Iron} = 2 \times 0.0272 \text{ mol}$$

$$= 0.0544 \text{ mol}$$

Iron 0.0544 mol is used in the preparation, which the used of iron (III) acetylacetonate equal to:

$$\text{Iron (III) acetylacetonate} = \frac{353.18}{0.97} \times 0.0544 \text{ g}$$

$$= 19.1635 \text{ g}$$

A.4 Zinc cobaltite

Zinc acetate and cobalt (III) acetylacetonate are used as the reactants.

1. Zinc acetate, 99.99%, molecular weight 183.46 g/mol.

   Zinc has atomic weight 65.39 g/mol.

2. Cobalt (III) acetylacetonate, 98%, molecular weight 356.26 g/mol.

   Cobalt has atomic weight 58.9332 g/mol.

Zinc acetate 5 g is used for preparation of zinc cobaltite. The reagent 5 g is consisted of zinc equal to:

$$\text{Zinc} \quad = \frac{65.39}{183.46} \times 5 \text{ g}$$

$$= 1.7821 \text{ g}$$

$$\text{Zinc} \quad = \frac{1.7821}{65.39} \text{ mol} = 0.0272 \text{ mol}$$

From the atomic ratio 0.5, the used of cobalt is equal to:

$$\text{Cobalt} = 2 \times 0.0272 \text{ mol}$$

$$= 0.0544 \text{ mol}$$

Cobalt 0.0544 mol is used in the preparation, which the used of cobalt (III) acetylacetonate equal to:

$$\text{Cobalt (III) acetylacetonate} \quad = \frac{356.26}{0.98} \times 0.0544 \text{ g}$$

$$= 19.7761 \text{ g}$$

APPENDIX B

CALCULATION OF THE CRYSTALLITE SIZE

Scherrer showed that the mean dimension of the crystallites is related to the pure x-ray diffraction broadening [31,37].

$$d = \frac{K\lambda}{\beta \cos\theta} \qquad (B.1)$$

Where, d = Crystallite size

K = Crystallite-shape factor = 0.89

λ = X-ray wavelength, for CuKα = 1.5418 Å

θ = Observed peak angle

β = X-ray diffraction broadening, rad

The X-ray diffraction broadening is the pure breadth of a powder reflection free of all broadening due to the experimental equipment, by using Warren's correction for instrumental broadening.

$$\beta^2 = \beta_P{}^2 - \beta_R{}^2 \qquad (B.2)$$

$$\beta = \sqrt{\beta_P^2 - \beta_R^2}$$

Where, β_P = X-ray diffraction broadening of observed peak, rad

β_R = X-ray diffraction broadening of instrumental, rad

Which is to say that the squared breadth of the pure diffraction profile equals to the squared of observed peak subtracted by the squared of the instrumental broadening profile. Standard α-alumina is used to observe the instrumental broadening.

Example B.1: The crystallite size of pure zinc chromite

The observed peak broadening = 63.8846º - 62.0000º

= 1.8846º

= 3.2892×10^{-2} rad

The instrumental broadening $= 5.6370 \times 10^{-3}$ rad

The pure diffraction profile $= \sqrt{\beta_P^2 - \beta_R^2}$ rad

$$= \sqrt{\left(3.2892 \times 10^{-2}\right)^2 - \left(5.6370 \times 10^{-3}\right)^2} \text{ rad}$$

$$= 3.2406 \times 10^{-2} \text{ rad}$$

$\beta \quad = 3.2406 \times 10^{-2}$ rad

$2\theta \quad = 63.1500°$

$\theta \quad = 31.5750°$

K $\quad = 0.89$

$\lambda \quad = 1.5418$ Å

The crystallite size $\quad = \dfrac{0.89 \times 1.5418}{0.032406 \times \cos 31.5750}$ Å

$$= 49.7024 \text{ Å}$$

d $\quad = 4.9702$ nm
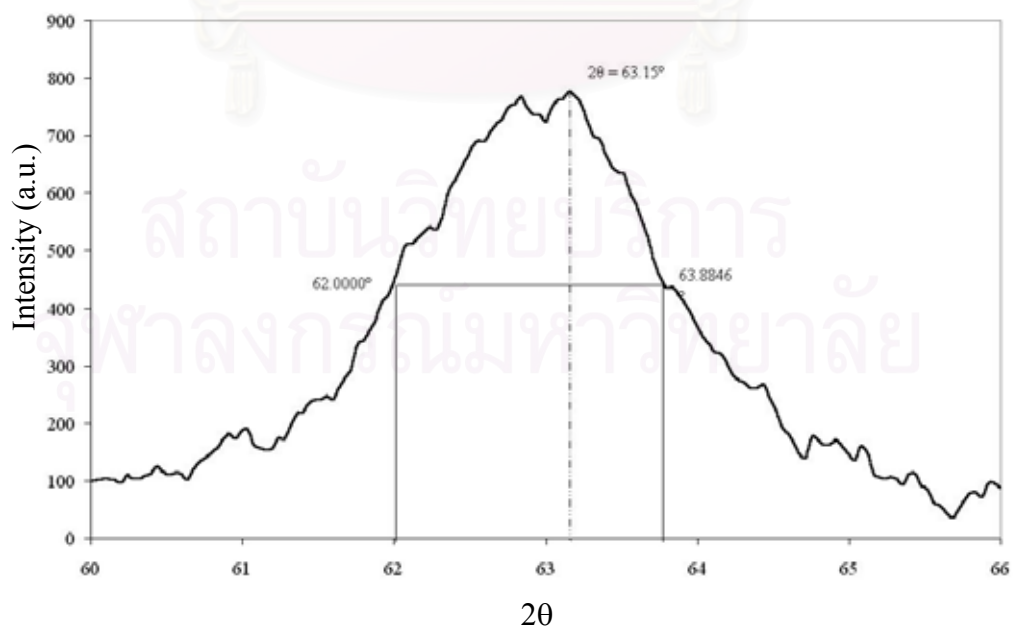
Figure B.1 The observation peak of zinc chromite to calculate the crystallite size
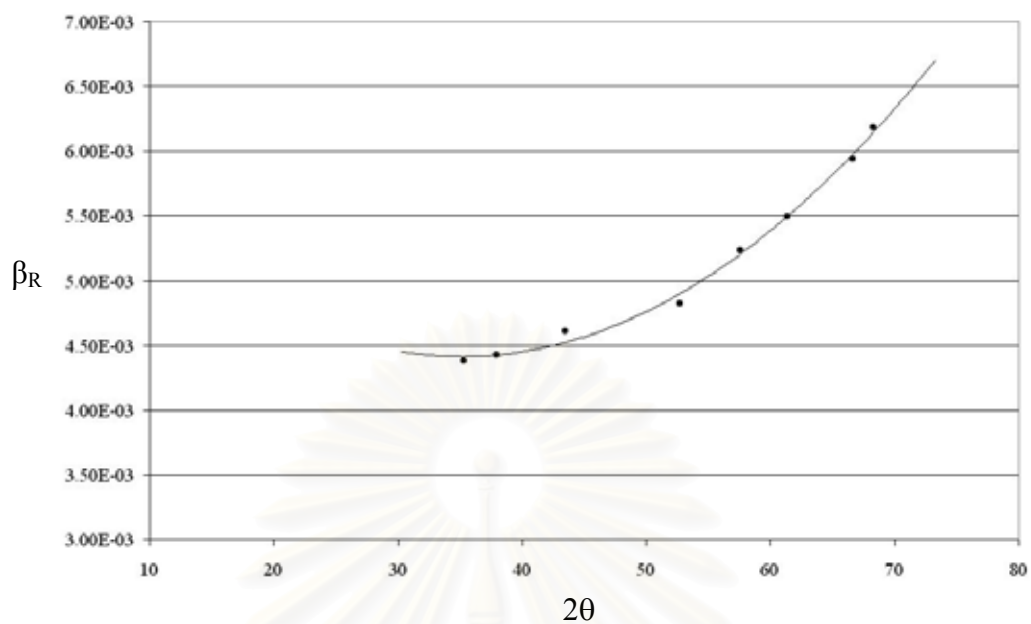
Figure B.2 The graph indicating the value of the line broadening attribute to the experimental equipment from the α-alumina standard

APPENDIX C

CALCULATION OF THE SPECIFIC SURFACE AREA

From Brunauer-Emmett-Teller (BET) equation [38]

$$\frac{p}{n(1-p)} = \frac{1}{n_m C} + \frac{(C-1)p}{n_m C} \qquad (C.1)$$

Where, p = Relative partial pressure of adsorbed gas, P/P_0

        P_0 = Saturated vapor pressure of adsorbed gas in the condensed

              state at the experimental temperature, atm

        P = Equilibrium vapor pressure of adsorbed gas, atm

        n = Gas adsorbed at pressure P, ml. at the NTP/g of sample

        n_m = Gas adsorbed at monolayer, ml. at the NTP/g of sample

        C = Exp $[(H_C - H_l)/RT]$

        H_C = Heat of condensation of adsorbed gas on all other layers

        H_l = Heat of adsorption into the first layer

Assume $C \to \infty$, then

$$\frac{p}{n(1-p)} = \frac{p}{n_m}$$

$$n_m = n(1-p) \qquad (C.2)$$

The surface area, S, of the catalyst is given by

$$S = S_b \times n_m \qquad (C.3)$$

From the gas law

$$\frac{P_b V}{T_b} = \frac{P_t V}{T_t} \qquad (C.4)$$

Where, P_b = Pressure at 0ºC

        P_t = Pressure at tºC

        T_b = Temperature at 0ºC = 273.15 K

        T_t = Temperature at tºC = 273.15 + t K

        V = Constant volume

Then, P_b $= (273.15 / T_t) \times P_t$ $= 1$ atm

Partial pressure

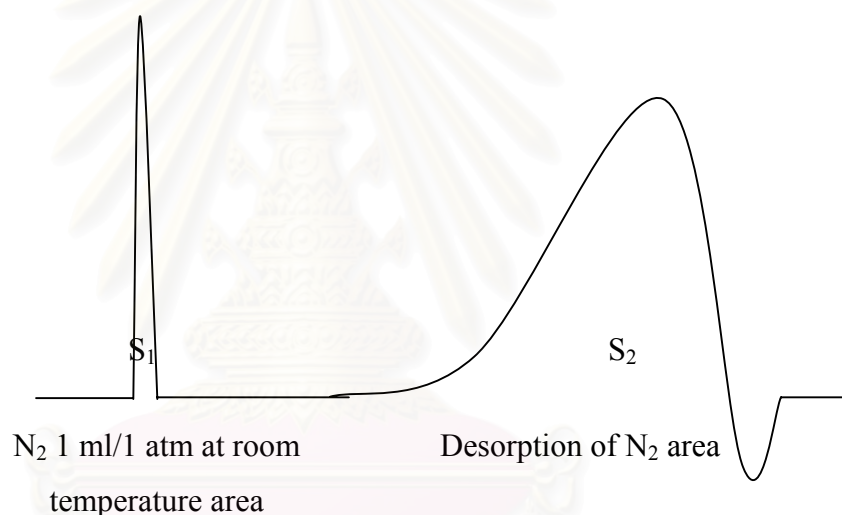$$P = \frac{[\text{Flow of }(He + N_2) - \text{Flow of He}]}{\text{Flow of }(He + N_2)} \qquad (C.5)$$

$$= 0.3 \text{ atm}$$

For nitrogen gas, the saturated vapor pressure equals to

P_0 $= 1.1$ atm

then, p $= P/P_0$ $= 0.3/1.1$ $= 0.2727$

To measure the volume of nitrogen adsorbed, n

N_2 1 ml/1 atm at room   Desorption of N_2 area

temperature area

$$n = \frac{S_2}{S_1} \times \frac{1}{W} \times \frac{273.15}{T} \text{ ml. /g of catalyst} \qquad (C.6)$$

Where, S_1 $= N_2$ 1 ml/1 atm at room temperature area

S_2 $=$ Desorption of N_2 area

W $=$ Sample weight, g

T $=$ Room temperature, K

Therefore,

$$n_m = \frac{S_2}{S_1} \times \frac{1}{W} \times \frac{273.15}{T} \times (1 - p)$$

$$n_m = \frac{S_2}{S_1} \times \frac{1}{W} \times \frac{273.15}{T} \times 0.7272 \qquad (C.2.1)$$

Whereas, the surface area of nitrogen gas from literature equal to

S_b = 4.373 m^2/ml of nitrogen gas

Then,

$$S = \frac{S_2}{S_1} \times \frac{1}{W} \times \frac{273.15}{T} \times 0.7272 \times 4.343$$

$$S = \frac{S_2}{S_1} \times \frac{1}{W} \times \frac{273.15}{T} \times 3.1582 \text{ m}^2\text{/g} \qquad\qquad (C.7)$$

APPENDIX C

CALCULATION OF THE SPECIFIC SURFACE AREA

From Brunauer-Emmett-Teller (BET) equation [38]

$$\frac{p}{n(1-p)} = \frac{1}{n_m C} + \frac{(C-1)p}{n_m C} \qquad (C.1)$$

Where, p = Relative partial pressure of adsorbed gas, P/P_0

P_0 = Saturated vapor pressure of adsorbed gas in the condensed

state at the experimental temperature, atm

P = Equilibrium vapor pressure of adsorbed gas, atm

n = Gas adsorbed at pressure P, ml. at the NTP/g of sample

n_m = Gas adsorbed at monolayer, ml. at the NTP/g of sample

C = Exp $[(H_C - H_l)/RT]$

H_C = Heat of condensation of adsorbed gas on all other layers

H_l = Heat of adsorption into the first layer

Assume $C \rightarrow \infty$, then

$$\frac{p}{n(1-p)} = \frac{p}{n_m}$$

$$n_m = n(1 - p) \qquad (C.2)$$

The surface area, S, of the catalyst is given by

$$S = S_b \times n_m \qquad (C.3)$$

From the gas law

$$\frac{P_b V}{T_b} = \frac{P_t V}{T_t} \qquad (C.4)$$

Where, P_b = Pressure at 0ºC

P_t = Pressure at tºC

T_b = Temperature at 0ºC = 273.15 K

T_t = Temperature at tºC = 273.15 + t K

V = Constant volume

Then, P_b $= (273.15/ T_t) \times P_t$ $= 1$ atm

Partial pressure

$$P = \frac{\left[\text{Flow of }(He + N_2) - \text{Flow of He}\right]}{\text{Flow of }(He + N_2)} \tag{C.5}$$
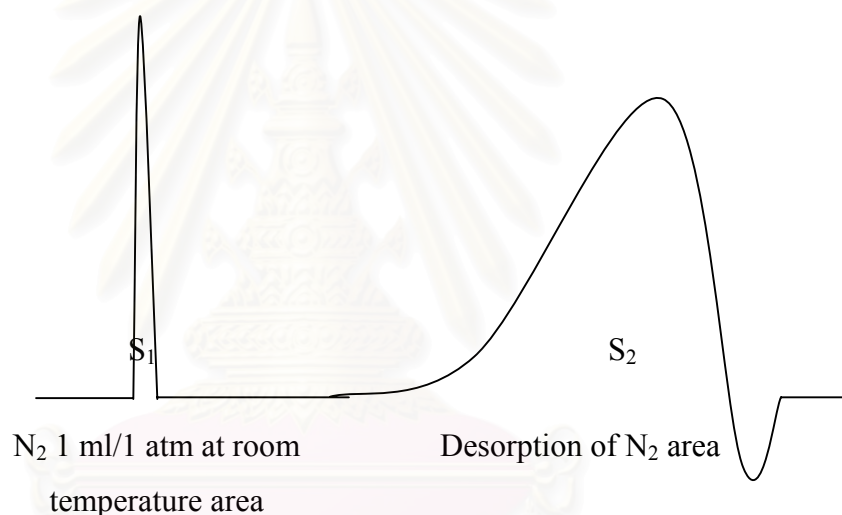
$$= 0.3 \text{ atm}$$

For nitrogen gas, the saturated vapor pressure equals to

P_0 $= 1.1$ atm

then, p $= P/P_0$ $= 0.3/1.1$ $= 0.2727$

To measure the volume of nitrogen adsorbed, n

N₂ 1 ml/1 atm at room   Desorption of N₂ area

temperature area

$$n = \frac{S_2}{S_1} \times \frac{1}{W} \times \frac{273.15}{T} \text{ ml. /g of catalyst} \tag{C.6}$$

Where, S_1 $= N_2$ 1 ml/1 atm at room temperature area

S_2 $=$ Desorption of N_2 area

W $=$ Sample weight, g

T $=$ Room temperature, K

Therefore,

$$n_m = \frac{S_2}{S_1} \times \frac{1}{W} \times \frac{273.15}{T} \times (1 - p)$$

$$n_m = \frac{S_2}{S_1} \times \frac{1}{W} \times \frac{273.15}{T} \times 0.7272 \tag{C.2.1}$$

Whereas, the surface area of nitrogen gas from literature equal to

S_b = 4.373 m^2/ml of nitrogen gas

Then,

$$S \quad = \quad \frac{S_2}{S_1} \times \frac{1}{W} \times \frac{273.15}{T} \times 0.7272 \times 4.343$$

$$S \quad = \quad \frac{S_2}{S_1} \times \frac{1}{W} \times \frac{273.15}{T} \times 3.1582 \ \text{m}^2/\text{g} \qquad\qquad (C.7)$$
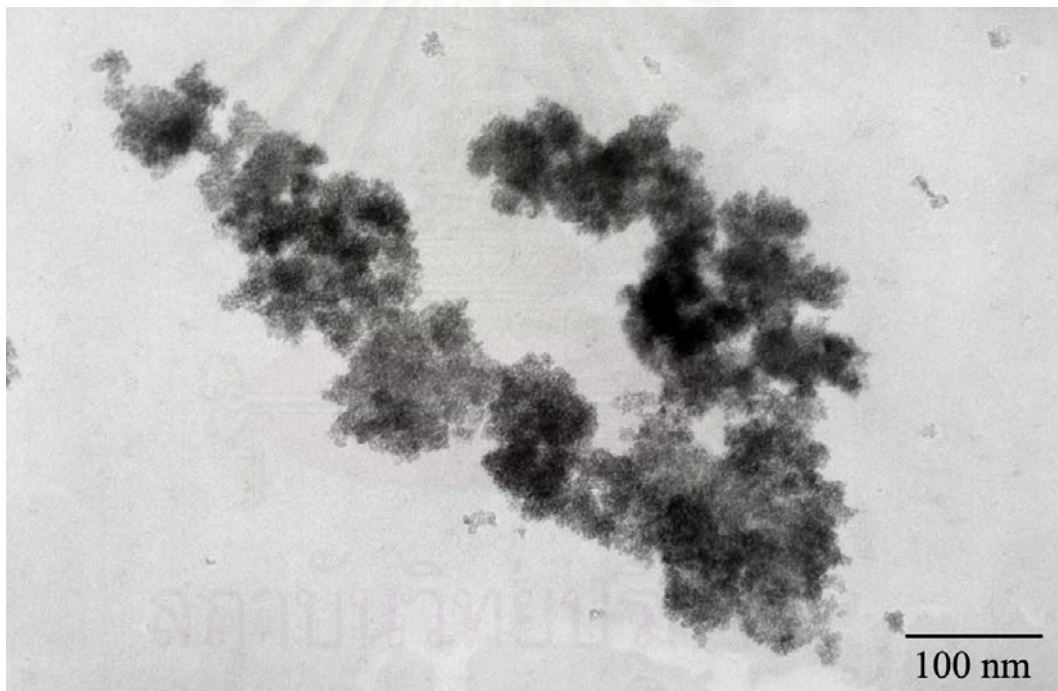
APPENDIX D

ESTIMATION OF THE PARTICLE SIZE
FROM TEM PHOTOGRAPH

Crystallite sizes measured from TEM photograph of the as-synthesized products and calcined products of the spinel type metal oxides were estimated as follows,

Example D.1: The measurement of as-synthesized crystallite size of zinc chromite prepared by the reaction-heating rate of 2.5ºC/min

Figure D.1 TEM photograph of as-synthesized zinc chromite (x150000)

At X150000 magnification, the scale is

150 mm   = 1 µm

            = 1000 nm

From TEM photograph, it was found that the crystallite size of the particles closed to each other and that was 0.8 mm. Therefore, the crystallite size observed by TEM is

Crystallite size $= \dfrac{1000 \text{ nm}}{150 \text{ mm}} \times 0.8 \text{ mm}$

Crystallite size $= 5.33$ nm

Example D.2: The measurement of calcined crystallite size of zinc chromite prepared by the reaction-heating rate of 2.5ºC/min at the calcination temperature 1000ºC

Figure D.2 TEM photograph of calcined zinc chromite at calcination temperature 1000ºC (x150000)

At X150000 magnification, the scale is

150 mm $= 1 \mu$m

$= 1000$ nm

From TEM photograph, it was found that the distribution of crystallite size of the calcined product was broad. Therefore, the crystallite size observed by TEM was averaged.

The measured crystallite sizes from TEM photograph were 8.2, 8, 7.2, 7, 6.8, 6.4, 6.2, 6, 5.8, 5, 4.6 and 4. The average crystallite size was

$$\text{Crystallite size} = \frac{8.2 + 8 + 7.2 + 7 + 6.8 + 6.4 + 6.2 + 6 + 5.8 + 5 + 4.6 + 4}{12} \text{ mm}$$

$$= 6.27 \text{ mm}$$

Therefore, the crystallite size observed by TEM is

$$\text{Crystallite size} \quad = \frac{1000 \text{ nm}}{150 \text{ mm}} \times 6.27 \text{ mm}$$

$$\text{Crystallite size} \quad = 41.8 \text{ nm}$$

VITA

Mr.Parinya Somrang was born on December 18th, 1976 in Lopburi Thailand. He received the Bachelor Degree of Chemical Engineering from Faculty of Engineering, King Mongkut's Institute of Technology Ladkrabang in 1998. His senior project had been accepted for the oral presentation in the 8th Congress of Asian Pacific Confederation of Chemical Engineering (APCChE), at Seoul Korea in 1999. He had been working in the field of process engineer before continued his Master's study at Chulalongkorn University in June 2000.